Modeling the electrorefining process and the effect of cathode design in a molten salt electrorefiner

by

B. KRISHNA SRIHARI

(ENGG02201104011)

Indira Gandhi Centre for Atomic Research, Kalpakkam

A thesis submitted to the
Board of Studies in Engineering Sciences
In partial fulfillment of requirements
for the Degree of

DOCTOR OF PHILOSOPHY

of

HOMI BHABHA NATIONAL INSTITUTE

October, 2015

Homi Bhabha National Institute

Recommendations of the Viva Voce Committee

As members of the Viva Voce Committee, we certify that we have read the dissertation prepared by **B. Krishna Srihari** entitled "**Modeling the electrorefining process and the effect of cathode design in a molten salt electrorefiner**" and recommend that it may be accepted as fulfilling the thesis requirement for the award of Degree of Doctor of Philosophy.

Chairman – Dr. M. Sai Baba **Date:** 11-4-16

Guide / Convener – Dr. B. Prabhakara Reddy Reddy **Date:** 11/04/2016

Examiner – Dr. Arindam Sarkar Arindam Sarkar 11/4/2016 **Date:**

Co-guide – Dr. P.M. Satya Sai (Retired) **Date:** 11. 04. 2016
f (Dean-Academic)

Member – Dr. T. Gnanasekaran **Date:** 11/04/2016

Final approval and acceptance of this thesis is contingent upon the candidate's submission of the final copies of the thesis to HBNI.

I hereby certify that I have read this thesis prepared under my direction and recommend that it may be accepted as fulfilling the thesis requirement.

Date: 11/04/2016
Place: Kalpakkam

Reddy
(Guide)

STATEMENT BY AUTHOR

This dissertation has been submitted in partial fulfillment of requirements for an advanced degree at Homi Bhabha National Institute (HBNI) and is deposited in the Library to be made available to borrowers under rules of the HBNI.

Brief quotations from this dissertation are allowable without special permission, provided that accurate acknowledgement of source is made. Requests for permission for extended quotation from or reproduction of this manuscript in whole or in part may be granted by the Competent Authority of HBNI when in his or her judgment the proposed use of the material is in the interests of scholarship. In all other instances, however, permission must be obtained from the author.

B. Krishna Srihari

DECLARATION

I, hereby declare that the investigation presented in the thesis has been carried out by me. The work is original and has not been submitted earlier as a whole or in part for a degree at this or any other Institution /University.

B. Krishna Srihari

List of Publications arising from the thesis

Journal

1. “Modeling the molten salt electrorefining process for spent metal fuel using COMSOL”, B. Krishna Srihari, S. Agarwal, B. Prabhakara Reddy, P.M. Satya Sai, B. Muralidharan, K. Nagarajan, Separation Science and Technology, 2015, 50, 2276-2283.
2. “Experimental studies and model validation for the optimization of electrodes configuration in a molten salt electrorefiner”, B. Krishna Srihari, B. Prabhakara Reddy, P Venkatesh, S. Agarwal, P.M. Satya Sai, K. Nagarajan, Separation Science and Technology, DOI: 10.1080/01496395.2016.1158190.

Proceedings of conferences

1. “Optimizing electrode surface area by COMSOL Multiphysics”, Bonasi Krishna Srihari, B. Prabhakara Reddy, P Venkatesh, K. Nagarajan, COMSOL Conference - 2013, Bengaluru, October 17-18, 2013.
2. “Effect of electrode configuration on the current and potential distribution in a molten salt electrorefiner”, Bonasi Krishna Srihari, Sourabh Agarwal, B. Prabhakara Reddy, K. Nagarajan, International Conference on Electrochemical Science and Technology - 2014, IISc Bengaluru, August 7-9, 2014.

(B. Krishna Srihari)

Dedicated to

My Parents

and

My Family

ACKNOWLEDGEMENT

I express my sincere gratitude towards Dr. K. Nagarajan, Former Director, Chemistry Group, Radio Chemistry Laboratory, Indira Gandhi Centre for Atomic Research, for granting me the privilege to carry out this dissertation work under his guidance. I acknowledge his valuable insight and persistent support.

I am very thankful to Dr. B. Prabhakara Reddy, Head, Pyroprocessing Studies Section, Chemistry Group, for providing me exciting and challenging research problems with excellent research facilities.

I am extremely thankful to Dr. P.M. Satya Sai, Former Deputy General Manager, Nuclear Recycle Board, Bhabha Atomic Research Centre Facilities, for giving valuable suggestions during our interactions.

I am grateful to Dr. M. Sai Baba, Chairman, Doctoral Committee and Associate Director, Resources Management Group, for his continuous encouragement. I am thankful to my other doctoral committee members: Dr. T. Gnanasekaran, Chemistry Group, Radio Chemistry Laboratory.

I would like to thank Shri Sourabh Agarwal, Chemical Technology Division, FRTG, for his great support, encouragement and in helping COMSOL modeling. And also thankful to Shri P. Venkatesh, Dr. S. Vannia Perumal, Dr. Manish Chandra, Dr. S. Ghosh, Dr. Vandarkhuzali and S. Nibedita Chemistry Group, for giving valuable suggestions and their co-operation, support and help during my research work.

I take immense pleasure in thanking Dr. P.R. Vasudeva Rao, Director, Chemistry Group and Indira Gandhi Centre for Atomic Research, for providing facilities to carry out my experiments.

I wish to record my sincere thanks to all my lab members, Shri. Kakum Perumal Mrs. Suganthi, Mrs. Lali, Mrs. Surya Kumari, Shri. Mariyappan, Shri. Ganapathi, Shri. Rajeev, Mrs. Anjali, Shri. Nedumaran, Shri. Arun, Vinod and RTC shift members for their kind help and support. I also wish to thank analytical laboratory members for helping in the analysis of experimental samples. I profoundly thank all the technical and non-technical members of chemistry group for their valuable co-operation during my research work.

I feel extremely fortunate to have friends like Ch. Mahendra, Dhanasekaran, I. Ravi, Anil K Soni, Ashutosh, Deepak, Mahesh, Maruthi, Karri Prasad, Pradeep, Sadu, Ramana, Avinash, Prasanna, Hari Prasad, Samba, Siva Kesava Reddy, Siva Srinivas, Srijan, Maasilamani, Suhail Malik and Yadgiri who were always with me in any situation. I would like to thank all my school and college friends who have encouraged me in all the ways.

I heartfelt gratitude to my parents, Shri. Venkataiah and Smt. Eswaramma, my wife Jyothi, brothers Shri. Balasubramanyam and Dr. Devender, sister-in-laws Smt. Sravanthi, and Smt. Maheswari, our children Vikranth, Aniket, Anirish, my father-in-law Kurmanthi and mother-in-law Smt. Padma and other relatives for their endless love, affection, support, and encouragement.

(B. Krishna Srihari)

CONTENTS

SYNOPSIS

1. Introduction

The fuel discharged from a nuclear reactor after irradiation still contains most of the fertile material (^{238}U or ^{232}Th) which was also the major constituent of the virgin fuel, significant amounts valuable fissile nuclides (^{235}U, ^{239}Pu, and/or ^{233}U) and large amounts of fission products. Reprocessing of the spent fuel is aimed at (1) recovering uranium and plutonium, and thorium if present, for reuse as nuclear fuels and; (2) removing the fission products. Several methods of reprocessing are currently known which can be grouped to aqueous and non-aqueous methods. Non-aqueous processes have many advantages over aqueous processes. Molten salts and molten alloys used in the non-aqueous processes are not susceptible to radiation degradation and hence the fuel could be reprocessed after cooling for a short time. This would be especially advantageous for Fast Breeder Reactors (FBRs) to reduce the doubling time and thus enhance the breeding ratio. The process steps involved are less compared to aqueous processes especially for metallic fuels. Compactness, nuclear proliferation resistance, and reduction of waste volumes and the radiotoxicity are additional advantages [1–6].

Pyrochemical reprocessing is one of the non-aqueous processes and among them, molten salt electrorefining is a pyrochemical reprocessing method especially advantageous for treating metallic fuels. In this process, the separation of the fuel materials and fission products is based on the thermodynamic stabilities of the chlorides of the respective metals. In the electrorefining process, the key process step of this pyroprocess flow sheet, carried out at 500^{0}C, the actinide uranium is recovered from the spent fuel anode by deposition as metal on to a solid cathode. Plutonium and other Transuranium (TRU) elements are electrodeposited as metals in liquid cadmium cathode. [7-9].

The process starts with chopping of the fuel pins. The chopped pieces of the pins are loaded into the electrorefiner where the alkali, alkaline earth and rare earth fission products whose chlorides are very stable are oxidized into molten eutectic LiCl–KCl salt. The noble metal fission products whose chlorides are the least stable stay in the anode along with cladding hulls. The deposit from the cathodes of the electrorefiner, whether solid cathode or liquid cadmium cathode is then distilled to remove the residual salt or cadmium, respectively and the U or U/TRU is consolidated into an ingot for fabrication into fuel. In the early years of development of the electrorefining process, liquid cadmium in which the anode basket containing chopped metal fuel pins was kept immersed served as the anode instead of the basket itself. The process is being developed in a few countries and yet to be demonstrated in industrial scale. In India also, where it is proposed to use metal fuels in future FBRs, development of the process in progress.

Several researchers investigated the electrorefining of spent metal fuel by various approaches, namely, experimental, thermochemical modeling and electrokinetic modeling. Some investigators have developed their own codes whereas some have used commercial packages. All the models are having their unique aspects depending on the application of the process.

In our laboratory also, these development efforts are in progress. In addition to the experimental efforts, a thermochemical model known as PRAGAMAN and an electrokinetic model (DIFAC) have been developed earlier [10, 11].

2. Thesis Objective

The objective of this thesis is to make a contribution to the modeling of the electrorefining process and that of design of the electrodes of a molten salt electrorefiner by developing our own code based on commercially available software and validates the same using laboratory scale experiments as well as literature data. Among the commercially available software's, COMSOL Multiphysics was chosen in view of the fact that it simulates the electrochemistry related problems and its Multiphysics capability (i.e.) the ability to couple any number of physics together like electrochemistry with chemical species transport or heat transfer or mathematical module etc, enabling more accurate results by minimizing the assumptions etc. These studies will be useful in understanding the pyrochemical processing of spent nuclear fuel and to develop the process from the present status of laboratory scale studies to scale up process development. This study thus gives important data for such a development.

3. Scope of the thesis

The following modeling and experimental work on the design of electrodes for the electrorefiner were carried out in this study and these will be discussed in the thesis:

- Developed the model for the electrorefining process using COMSOL Multiphysics [12] in which three modules of the software were coupled together and studied the electrotransport behavior of uranium and plutonium from liquid cadmium anode to solid cathode and validated the model with experimental data from literature.
- Developed the model to study the effect of the electrode configuration for achieving higher throughput and validated the model with experimental studies carried out by us as well as with experimental data from literature.
- Studied the electrodeposition of uranium using different shapes of the cathode both by modeling and by experimental work

4. Experimental and modeling techniques

In this work, for studying the electrotransport behavior of uranium and plutonium, three modules of COMSOL Multiphysics [12] are coupled together. Those are: (1) the secondary current distribution (siec) of electrochemistry module is used for simulating the electrochemical reactions and the potential and current distributions in the electrochemical cell (2) The transport of the diluted species (chds) of the chemical species transport module is used for simulation of mass transfer of each species through the diffusion layer and (3) the general form of ODE (g) in ODE (Ordinary Differential equation) interfaces of mathematical module is used for solving the material balance equation for each species. Simulated the effect of electrode configuration on the potential and current density distributions by the primary current distribution (piec) of electrochemistry module and validated. The Electrodeposition, Secondary current distribution (edsec) interface of electrochemistry module was used to describe the electrotransport of uranium from solid anode to solid cathode for three different shapes of the cathodes.

All the experimental electrochemical measurements were carried out using AUTOLAB/PGSTAT30 with IF030 interface. A glove box facility was used to maintain inert atmosphere during electrochemical experiments. Davis and Gray method was used to analyze the concentration of uranium present in the electrolyte salt. Oxygen and moisture analyzers were used to measure the levels of these impurities in argon in the glove box in ppm level. Purification towers in the recirculation system enable maintenance of argon gas purity.

5. Results and Discussion

5.1. Modeling the molten salt electrorefining process

A 2D-axis symmetric model was developed for an electrorefiner having liquid cadmium as the anode and a solid rod as the cathode. In this model, uranium and plutonium get oxidized at the liquid cadmium anode and reduced at the solid cathode as per the following half-cell electrochemical reactions:

$$\mathrm{U} \rightarrow \mathrm{U}^{3+} + 3\mathrm{e}^- \qquad \mathrm{E}_{\mathrm{U}}^{0} = -1.10\ \mathrm{V\ vs\ Ag/1\ wt\%AgCl} \qquad \text{(anode)} \qquad (1)$$

$$\mathrm{Pu} \rightarrow \mathrm{Pu}^{3+} + 3\mathrm{e}^- \qquad \mathrm{E}_{\mathrm{Pu}}^{0} = -1.40\ \mathrm{V\ vs\ Ag/1\ wt\%AgCl} \qquad \text{(anode)} \qquad (2)$$

$$\mathrm{U}^{3+} + 3\mathrm{e}^- \rightarrow \mathrm{U} \qquad \mathrm{E}_{\mathrm{U}}^{0} = -1.10\ \mathrm{V\ vs\ Ag/1\ wt\%AgCl} \qquad \text{(cathode)} \qquad (3)$$

$$\mathrm{Pu}^{3+} + 3\mathrm{e}^- \rightarrow \mathrm{Pu} \qquad \mathrm{E}_{\mathrm{Pu}}^{0} = -1.40\ \mathrm{V\ vs\ Ag/1\ wt\%AgCl} \qquad \text{(cathode)} \qquad (4)$$

The electrotransport of U and Pu from the liquid cadmium anode to solid cathode and their subsequent deposition on the solid cathode was modeled and validated. The variation in the concentrations of U and Pu in the molten salt electrolyte as well as in liquid cadmium anode with time could be predicted by the model. The concentration of uranium was higher than that of Pu in the liquid cadmium anode in the initial stages and as the deposition of U on the cathode progressed, the concentration of uranium became lower in the later stages. The rate of decrease of U concentration in the anode was almost the same until more than 98% of it got deposited. At this point, Pu remained in the anode itself until this stage and only uranium was getting transferred to the cathode. Pu starts getting transferred to the cathode from this value. Hence the rate of decrease of plutonium at the anode is zero until this stage and later it becomes higher. So, the rate of transfer of Pu to the cathode increases at later stages and becomes higher than that of U. The results from COMSOL model are in general in good agreement with the experimental data from literature [13]. It was also be able to predict the amounts of U and Pu deposited on the solid cathode with the progress of electrorefining. As shown in Fig.1, for a starting feed composition of 1.61 wt% of U and 1.82 wt% of Pu in 4.4 kg of electrolyte salt, 1.01 wt % of U and 0.59 wt % of Pu in 16 kg of liquid cadmium, the U deposition on the solid cathode increased linearly with time until 52 hours and there is no further deposition subsequently. There is no Pu deposition on the solid cathode until 52 hours, as

$PuCl_3$ (ΔG_f = -62.4 Kcal/gmole equivalent of Cl^- at 773 K) is more stable compared to UCl_3 (ΔG_f = -55.2 Kcal/gmole equivalent of Cl^- at 773 K). After 52 hours, there is a sudden increase in the Pu to U ratio in the molten salt, which results in Pu deposition. It was also observed that, Pu to U ratio in the molten salt as well as in the liquid cadmium anode increases with the progress of electrorefining. Variation of cell voltage was also simulated and validated with cell voltage obtained from literature [14]

5.2. Effect of electrode configuration

The key feature in the design of a molten salt electrorefiner is the potential and current distribution analysis. In this study, the effect of electrode configuration on the potential and current distribution in a molten salt electrorefiner was studied by carrying out uranium electrorefining experiments and by modeling using COMSOL Multiphysics. Although there are three types of distribution of current and potential (primary, secondary and tertiary), only primary potential and current density distributions were analyzed, as a first approach. This approach simplifies the analysis by considering only the cell geometry. The developed model was validated with the experimental results of our electrorefiner set up and also with the literature data.

5.2.1. Parallel and staggered arrangement of electrodes

A perforated anode basket and an SS 430 solid rod were used as the anode and the cathode respectively. Two pairs of anodes and cathodes were used for electrorefining. Experiments were carried out with the two pairs of electrodes arranged in a parallel as well as staggered configuration. A 2D model was developed with the centre to centre distance between the each of four electrodes in each direction maintained at 42 mm in both the parallel and staggered arrangements. A cell voltage of 0.2 V was imposed.

In the parallel arrangement of electrodes, the potential was distributed only in the space between the electrodes and electrodeposition occurred only on one face of the cathode. The current distribution was also observed between one anode and one cathode facing each other in the parallel arrangement, whereas for the staggered arrangement, current distribution was observed from all the four faces of the anodes to all the sides of the two cathodes. The cell resistances were calculated using the model and compared with the presently investigated experimental values and also with available literature data.

5.2.2. Effect of variation of the distance between the electrodes

The distance between the anode and cathode was kept as 3 and 6 cm and its effect on the electrodeposition of uranium was experimentally determined. A 2D model was developed for electrotransport of uranium from the perforated anode basket to solid cathode with various distances (2-8 cm) between anode and the cathode. The potential and current distributions were similar to that observed for the parallel arrangement of electrodes. It was also observed that the cell resistance increased with increase in the center to center distance between the electrodes. The cell resistances computed using the model is in very good agreement with the experimental values.

5.2.3. Effect of having an insulating disc at the bottom of the solid cathode

The electro-deposition of uranium was also investigated with and without an insulating ceramic disc at the bottom of the solid cathode. In these experiments, liquid cadmium containing a known amount of uranium was used as the anode. A 2D axisymmetric model was developed due to the symmetry in the electrochemical cell. The results show that the solid cathode with insulation had an advantage of avoiding uranium dendrites growth towards liquid cadmium anode without any significant loss in the performance, as the increase of cell resistance is only 11 % for the solid cathode with insulation compared to that without insulation.

5.2.4. Effect of parameters of the Cd cathode

Liquid cadmium taken in an alumina crucible was used as the cathode and the cadmium pool at the bottom of the electrorefiner was used as the anode, for this study. The concentration of uranium in the liquid cadmium anode was approximately 2 wt%. Liquid cadmium cathode was immersed in the electrolyte salt up to known height (‘h_1’). The height of the empty space inside the alumina crucible above liquid cadmium was taken as ‘h_2’ and the surface area of the cadmium cathode was ‘S’. A 2D axisymmetric model developed and the potential and current density distributions were calculated with various elevations of the Cd cathode. The cell resistances computed using the present model was compared with the experimental results for two sets of values of h_1, h_2 and S. Simulations were also carried out for the experimental conditions described by Kobayashi et al. [14]. It was observed that with increase in the height of the immersed region (h_1) of the crucible, the cell resistance decreased due to the decrease in the distance between the anode and cathode. Increasing the height of empty space of crucible (h_2) resulted in increase in the cell resistance and increasing the Cd cathode surface area led to decrease in the cell resistance, as is expected.

5.2.5. Effect of solid cathode surface area

The 2D axisymmetric model was used to do computations with various surface areas of the cathode and liquid cadmium as anode for electrodeposition of uranium. The potential and current density distributions were evaluated. It was observed that with increase in the cathode surface area, the cell resistance decreased and current increased, which results in higher throughput of electrorefiner. But further increase in the surface area would lead to polarization of liquid Cd anode and electrotransport would be interrupted [15].

5.2.6. Cell resistance sensitivity study

A sensitivity analysis was performed to determine which of the two parameters, namely, cell voltage and electrical conductivity more significantly affects the cell resistance. It was observed that cell resistance is more sensitive to the electrolyte conductivity and there is no influence of cell voltage on cell resistance.

5.3. Effect of shape of the cathode

Electro-deposition of uranium was investigated with cathodes of three different shapes (Cylindrical, rectangular and Stirrer type) made up of SS 430. A perforated anode basket containing uranium was used as the anode. Electrodeposition of uranium on each cathode was performed, when the surface areas for all of the cathodes were maintained the same as a first approach. It was found that the current efficiency was approximately the same for all the cathodes as expected. As a second approach the same lengths of the cathodes were dipped into the electrolyte and the electrodeposition of uranium was performed. Higher current efficiency was observed for the stirrer type of the cathode. The potential distribution between anode and cathode was also evaluated.

Thesis Outline

The thesis is divided into 6 chapters; the introductory Chapter 1 discusses briefly the need of nuclear energy, the pyrochemical reprocessing methods, molten salt electrorefining process, and the literature survey on the various modeling studies. At the end of the chapter, the objective and the scope of the thesis are also given. Chapter 2 discusses the fundamental theories, and concepts used for modeling the electrorefining, chemicals used for the preparation of electrolyte salts, experimental setup and facilities and analytical methods. Chapter 3 discusses the development of electrorefiner model and validation of the developed model with the literature data. Chapter 4 explains the studies on the effect of electrode configuration in a molten salt electrorefiner by experimental techniques, development of the model and its validation with experimental results. Chapter 5 deals with the effect of different shapes of the solid cathode on the electrodeposition of uranium by experiments as well as by modeling. Chapter 6 concludes the thesis by discussing the limitations of the developed model and experimental observations and future studies that need to be taken for further development of model for the electrorefining process.

References

[1] M. Benedict, T.H. Pigford, Nuclear Chemical Engineering, H.W Levi, 2nd edition, p 457-557.

[2] Y.I. Chang, The Integral Fast Reactor, Nucl. Technol. 88 (1989) 129-138.

[3] J.J. Laidler, W.E. Miller, T.R. Johnson, J.P. Ackerman, J.E. Battles, IFR fuel cycle pyroprocess development, Report ANL/CMT/CP-77849, Argonne, IL, USA, 1992.

[4] J.J. Laidler, Report ANL/CMT/CP7893, Pyrochemical Recovery of Actinides, Argonne National Laboratory, Argonne, IL, USA, 1993.

[5] J.P. Ackerman, Chemical Basis for Pyrochemical Reprocessing of Nuclear-Fuel, J. Ind. Eng. Chem. 30 (1991) 141-145.

[6] J.G. Kim, J.H. Lee, I.T. Kim, E.H. Kim, Fabrication of a Glass-Bonded Zeolite Waste Form for Waste LiCl Salt, J. Ind. Eng. Chem. 13(2) (2007) 292-298.

[7] J.L. Willit, W.E. Miller, J.E. Battles, Electrorefining of uranium and plutonium-A literature review, J. Nucl. Mater. 195(3) (1992) 229-249.

[8] K. Uzomi, M. Iizuka, T. Kato, T. Inoue, O. Shirai, T. Iwai, Y. Arai, Electrochemical behaviors of uranium and plutonium at simultaneous recoveries into liquid cadmium cathodes, J. Nucl. Mater. 325 (2004) 34-43.

[9] T. Koyama, M. Iizuka, Y. shoji, R. Fujita, H. Tanaka, T. Kobayashi, M. Tokiwai, An Experimental Study of Molten Salt Electrorefining of Uranium Using Solid Iron Cathode and Liquid Cadmium Cathode for Development of Pyrometallurgical Reprocessing, J. Nucl. Sci. Technol. 34(3) (1997) 384-393.

[10] S. Ghosh, B. Prabhakara Reddy, K. Nagarajan, P.R. Vasudeva Rao, PRAGAMAN: A computer code for simulation of electrotransport during molten salt electrorefining, Nucl. Technol. 170 (2010) 430-443.

[11] A. Venkatesh, S. Ghosh, S. Vandarkuzhali, B. Prabhakara Reddy, K. Nagarajan, P.R. Vasudeva Rao, Modeling the anodic behavior of U, Zr, and U-Zr alloy in molten LiCl-KCl eutectic, Nucl. Technol. 182 (2013) 98-110.

[12] COMSOL Multiphysics user guide and model library, version 4.4, COMSOL 4.4 (2013).

[13] Z. Tomczuk, J.P. Ackerman, R.D. Wolson, W.E. Miller, Uranium transport to solid electrodes in pyrochemical reprocessing of nuclear fuel, J. Electrochem. Soc. 139 (1992) 3523-3528.

[14] T. Kobayashi, M. Tokiwai, E.C. Gay, Investigation of cell resistance for molten salt electrorefining of spent nuclear fuel, J. Nucl. Sci. Technol. 32(1) (1995) 68-74.

[15] T. Nishimura, T. Koyama, M. Iizuka, H. Tanaka, Development of an environmentally benign reprocessing technology – pyrometallurgical reprocessing technology, Prog. Nucl. Energ. 32(3/4) (1998) 381-387.

List of Figures

List of Tables

Abbreviations

PHWR	Pressurized Heavy Water Reactor
FBR	Fast Breeder Reactor
FBTR	Fast Breeder Test Reactor
PFBR	Prototype Fast Breeder Reactor
AHWR	Advanced Heavy Water reactor
BWR	Boiling Water Reactor
MA	Minor Actinides
HLW	High Level Waste
IAEA	International Atomic Energy Agency
PUREX	Plutonium Uranium EXtraction
THORP	THermal Oxide Reprocessing Plant
TBP	Tri-n-ButylPhosphate
RE	Rare Earths
TRUEX	TRansUranic EXtraction
DIAMEX	DIAMideEXtraction
FP	Fission Products
RIAR	Russian Institute of Atomic Reactors
ANL	Argonne National Laboratory
MOX	Mixed Oxide
ITU	Institute of Trans Uranium
IFR	Integral Fast Reactor
IGCAR	Indira Gandhi Centre for Atomic Research
ER	Electrorefiners
CFD	Computational Fluid Dynamics

FEM	Finite Element Method
TRAIL	Transportation of Actinides in Electrorefiner
CRIEPI	Central Research Institute of Electric Power Industry
LCA	Liquid Cadmium Anode
LCC	Liquid Cadmium Cathode
GPEC	General Purpose Electrochemical Simulator
COMSOL	Computer Solution
ERAD	Enhanced REFIN with Anodic Dissolution
DIFAC	DIFfusion of Actinides in EleCtrorefiner
ODE	Ordinary Differential Equation
PID	Proportional Integral Derivative
UHP	Ultra High Pure
SS	Stainless Steel
BARC	Bhabha Atomic Research Centre
WE	Working Electrode
CE	Counter Electrode
RE	Reference Electrode
GUI	Graphical User Interface
PDE	Partial Differential Equation

Nomenclature

U	Uranium
Pu	Plutonium
Th	Thorium
Np	Neptunium
Am	Americium
Cm	Cerium
Kr	Krypton
I	Iodine
Zr	Zirconium
Nb	Niobium
Ru	Ruthenium
Rh	Rhodium
Pd	Palladium
Ag	Silver
Pt	Platinum
Cr	Chromium
Ni	Nickel
Fe	Iron
Cd	Cadmium
M^{n+}	Metal Ion
M	Metal
N	Number of electrons or valency
Q	Quantity of electricity in coulombs
Δm	Number of moles of material deposited

I	Current in amperes
T	Time in seconds
F	Faraday’s constant (96500 $C.mol^{-1}$)
H	Current efficiency (%)
Siec	Secondary Current Distribution
Tds	Transport of Diluted Species Interface
N_i	Flux of species i ($mol/m^2.s$)
z_i	Concentration (mol/m^3) of the species i
D_i	Diffusion coefficient (m^2/s) of species i
z_i	Number of electrons participated in the reaction of species i
$u_{m,i}$	Mobility (s. mol/kg)
$\emptyset_l$	Electrolyte Potential, (V)
U	Velocity (m/s)
i_l	Current density in the electrolyte, (A/m^2)
c_i	Concentration of species i, (mol/m^3)
σ_l	Electrolyte conductivity, (S/m)
$E_{eq,m}$	Equilibrium Potential, (V)
η_m	Activation Overpotential, (V)
ϕ_s	Electrode potential, (V)
$i_{loc,m}$	Local charge transfer current density for reaction m, (A/m^2)
i_0	Exchange Current Density, (A/m^2)
α_a	Anodic charge transfer coefficient
α_c	Cathodic charge transfer coefficient
R	Universal gas constant

C_R	Dimensionless expression of reduced species
C_O	Dimensionless expression of Oxidized species
R	Reaction rate expression for the species, (mol/ (m^3·s))
D	Diffusion coefficient, (m^2/s)
$C_{b,j}$	concentration of the species *j* in the bulk, (mol/m^3)
$i_{o,norm}$	Normalized current density,
$E^{o}_{red,j}$	standard potential of species j, (V)
T	Temperature, (K)
γ_j^{salt}	Activity coefficient of the species *j* in salt
γ_j^{Cd}	Activity coefficient of the species *j* in Cadmium
$C^*_{Ox,j}$	Concentration of species *j* at the salt side of the cadmium-salt interface
$C^*_{Red,j}$	Concentration of species *j* at the cadmium side of the cadmium – salt interface
$C_{Ox,j}$	Concentration of *j* at the salt side of the solid electrode-salt interface
I_{app}	Total current, A
A	Electrode surface area, m^2
V_{salt}	Molten salt volume, (m^3)
$C_{b,j}^{salt}$	Bulk concentration of species *j* in the molten salt (mol/m^3)
V_{Cd}	volume of cadmium, (m^3)
$C_{b,j}^{Cd}$	Bulk concentration of species *j* in cadmium, (mol/m^3)
α_U	Transfer coefficient for U
α_{Pu}	Transfer coefficient for Pu
W_{salt}	Molten salt weight, g
W_{Cd}	Cadmium weight, g
D_U^{salt}	Diffusion coefficient of uranium in salt, cm^2/s

D_{Pu}^{salt}	Diffusion coefficient of plutonium in salt, cm^2/s
D_{U}^{Cd}	Diffusion coefficient of uranium in cadmium, cm^2/s
D_{U}^{Cd}	Diffusion coefficient of plutonium in cadmium, cm^2/s
$E_{red,U}^{o}$	Standard potential of uranium, (V)
$E_{red,Pu}^{o}$	Standard potential of plutonium, (V)
Δ	Diffusion layer thickness in molten salt and cadmium, (cm)
γ_{U}^{salt}	Activity coefficient of uranium in molten salt
γ_{Pu}^{salt}	Activity coefficient of plutonium in molten salt
γ_{U}^{Cd}	Activity coefficient of uranium in cadmium
γ_{Pu}^{Cd}	Activity coefficient of plutonium in cadmium
σ_{salt}	Molten salt conductivity, (S/m)
$i_{u,o,norm}$	Normalized exchange current density for uranium, (A/m^2)
$i_{Pu,o,norm}$	Normalized exchange current density for plutonium, (A/m^2)
Z	Charge number

Chapter1

Introduction

1.1. Nuclear Energy

Energy consumption is increasing everyday with the growth of economies. To satisfy these high energy demands, we cannot simply rely on the conventional, non-renewable energy resources, as they are limited and they also add a large amount of pollutants into our environment contributing at a large scale to global warming. Today the standard fossil fuels, coal, gas and oil are contributing to 75% of the world energy production. But these fossil fuels would get exhausted in the near future. On account of these reasons, the world needs fuels which could satisfy the energy demand and at the same time are devoid of emission of the green house gases as well as are amenable to safe disposal of the generated waste. Nuclear energy and the renewable energy resources like hydro, solar, wind, biomass etc. would meet these criteria. But the availability of energy from these renewable resources depends on the atmospheric conditions and will vary depending on the season. Of the above said resources, hydro and nuclear, are the only suitable ones for the large scale electricity production. Thus nuclear energy has an important role to play in fulfilling the energy demands of the world. According to some of the scenarios envisaged for the future, the production of nuclear energy would be to an extent of 5 Gtoe (Giga tons of oil equivalent) in 2050, which would represent about 20% share of the world's energy production [1].

Indian electricity sector has grown manifolds in size and capacity, since independence. This growth comprises of thermal, hydel, nuclear and also non conventional energy sources like solar, wind and tidal. But the demand for electrical energy is increasing and it has been envisaged to be about 1300 GW (Giga watts electric) by 2050. The main objective of Department of Atomic Energy in India is to meet 25% of this energy demand (i.e.) 275 GW through nuclear energy. [2, 3].

1.2. The Indian Nuclear energy program

Dr. Homi Bhabha, the father of the Indian nuclear energy formulated a three stage nuclear programme for the nuclear energy development in India based on the fact that India has very limited resources of uranium and abundant resources of thorium. The three stage programme is based on the closed fuel cycle wherein the irradiated fuel is reprocessed to recover the valuable uranium and plutonium from it and recycle them for efficient utilization of the available nuclear resources [4]. The schematic of the three-Stage Nuclear Programme in India is shown in Fig 1. The three stages of nuclear energy development are the following:

1. Setting up of natural uranium fuelled, heavy water moderated Pressurized Heavy Water Reactors (PHWRs) in the first stage. These exploit the low energy neutrons to cause fission and are known as thermal reactors.
2. Setting up of Fast Breeder Reactors (FBRs) having desirable rapid growth characteristics (i.e. short doubling time) in the second stage and they will be based on plutonium.
3. Setting up of thorium fuelled reactors in the third stage.

In the first stage of the programme, mainly, natural uranium in the form of uranium oxide is being used as fuel material. Natural U contains approximately 0.7% ^{235}U and remaining ^{238}U. Only ^{235}U is the fissile material which undergoes fission reaction in these thermal reactors. The fertile material, ^{238}U produces ^{239}Pu by absorbing a neutron. At present most of the nuclear power reactors in India are Pressurized Heavy Water Reactors (PHWR) in which natural uranium in the form of uranium oxide is the fuel material. The fuel discharged from these reactors contains ^{239}Pu, residual ^{235}U and ^{238}U.

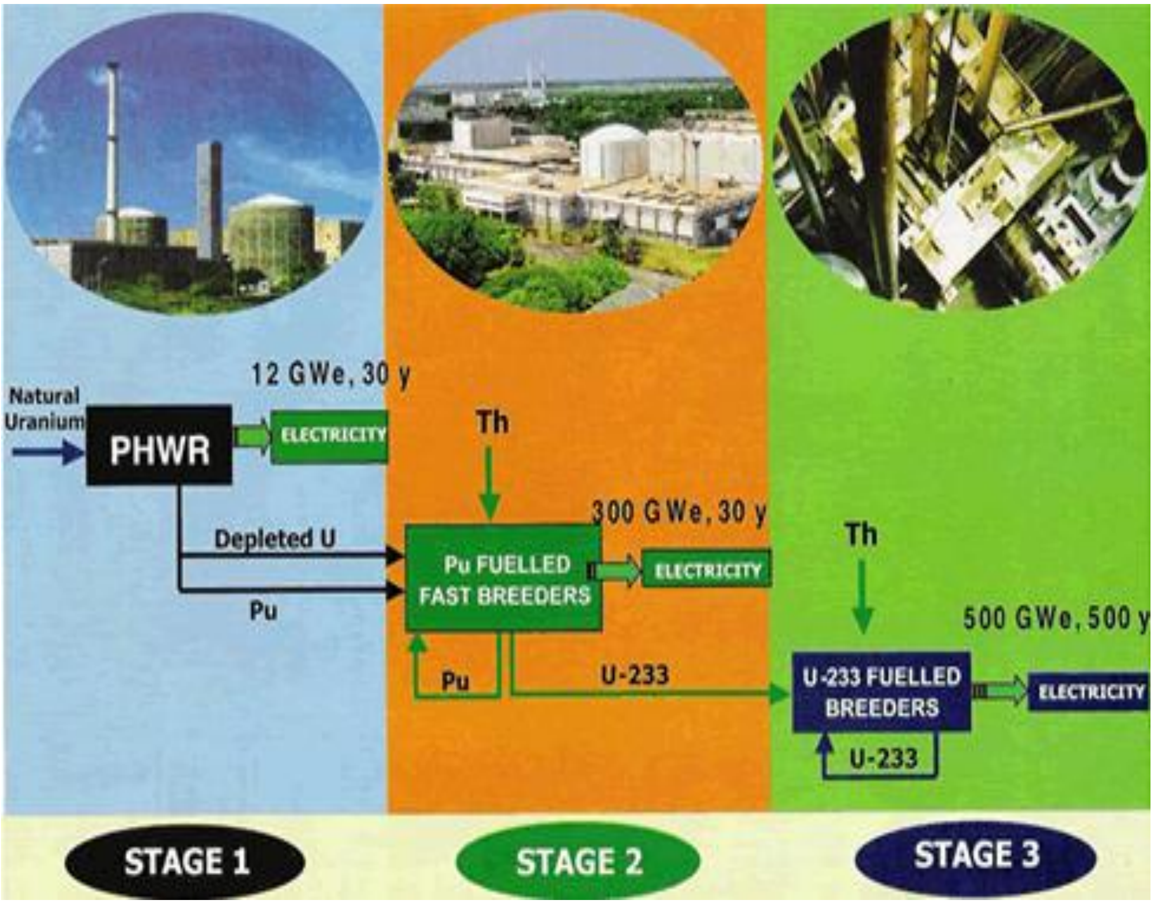

Fig. 1.1. The Three Stage Nuclear Programme in India

In the second stage, the ^{239}Pu generated in the first stage is fed into a Fast Breeder Reactor (FBR) together with the unused ^{238}U from the first stage. The nuclear fission reaction in the breeder reactor uses ^{239}Pu for energy and converts ^{238}U into ^{239}Pu, thus breeding its own fuel. Also FBRs more efficiently utilize ^{238}U compared to thermal reactors. Fast breeder reactors will use U-Pu combination in the fuel. They would enable a power generation capacity as high as 350 gigawatts (electric) [5]. The Fast Breeder Test Reactor (FBTR) at Kalpakkam uses a (U, Pu) carbide fuel whereas the next three power reactors including the Prototype Fast breeder Reactor (PFBR) which is at an advanced stage of construction will be based on (U, Pu) mixed oxide fuel.

The third stage involves another kind of breeding. The core of the FBRs will be loaded with blanket fuel pins containing ^{232}Th, another fertile material. During the operation of the FBR, it undergoes conversion to ^{233}U (another fissile isotope of uranium). The reactors of the third stage are thermal reactors using the fuel containing ^{232}Th and ^{233}U. The operation of the reactor produces more U^{233}. A 300-MW prototype the Advanced Heavy Water reactor (AHWR) was developed and is scheduled to be built in 2016. It is expected to start generating electricity by 2023 so that the available resources of thorium can be utilized efficiently [6].

1.3. Nuclear Fuels

Generally a reactor fuel, as was also discussed above, must comprise a fertile and a fissile material where the fissile material sustains the fission chain reaction producing energy and the fertile material absorbs neutron to produce the fissile material. The chemical forms of the fuel materials may be different, the choice of which would be based on the respective advantages and disadvantages. It can be generalized as follows: the nuclear fuel would be either uranium alone or along with plutonium in the form of metal or oxide or carbide or nitride. Natural Uranium oxide is used as the fuel in PHWRs. However, there is another type of thermal reactor in Tarapur, namely, Boiling Water Reactor (BWR) which uses Light Water as the moderator and the coolant. It uses enriched uranium oxide as the fuel. Instead of enriching uranium in ^{235}U isotope, a mixture of natural uranium and plutonium oxides can also be used as fuel in this reactor. As mentioned earlier, the FBTR at Kalpakkam, the forerunner for the second stage is using a unique uranium-plutonium mixed carbide fuel as the reactor and the first 500 MW commercial fast reactor, namely, the PFBR is based on a uranium-plutonium mixed oxide fuel. However, the future fast reactors of the next decade would be based on metallic fuel, an alloy of uranium, plutonium and zirconium. The metallic form offers several advantages in terms of thermal conductivity and has the highest potential for breeding. The fuel cycle to be discussed below and the reprocessing step of the fuel cycle will depend on the chemical form of the fuel.

1.4. Nuclear Fuel Cycle

A nuclear fuel cycle comprises the various processes involved in producing electricity by making use of nuclear materials and returning them to normal state. The complete set of processes to make nuclear fuel containing uranium for a thermal reactor from uranium ore is known as front end of the nuclear fuel cycle. The processes in the front end of the nuclear cycle are mining and milling, conversion, enrichment and fuel fabrication. During irradiation in a reactor, fission products and heavier actinides, like Np, Am and Cm (also known as minor actinides) are produced and the fuel removed from the reactor, known as the spent fuel, thus will contain U, Pu, fission products and Minor Actinides (MA). Separation of the valuable fuel materials, U and Pu from the fission products and MA in the spent fuel is known as reprocessing. The waste that is produced during reprocessing is highly radioactive and has to be disposed in a safe manner so as not to harm the environment. The reprocessing and waste management processes are known as the back end of the fuel cycle. The thermal reactor fuel cycle is shown in Fig. 2.

1.4.1. Fast Reactor Fuel Cycle

In a fast reactor fuel cycle, though the process steps are almost similar to that of a thermal reactor fuel cycle, some of the steps in the front end of fuel cycle are different. Since the feed for fast reactor fuel fabrication is depleted uranium (whose ^{235}U content is less than that of natural U) and plutonium from thermal reactor fuel cycle, there are no processing of ore and the associated steps. A fast reactor fuel cycle is shown in Fig. 3.

Fig. 1.2. Thermal reactor fuel cycle

Another significant difference between the above fuel cycle and the thermal reactor fuel cycle is the recovery of valuable fission products and minor actinides from the high level waste (HLW) produced during reprocessing. The main concern in the disposal of radioactive waste is related to long-lived radionuclides; some of them will remain hazardous for tens of thousands of years. By partitioning (chemical separation) and transmutation (radionuclide conversion), it is possible to reduce the long-lived components of the high level liquid waste.

Though lot of development work has been carried out worldwide on these partitioning process steps, it is not part of any currently practiced fuel cycle. In that sense, the above fuel cycle is somewhat futuristic. However, the above fuel cycle except the partitioning step is followed in Russia and France.

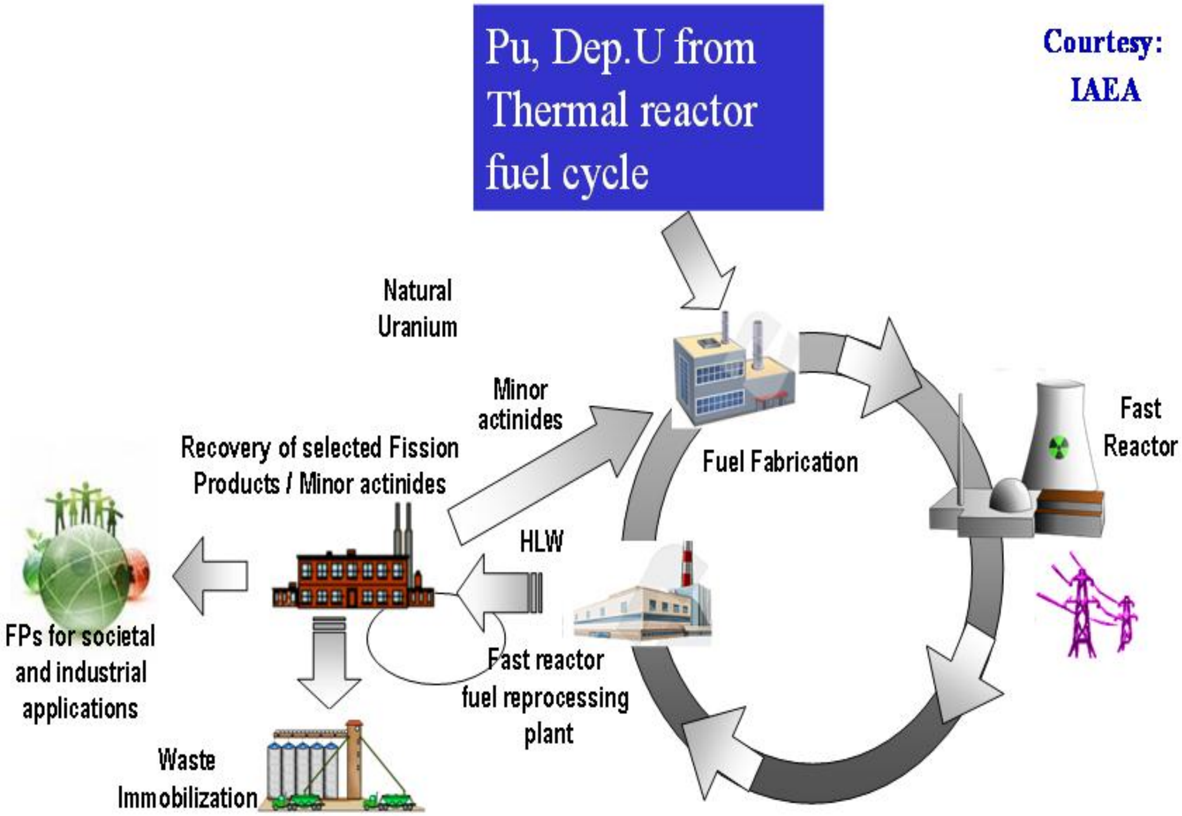

Fig. 1.3. Fast Reactor Fuel Cycle

1.5. Reprocessing of spent nuclear fuel

Nuclear fuel reprocessing forms the major step of the back end of the fuel cycle. As discussed above, it is aimed at the recovery of U and Pu from the other constituents of the spent fuel, namely, fission products and MA and reuses them for nuclear fuel fabrication. There are various reprocessing methods developed in the world. These can be broadly classified into (a) Aqueous Reprocessing Methods and (b) Non-Aqueous Reprocessing Methods.

1.5.1. Aqueous reprocessing methods

1.5.1.1. PUREX Process

Among the aqueous processes, the PUREX (Plutonium Uranium Extraction) process is the most widely used. The PUREX process was developed in the USA in late 1940s and was first used at US Atomic Energy Commission's Savannah River Site in 1954 [7]. The PUREX process has subsequently been used commercially by France at the LaHague plant of COGEMA [8], and is the basis for the recently operational THORP (Thermal Oxide Reprocessing Plant) plant at Sellafield in the U.K. [9], as well as the planned Rokkasho-mura plant in Japan [10].

It has been and is being used for reprocessing all the thermal reactor fuels in India and the carbide fuel from FBTR. It will also be used for the reprocessing of the oxide fuel from PFBR and future fast reactors.

In the PUREX process, tetravalent uranium and plutonium are separated from the spent fuel by dissolution of the fuel in nitric acid and solvent extraction using tri-n-butylphosphate (TBP), as the extractant in diluents like dodecane or paraffin. The trivalent americium and curium are not extracted by TBP. They remain in the raffinate together with the bulk of fission products, which is treated as the High Level Waste (HLW). Gaseous products like ^{85}Kr and ^{129}I are separated in the off-gas during the spent fuel dissolution. Separation of MA (Am and Cm) and some fission products, mainly Rare Earths(RE) from the HLW is achieved in the modified flow sheet known as the extended PUREX process

[11, 12] . For this separation there are three alternatives. One is based on the coextraction of trivalent MA and trivalent fission products. The other two are based on the selective extraction of MA from HLW either by oxidation of the trivalent and tetravalent MA to a higher oxidation state followed by an extraction process or using selective extractants to separate trivalent MA from trivalent RE. For the coextraction of MA and RE different processes are under development, viz. TRUEX, DIAMEX, DIPDA, TALSPEAK, and TRPO using different solvents.

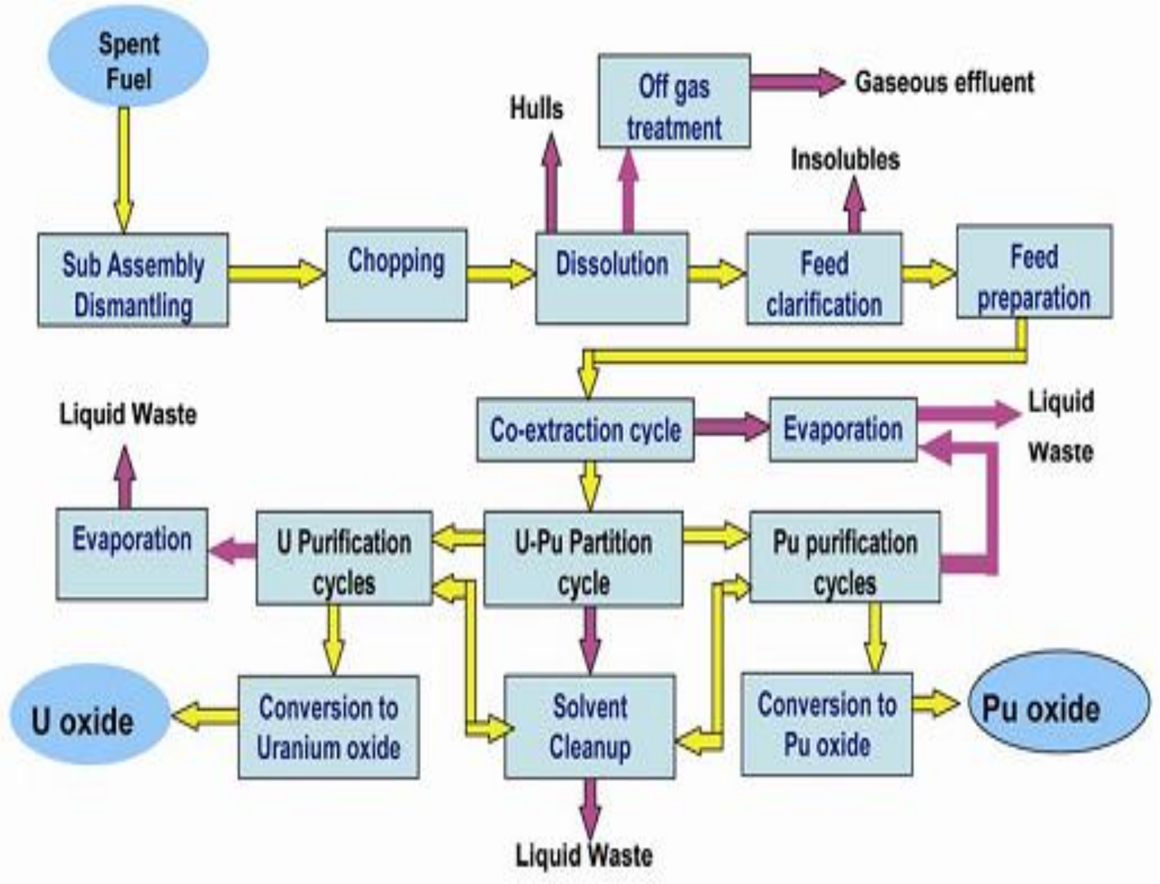

Fig. 1.4. Schematic of PUREX process flow sheet

The biggest advantage of the aqueous PUREX process is that it is well developed over the years and has been the workhorse of several reprocessing plants in various countries.

Further, being a process based on aqueous and organic solvents, it is amenable for continuous operation. It offers high decontamination factors of the order of 10^7 for the fission products which is a measure of the extent of separation of the fission products from the spent fuel resulting in large reduction of radioactivity. There are certain disadvantages too in this process. The presence of aqueous solvents makes criticality (uncontrolled chain reaction) based accidents a highly probable one. The organic solvents are susceptible to radiolytic degradation and hence this process will not be compatible with highly radioactive spent fuels as will be encountered with fuels cooled for short time. Also the waste produced is in the form of liquid whose volumes are very large. Another specific problem with respect to fast reactor fuel reprocessing is that the high concentrations of plutonium in the fast reactor fuel would lead to problems related to third phase formation, when the plutonium loaded in the organic phase exceeds a limiting value. Third phase formation refers to the splitting of the organic phase into two layers, leading to incomplete recovery of plutonium.

1.5.2. Non – aqueous reprocessing

Non-aqueous methods of fuel reprocessing exclude the use of both aqueous and organic media, and are based on the use of liquid metals and molten salts, usually at high temperatures. Non-aqueous methods are the potential alternatives to aqueous processing methods [13]. Some of the non-aqueous methods utilize the differences in the physical properties of the compounds of fuel materials, U and Pu and those of the fission products to achieve the separation. An example of such methods is the fluoride volatility process based on the differences in the vapor pressures of the fluorides. There are other methods that use the differences in the thermodynamic stabilities of the compounds of fission products and fuel materials. Examples are the melt refining process based on the differences in the stabilities of oxides and the molten salt electrorefining (to be discussed in detail later) based on that of chlorides. Of the various non-aqueous methods, those using oxidation reduction reactions rather than physical property differences are termed as pyrochemical processes. The prefix 'pyro' indicates the high temperatures involved in these processes. These methods are characterized by much lower separation factors (100 to 1000) compared to the aqueous reprocessing methods. Such lower separation factors are pose no problems for fast reactors, as they can accept higher levels of impurities in the fuel and hence possibly decrease the cost of reprocessing.

The advantages of non-aqueous reprocessing methods over the aqueous methods are:

1) Ability to reprocess spent fuels containing Minor Actinides (MA) and fuels cooled for shorter periods. As these fuels are highly radioactive, they would cause radiolytic degradation of the organic extractants in the aqueous process whereas the inorganic molten salts and alloys used in these processes are more radiation resistant.
2) In a given volume of the reaction vessel, more amount of fuel can be processed making the equipment and hence the plants more compact compared to aqueous based plants. It enables co-location of the reprocessing plants with the reactor itself, obviating the need for transport of spent fuel and refabricated fuel across long distances.
3) The waste produced is in solid form and hence the waste volumes are much lower.
4) In these processes, plutonium is never separated alone in the pure form. It is always accompanied by U and some amount of fission products (FP) and MA. Hence the processes have very high intrinsic proliferation resistance.

The above advantages are applicable for all the non-aqueous processes. The following advantages are more specifically offered by the molten salt electrorefining process which is relevant for this study:

i). The number of process steps are less compared to aqueous process, when reprocessing of metallic fuels are considered, as U and Pu are maintained in the metallic state throughout the process. In the aqueous PUREX process, the end product is oxide and process steps are needed to convert it to metal.

ii). The MA, unlike in the aqueous process, accompany Pu to the refabricated fuel and they cannot be separated. This aspect known as the Actinide Recycle Potential reduces the waste management problems, as it reduces the radiotoxicity of the HLW.

There are also disadvantages of the non-aqueous methods:

1) The high process temperatures along with the corrosive molten halide salts used in these processes enhance the corrosion potential of the processes, requiring selection of compatible materials a pre-requisite.
2) Since the molten salts are hygroscopic and the actinide metals are pyrophoric in nature, these processes need high purity inert atmosphere with extremely low levels of moisture and oxygen.
3) Aqueous reprocessing methods enable very high throughputs and sufficient industrial maturity to handle large volumes of discharged fuels whereas the non-aqueous processes are not yet developed in industrial scale.
4) Reprocessing involves operation inside hot cells which are remotely operated. The PUREX process involving organic and aqueous solvents in liquid form is amenable for

remotization and automation whereas the adaptation of non-aqueous processes involving solids to remotization requires development work.

5) These processes are batch processes which make them less competitive economically compared to the PUREX process.

Three non-aqueous methods that are currently receiving the major focus of attention in different countries [14–17]. They are:

a) The oxide electrowinning method for oxide fuels (originally developed by the Russian Institute of Atomic Reactors (RIAR), Russian Federation)
b) The fluoride volatility process of oxide and metallic fuels (developed by France, the Russian Federation, Japan and the USA)
c) The molten salt electro-refining method for metallic fuels (originally developed by the Argonne National Laboratory (ANL), USA)

1.5.2.1. Oxide electrowinning method

Oxide electrowinning method was developed to recover uranium and plutonium mixed oxides from the spent mixed oxide (MOX) fuel by MOX co-deposition process [18]. Fig. 5 shows the process flow sheet of the Oxide Electrowinning method. The process involves five main steps. Those are:

1. Chlorination of the fuel in the presence of molten NaCl–KCl or NaCl–CsCl to ensure complete dissolution of the fuel components in the salt.

2. Electrolysis to deposit part of UO_2 on a cathode free from Pu. Some noble metals FPs (Zr, Nb, Ru, Rh, Pd, and Ag) are also deposited on the cathode along with UO_2.

3. Co-deposition of bulk of UO_2 and PuO_2 on a cathode which are free from fission products (FPs).

4. Additional electrolysis to deposit the remaining UO_2 and PuO_2

5. Phosphate precipitation: This operation is carried out by introducing sodium phosphate into the melt. As a result, the impurities mainly RE, precipitate from the electrolyte salt, in the form of their respective phosphates which are insoluble in molten chlorides as well as in water.

In this process, a mixture of oxygen and chlorine gases is used as the flowing gas and its composition and the flow rate were important parameters for reducing bottom precipitation of PuO_2 during electrolysis in the process steps 2 and 3. If the oxygen concentration is more, PuO_2 will be precipitated.

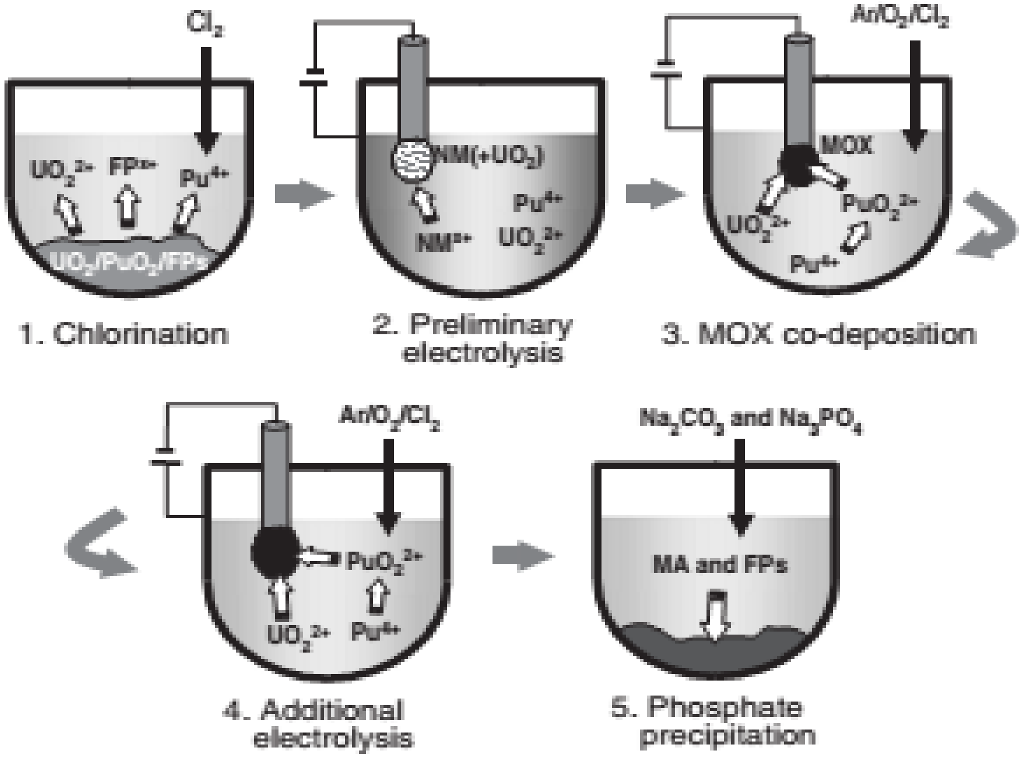

Fig. 1.5. Process flow sheet of the oxide electrowinning process

1.5.2.2. Fluoride volatility process

The fluoride volatility process is based on the differences in the volatilities of fluorides as well as in their absorption characteristics by the fluorides of alkaline and alkaline earth metals. The process was developed in the early 1960's in the USA [19] and the former Soviet Union [20]. In this process, the oxide fuels are oxidized to U_3O_8 and charged to a fluidized bed of alumina through which a fluorinating gas such as F_2, ClF_3 or BrF_5 is passed. Of the fluorides of the fuel materials U, and Pu and those of the fission products, UF_6 and PuF_6 are separated from the less volatile fission product fluorides and are absorbed in the alkaline earth fluorides. Before the adsorption process of the volatiles in the alkaline earth fluorides, the solid waste is separated from the volatile fractions. Then UF_6 and PuF_6 are converted to UO_2 and PuO_2. Schematic of the process is presented in Fig. 6 [21].

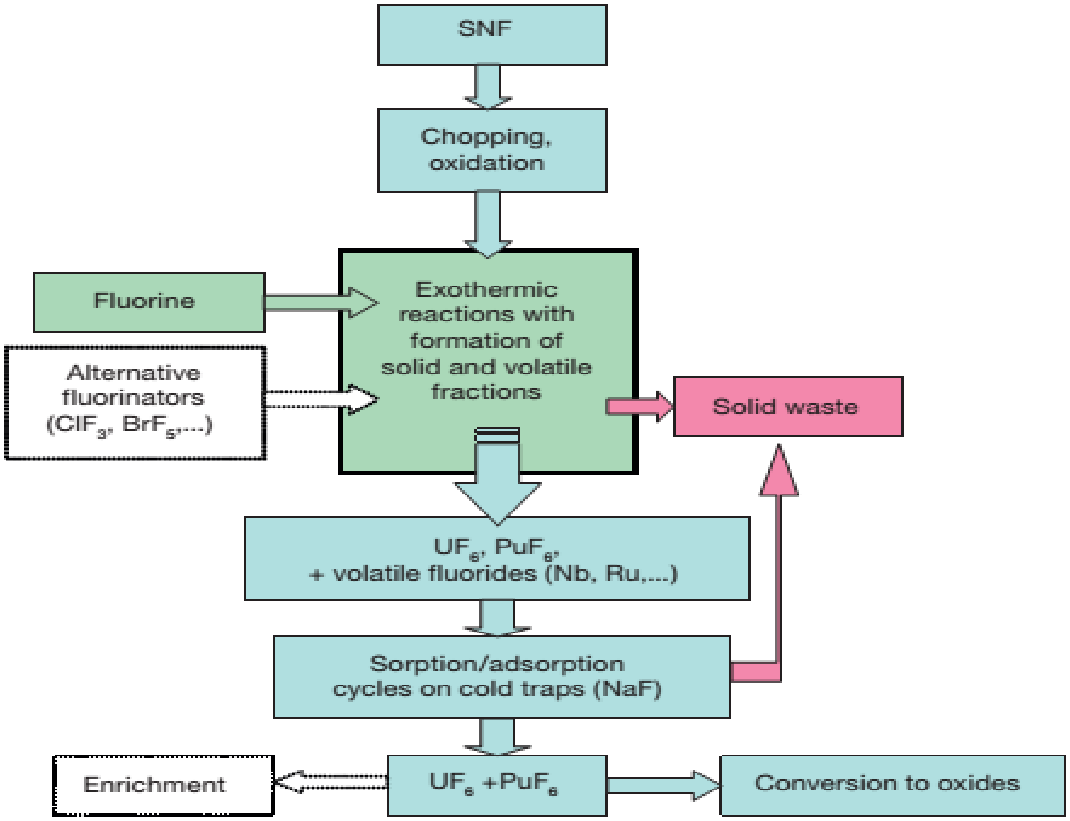

Fig. 1.6. Schematic flow sheet for the fluoride volatility process

1.5.2.3. Molten salt electro-refining process

The molten salt electrorefining process is being studied in our Institute in India, the Korean Atomic Energy Research Institute of Republic of Korea and the Institute of Trans Uranium (ITU) Elements, Karlsruhe. Compared to the other two methods discussed above, the molten salt electrorefining process being the relevant process for the present study, it will be discussed in detail further:

The molten salt electrorefining process was developed as part of the Integral Fast Reactor (IFR) programme in the USA. The IFR fuel cycle is based on reprocessing of its spent U–Pu–Zr alloy fuel using this electro-refining process. The schematic diagram of an electrorefining cell is shown in Fig.7. This process flow sheet involves the following steps:

a) Chopping of fuel pins containing spent fuel into pieces and loading into a basket and making the basket as the anode of the electro-refining cell

b) Addition of $CdCl_2$ to the electro-refining cell, operated at a temperature of 773 K, to transfer most of the actinides, sodium and FPs as chlorides to the electrolyte (eutectic mixture of KC1 and LiCl)

c) Deposition of uranium metal as dendrites on a solid cathode (dendritic deposit)

d) Introduction of a liquid cadmium cathode in the cell as the pre-determined concentration of Pu is reached in the electrolyte to deposit Pu and the remaining actinides, including an approximately equal amount of uranium on the liquid cadmium cathode.

As was mentioned earlier, the molten salt electrorefining process is based on the thermodynamic stabilities of the chlorides of fuel materials and fission products. When electrorefining is carried out, the alkali, alkaline earth and rare earth elements, whose chlorides are highly stable, readily go to the molten salt electrolyte and remain there. They are not easily reduced. The noble metal fission products, namely, Pd, Pt etc. whose chlorides are the least stable do not get oxidized at the potentials applied for electrorefining; so they remain in the anode itself along with the cladding components, Fe, Cr, Ni etc. whose chlorides are also less stable. The fuel materials, U, Pu, MAs whose chlorides are of intermediate stability get oxidized, go to the electrolyte as chlorides and get reduced to be deposited as metals on the solid cathode and liquid cadmium cathode. Zr which is also a fuel component remains in the anode.

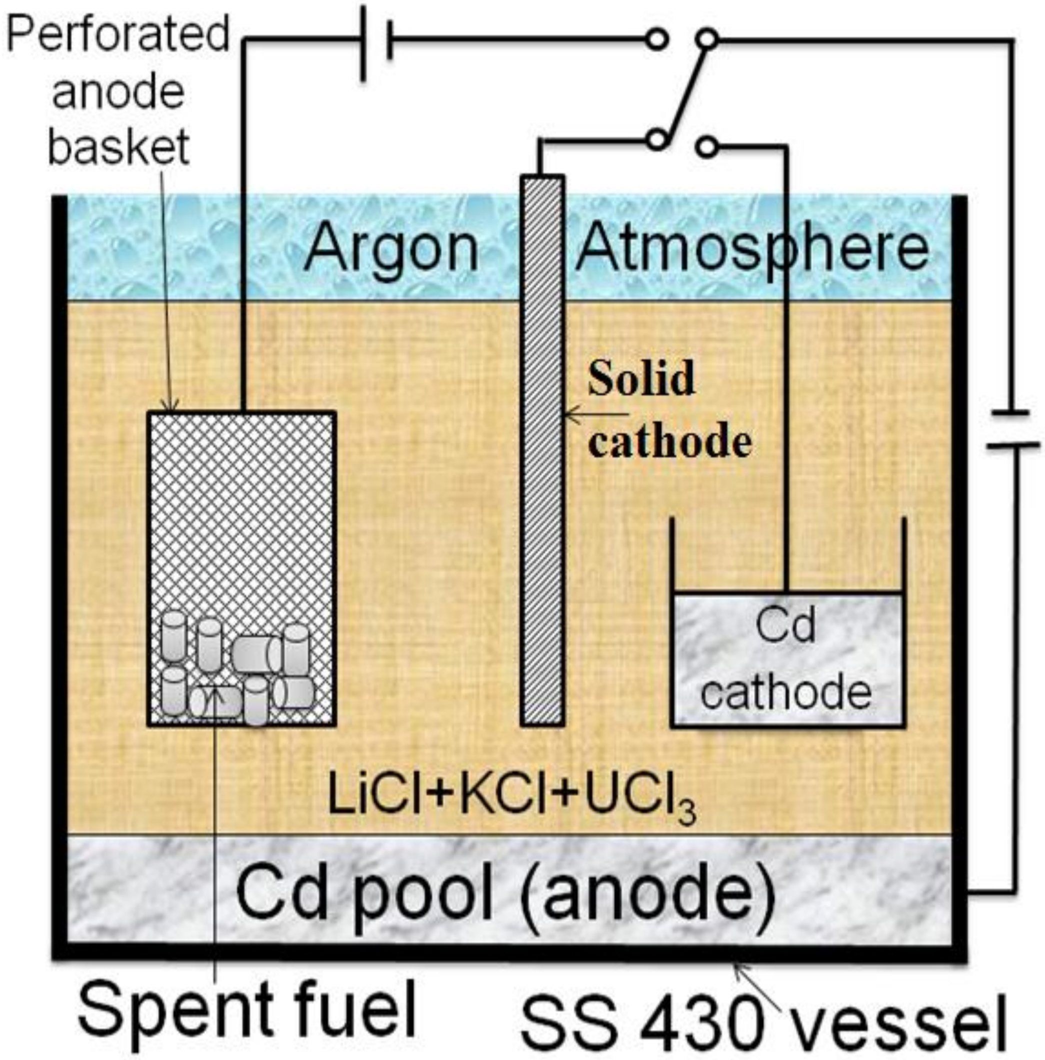

Fig. 1.7. Schematic diagram of the electrorefining cell

A cylindrical rod of low carbon steel (zirconium, molybdenum or uranium may be used) is used as the cathode for the selective deposition of uranium. The higher thermodynamic stability of $PuCl_3$ compared to UCl_3 makes the deposition of plutonium on the solid cathode impossible, unless the $PuCl_3$ to UCl_3 ratio is >2 which is not realizable under normal process conditions. However, co-deposition of uranium and plutonium on the liquid cadmium cathode is enabled by the lower activity coefficient of plutonium in cadmium compared to that of uranium. The activity coefficient being lower for Pu indicates that Pu will be more stabilized in Cd than U due to intermetallic compound formation in the case of Pu.

The cathode deposits are removed from the electrorefining cell after the process is completed. The dendritic deposit of uranium on the solid cathode is covered with salt from the electrolyte and it is separated from the salt by distilling off the salt in the process step known as the ‘cathode processing step’. Similarly, U and TRU elements deposited on the liquid cadmium cathode are separated from cadmium through distillation. Then the residual U (in the case of solid cathode) and U, Pu, MA in the case of liquid cadmium cathode are melted to form ingots. Ingots of U and U-Pu-MA alloy ingots are used for the fabrication of fuel elements by using the injection casting process [21].

A major fraction of the salt as well as Cd are recycled back into the electrorefiner, leaving only a small fraction in the waste [22]. The molten salt electro-refining process generates two waste streams: a salt stream that does not contain TRU elements and a stream of metals containing TRU element traces. The metal waste originates from the anode and it contains the noble metals including Zr, cladding hulls and traces of TRU. Accordingly, two waste forms are produced, namely a ceramic waste form and a metal waste form. The process flow sheet of the process is presented in Fig. 8. Although the molten salt electro-refining process was developed for treating spent metallic fuels, it can be used for the reprocessing of spent nitride or carbide fuels as well. Since nitride or carbide fuels have high electrical conductivity, they could be used as the anode of an electro-refining cell, and U and Pu metals from the spent fuel can be deposited on the cathode during the process. Studies carried out in Japan have also shown that in situ nitriding in liquid cadmium used as a cathode is possible.

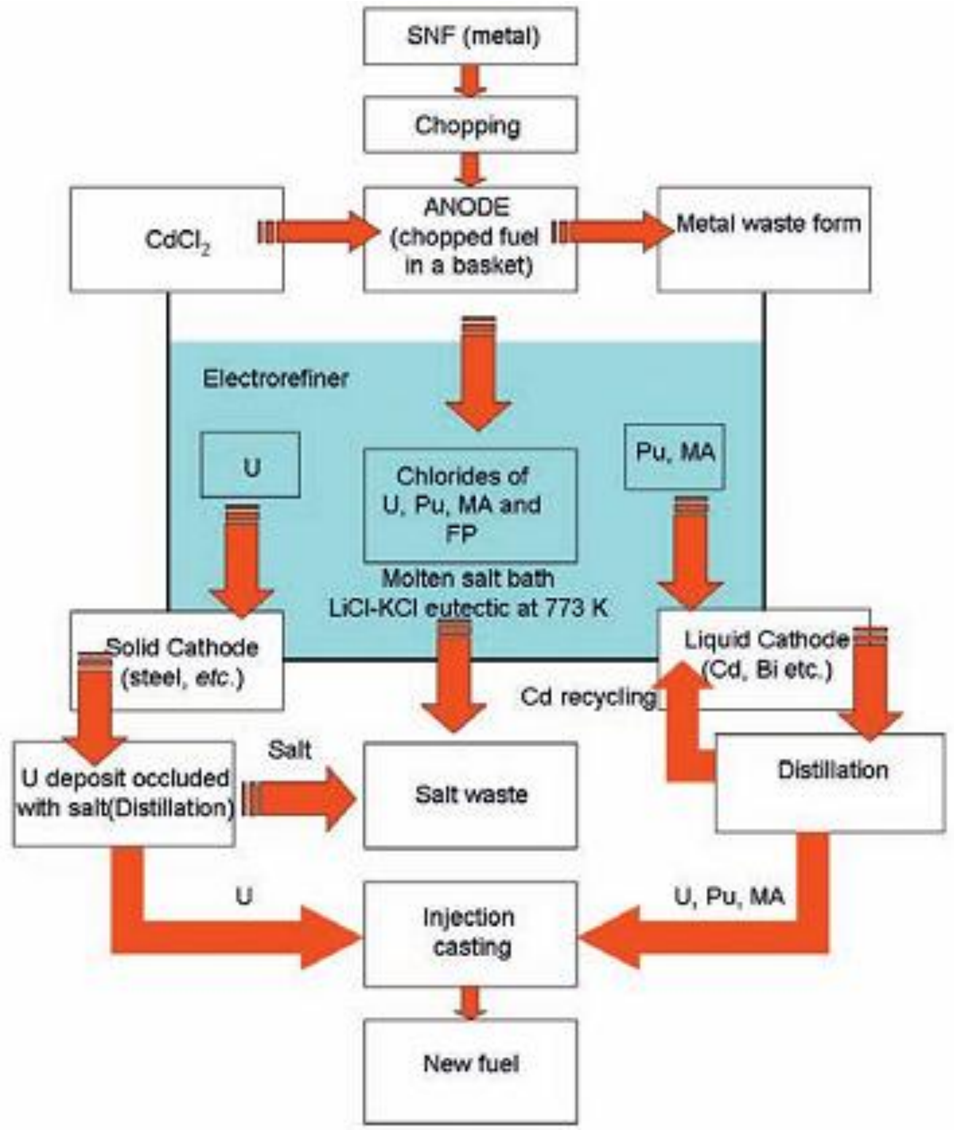

Fig. 1.8. Flow sheet of the molten salt electrorefining process

1.6. Reprocessing of the metallic fuel and the Indian perspective

As was discussed in 1.3, the future fast reactors of India will be based on metallic fuel. The choice of metallic fuel is based on the highest breeding ratios offered by the metallic fuels. The metallic fuels were developed for the fast reactor programme in the USA. U-19Pu-10Zr was used as the reference fuel in the Integrated Fast Rector Programme pursued by Argonne National Laboratory, USA [23-26].

Indian metal fuelled reactors will also be based on U-Pu-Zr alloy fuels. As discussed above in the sections on non-aqueous reprocessing methods, molten salt electrorefining method is ideally suited for reprocessing of metallic fuels. However, limited experience exists worldwide with this process.

Hence development of the molten salt electrorefining process technology is being pursued in Indira Gandhi Centre for Atomic Research (IGCAR), Kalpakkam. Laboratory scale studies on electrorefining and the associated processes have been initiated in the nineties and studies have been carried out on U, U-Ce-Pd and U-Pu-Zr alloys [27 - 29]. Studies on U and U-Zr alloys have also been carried out at 1 kg scale in an engineering scale demonstration facility [30].

Electrochemical studies on the reduction behavior of the various ions have been carried out using transient electrochemical techniques [31, 32]. In parallel, thermochemical and eletrokinetic modeling of the electrorefining process have been carried out [33-35]. Further development work is needed to scale up the process for applying it at industrial scale. Hence, as a part of these development efforts, in this study, modeling the electrorefiner and validation of the model using experimental investigations has been carried out.

1.7. Literature review of the experimental and modeling approaches on the molten salt electrorefining process

Several researchers investigated the electrorefining of spent metal fuel by various approaches, namely, experimental, thermochemical modeling and electrokinetic modeling. Some investigators have developed their own code whereas some have used commercial packages. The summary of a survey of the literature on these approaches is discussed in this section.

Miller et al. [36] studied that the deposited uranium and plutonium together at a liquid cathode, after the $PuC1_3$ to UCl_3 ratio in the electrolyte salt was greater than 2:l. They also performed the electrorefining of spent nuclear fuel using a hollow cathode and a solid anode so that the anode is nearer to the cathode, resulting in higher transport of uranium/plutonium. Lee et al. performed the electrorefining experiments with an anode composed of U, Y, Gd, Nd and Ce in the KCl–LiCl and LiF–NaF–KF (FLINAK) eutectic melts at 500 and 600˚C, respectively. Uranium was the major component in the cathode deposits, and the separation factors of the uranium with respect to the rare earths (RE) were nearly the same in both electrolytes. The concentrations of REs in the molten salts as well as cathode deposits increased sharply at above 1.9 V, which is the decomposition potential of the REs. The cathode current efficiencies rapidly decreased as the applied potential increased, and the highest separation factor was achieved at −1.5 V, which is little higher value than the reduction potential of the uranium [37].

The pyrochemical reprocessing flow sheet of spent nuclear fuel was developed based on electrorefining in molten LiCl-KCl salt using aluminium solid cathode [38]. Choice of aluminium as the cathode stems from the higher separation factors achievable for the REs with respect to U and Pu. After the deposition process, the actinides were recovered from the deposited actinide-aluminium alloy by chlorination process.

KAERI developed a novel electrorefiner with 24 graphite cathodes, a rotating mesh type anode basket consisting of 4 cartridges and a bucket-type deposit retriever to increase the throughput of an electrorefiner in the electrorefining process [39]. A rotating scraper was used to scrap the dendritic uranium deposit and put it in the bucket.

Many laboratory scale studies have been carried out in various laboratories. However, design optimization of electrorefiners (ERs) is required to reach high uranium throughput that improves economic competitiveness and reduces environmental impact [40 - 44]. It is important to understand electrochemical phenomena in order to design an electrorefiner (ER) system suitable for pyroprocessing, particularly one equipped with complicated electrodes. Computer simulation of the electrochemical cells is an effective tool for the visualization of processing parameters such as the potential distribution, current density, and concentration profile and for the optimization of the electrorefining process.

Several researchers have reported numerical methods for simulating the electrorefining process of spent nuclear fuel. Initially the models were relatively simple, and were based primarily on the concepts of thermodynamics and diffusion. Gradually models have become more sophisticated to handle many other phenomena. A number of models have been developed in order to calculate and to maintain track of the material balance in electrochemical processing. The capability to calculate the process outcome using modeling saves time and energy. While there are several computer codes developed to predict the behavior of ER, each is unique in its own way. While some of the new modeling approaches in 2D or 3D are useful to describe the details of the process by combining effects of fluid flow and electrochemistry, they are either computationally burdensome or specific to a given design. Most of the less computationally intensive models have issues such as modeling capability. In recent years, focus has shifted to account for phenomena in a more integrated fashion, including the effects of fluid flow. Many of the recent models rely on CFD and FEM. One hallmark of these simulations is the long computation time required for their completion. Most are constructed by including some set of electrochemistry relations in a CFD analysis. However, there are many levels of detail which can still be included in a 3D model, and there is more work to be done in this area.

Johnson at Argonne National Lab (ANL) [45] developed a model based on chemical equilibrium to predict the electrorefiner behavior. In 1991, ANL developed PYRO, one of the first computer models for a uranium electrorefiner. It also relied solely upon thermodynamic considerations for predictions. Despite its simplicity, it helped to optimize ANL's electrorefiner operations [46]. A simulation code named TRAIL [47] was developed by CRIEPI (Central Research Institute of Electric Power Industry) in Japan, based on thermodynamics and steady state diffusion for the molten salt electrorefining process of spent metallic nuclear fuel from the IFR. Diffusion layer thickness was calculated from the polarization experiments. The optimized values for the diffusion layer thickness at the solid cathode and liquid cadmium anode were both equal to 0.002 cm and that at liquid cadmium cathode was 0.003 cm. The TRAIL code was validated with the experimental data of Tomczuk et al [48]. These authors performed electrorefining with dual cathodes; a solid cathode at the intial stages of electrorefining and a cadmium cathode later. The deposition on the Cd cathode can be controlled by adjusting the timing of switching of the cathode in the dual cathode operation.

Shortly after, DEVON [49] code was developed as an extension to TRAIL and it includes the effects of the electrolyte resistance on electrodes that are not on equipotential surfaces. In this upgrade, the electrodes are modeled in two dimensions in order to show more detail. The results compared very well with the measured cell potentials, but the model did not account for activation overpotential. This means that the predicted potential distributions are slightly skewed. Nonetheless, it appears to be a useful code, when the assumptions are met. Diffusive mass transfer often limits the reaction rate in electrochemical systems. In particular, diffusion affects the concentration at the electrode surface. At the electrode surfaces, a thin laminar fluid layer is formed (within 2 mm to 1 mm of the surface). The only way that material can cross this boundary is via diffusion and electromigration. This is because the flow is parallel to the electrode, and there is no turbulence.

A numerically simulated thermochemical model was developed by Nawada and Bhat [50] for the electrotransport of U and Pu in a molten salt electrorefiner and like the Johnson's model [Johnson 1988] this model also depends on Gibbs energies of formation of the chlorides of fuel materials and fission products and the equilibrium constants. But it does not depend upon the electrochemical properties such as standard potential. An electrorefiner with liquid cadmium anode and liquid cadmium cathode was envisaged. 16 conditions of electrorefiner cell operation were categorized, based on the saturation condition of the electrodes with respect to U and / or Pu. Electrotransport was simulated for all the realistic conditions. Using algebraic equations, the variation of concentrations of U and Pu in the salt phase and the two electrodes (LCA and LCC) were computed for each condition of anode and cathode with respect to saturation.

Ahluwalia and Hua [51, 52] developed a computer code named General Purpose Electrochemical Simulator (GPEC) to determine the partial currents carried by Zr and Cd upon oxidation at the liquid anode and the extent to which they are reduced at the cathode and time dependent curves for different electrorefiner operations. It considers both Butler–Volmer kinetics and steady state diffusion. Iizuka et al. modeled electrorefining with the U–Pu–Zr ternary alloy anode based on the one-dimensional diffusion layer of CRIEPI/ITU electrorefining studies [47], and this model was validated with the experimental results. In this study, they explained about the presence of another diffusion barrier, called the passive layer, near the anode, which is rich in Zr [53]. They assumed that this passive layer is highly viscous at the temperature of the experiment and that the diffusion coefficients of the ions in this layer are lower due to the increase in viscosity. They proposed that it is necessary to determine the solubilities and diffusion coefficients of uranium, plutonium and zirconium in the diffusion layer containing zirconium metal residue for more accurate calculations [54].

A numerical model for a high-throughput electrorefiner was developed [55, 56] for spent metallic nuclear fuel by using a commercial, computational fluid dynamics code, ANSYS CFX. A graphite cathode bundle was designed to recover a high-purity uranium product continuously without noble metal contamination. The dependence of the morphology of the uranium dendrite on the molten salt flow, the mixing behavior of the molten salt and collection behavior were evaluated by varying the process parameters such as the rotation speeds of the stirrer and the anode basket and also the effects of the void fraction of the anode basket. The results show that the rotation speeds of the anode basket and the central screw agitator were the main parameters in determining homogeneous mixing of the molten salt. The fine uranium dendrite tended to be affected by the molten-salt flow. The distributions of the electric field and the electrodeposition behavior were also evaluated numerically, and an optimum electrode configuration was suggested.

A three-dimensional analysis of an electrorefiner based on momentum and mass transfer was carried out by using the ANSYS®CFX-11.0 code [57]. In this model both the anode and cathode were rotating at 100 and 50 rpm respectively. Diffusion boundary layers were obtained from the concentration profiles by using the calculated fluid dynamic contours. The electrochemical reaction within the diffusion boundary layer was calculated by using a one-dimensional analysis model (REFIN). A three-dimensional multispecies and multi-reaction modeling approach [58] was developed for electrorefining to treat spent nuclear fuel. Electro-fluid-dynamic behavior is analyzed by the coupling of one-dimensional electrochemical reaction analysis code and three dimensional CFD code. The current density distribution patterns were analyzed for various electrode rotational speeds and diverse applied currents. They computed the local concentration distribution and local multispecies current density distribution. Bae et al. developed a code based on the commercial computational fluid dynamics code, ANSYS CFX-10.0 for a three-dimensional analysis of diffusion boundary layer and deposition rate, in combination with the one-dimensional electrochemical analysis model, REFIN in PEACER for the lead bismuth cooled fast reactor fuel cycle [59]. Simulation results are used to estimate overall decontamination factor of PEACER pyrochemical process. The spent fuel from the lead bismuth cooled fast reactor, PEACER also called as heavy liquid metal reactor transmutation by pyroprocessing techniques and actinides and long living fission products sent for fuel fabrication and short living low level sent to land disposal [60]. Hoover et al. developed a model based on the Butler-Volmer equation to study the kinetics of the electrorefining system [61].

A 3D electrorefining model was developed to calculate the cell potential changes with five differently assumed real anode surface area cases and the results were compared with experimental results [62]. A 2D electrorefining model was also developed to indentify the uncertainty factors in material properties, heterogeneous material distribution, surface roughness, and current efficiency. They also found that the anode materials would be dissolved both in the axial and radial directions at least for low burn-up metallic fuels after active liquid sodium bonding was dissolved.

Kim et al [63] successfully simulated the electrodeposition behavior of uranium using the COMSOL Multiphysics electrodeposition modules, which are part of a commercial program for Multiphysics. The electrochemical parameters considered in this study are the exchange current density distribution and electrode arrangement. The application of a numerical model to design an electrorefiner for spent metallic nuclear fuel is discussed with respect to throughput, impurity contamination and operating mode. Tertiary current density distribution module was applied and the calculated results were validated with experimental data. ERAD (Enhanced REFIN with Anodic Dissolution) is another general ER model that can be applied to various ER configurations by adjusting various geometric parameters such as electrode areas and diffusion boundary layer thicknesses [64, 65]. ERAD was developed by modifying REFIN in a number of ways. A model was added to describe the dissolution of spent fuel from a solid anode.

Zhang developed a kinetic model based on the diffusion control assumption. The model has the capability to predict the kinetic features of materials dissolution/deposition at anodes/cathodes of the electrorefiner and the evolution of the partial currents of the species involved, the potentials of the electrodes, and the concentrations of the species in the molten salt. The model was validated by comparing with available experimental data [48]. This model does not consider the materials diffusion and nucleation effects at the solid electrode surface. The model also does not address the formation of rare earth element-cadmium compounds and the rare earth contaminations to the actinide metal product [66].

1.8. Scope of the thesis

As was mentioned above, as a part of the efforts towards development of pyrochemical reprocessing for spent metal fuels from the future fast reactors, two models have been developed in our Institute. One is thermochemical model, named, PRAGAMAN [33]. It is based on thermochemical equilibria among the species in the anode, cathode and the electrolyte salt as the model of Johnson [45] and Nawada [50]. It also depends on the conditions that exist in the anode and cathode regarding the saturation conditions with respect to U and/or plutonium. However, PRAGAMAN can handle electrorefining with solid anode and any type of cathode whereas the other two models are used with liquid cadmium anode only. The second model developed in our Institute, named, DIFAC, is an electrokinetic model based on diffusion layer theory. [29].

These models are independent of the size of the electrorefiner. When the scaling up of the process is desired, developing a model that could take into account the size of the electrorefiner, the configuration, the number and the arrangement of the electrodes etc. to compute the process throughput will be more useful than the existing models. Further, even though, as the literature review above shows, a number of investigators have developed models, they are not available for other institutes and hence each country needs to develop its own model or code. Hence with a view to developing such a model, research work was taken up which forms the basis of this thesis.

This study focused on computer simulation of the processes that takes place in the electrorefiner and validation of the computer simulation model with experimental results carried out at laboratory scale. Also the effect of electrode configurations on the potential and current distribution in a molten salt electrorefiner was modeled which was also validated with laboratory scale experiments. Simulation of the electrochemical reactions at the electrode surfaces was based on the time dependent 2D axisymmetric COMSOL Multiphysics model [67]. The model was validated with experimental data. The model was used to determine the mass of uranium deposited at solid cathode and the variation of uranium and plutonium concentrations in the molten salt and liquid cadmium anode. In addition, the operation time for the electrochemical process was estimated using the COMSOL model, based on the operational and geometrical parameters of the electrorefiner.

The electrochemistry module, the chemical species transport module and the mathematics module of the COMSOL Multiphysics package are used for this simulation. The secondary current distribution (siec) of electrochemistry module is used for simulating electrochemical reactions and the potential and current distribution in the electrochemical cell. Transport of diluted species (tds) of chemical species transport module is used for simulation of mass transfer of each species through the diffusion layer and the general form of ODE (g) in ODE interfaces of mathematical module is used for solving the material balance equation for each species. The three modules are coupled to each other and solved simultaneously.

One of the important key factors in the design of molten salt electrorefiner is the potential and current distribution analysis which was determined by experimental studies at lab scale and also modeling using COMSOL Multiphysics.

The effect of the arrangement of electrodes and the distance between the electrodes were analyzed in which solid Uranium rod acts as anode and SS430 solid rod acts as cathode. The solid cathode used in the electrorefiner is attached with an insulating disc at the bottom to avoid the electrode deposition occurring at the bottom of the cathode which could fall into the electrorefiner. The effect of solid cathode with and without insulation was also studied.

The effect of the liquid Cd cathode positioned at different elevations in the electrorefiner and that of the surface area of the solid cathode were also analyzed for an electrorefiner in which liquid Cd cathode acts as anode. The sensitivity analysis of the parameters was performed.

Computer based simulations of the electrochemical separation of the U and Pu and effect of electrode configurations concept presented in this study have provided the parameters for a large scale electrorefiner which could be used in the design of a large scale electrorefiner.

Electrochemical processing of spent nuclear fuel plays an important role in the development of the next generation fast reactors and also the technologies that will close the nuclear fuel cycle. This study thus gives important data for such a development.

Chapter 2

Materials, Experimental methods and modeling techniques, equipments and facilities

2.1. Introduction

In this chapter, the experimental methods employed and details of modeling used in the present work are discussed. The chemicals used in the experiment and its preparation procedures are also discussed here.

2.2. Chemicals and its purification

The chemicals mainly used for the electrochemical studies on high temperature molten salts were anhydrous LiCl (≥ 99 % from M/s. Chempure private limited, Kolkata) and KCl (≥ 99% from M/s. Ranbaxy fine chemicals, India). The salts were free flowing, crystalline, white powders. The eutectic salt of the composition, 41 mol% KCl – 59 mol% of LiCl, was used as the electrolyte in the electrorefining process due to its relatively low melting temperature, (approximately 353^{o}C) as shown in the phase diagram, Fig 2.1. Due to the extremely hygroscopic nature of the LiCl and KCl salts, a purification step is necessary before the salt could be used as the electrolyte for the electrochemical reactions. Various standard purification methods are available for purification. A short account of various purification methods used here are described below. Besides being low melting, the eutectic electrolyte salt has other advantages such as good thermal stability, wide span of electrochemical window, absence of strongly acidic or basic properties, high conductivity and fluidity and commercial availability of its components as reagent grade salts. Further, the low melting point and its chemical reactivity is such that glass can be utilized as a material of construction. The only disadvantage is the high operating temperatures [68]. A summary of various properties of eutectic mixture of LiCl-KCl are shown in Table 2.1.

Table 2.1. Physical properties of LiCl-KCl eutectic salt

Parameter	**Value or equation**
$T_{melt,LiCl}$	610 ^oC
$T_{melt,KCl}$	770 ^oC
$T_{melt,LiCl\text{-}KCl}$	355 ^oC
Density, $\rho_{LiCl\text{-}KCl}$	$\rho(T) = 2.0286 - (5.267\times10^{-4})T$
Density, $\rho_{LiCl\text{-}KCl,\ 500^oC}$	1.62 g/cm^3

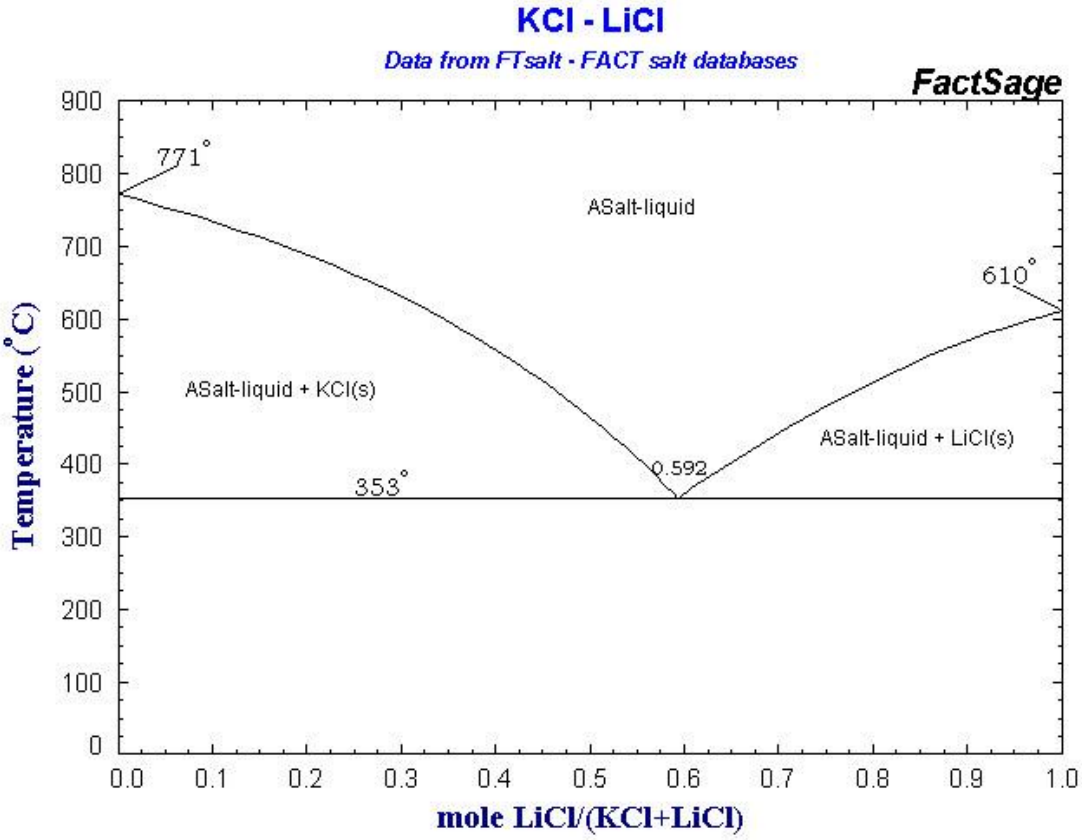

Fig. 2.1. Phase diagram of the LiCl-KCl

2.2.1. Vacuum drying

Vacuum drying is one of the purification methods generally employed for the salts. In this process, the LiCl and the KCl are dried separately by first slowly heating the salts to 150°C to 200°C under vacuum (less than 0.1 mbar) to remove moisture (major impurity content) and other easily volatile impurities. The material (LiCl or KCl) is placed in a suitable vessel and exposed to vacuum. A tilting vacuum oven made by M/s. Technico Company was used for drying the salts, a rotary vacuum pump, model no ED-6 of M/s. Vacuum Techniques, Bangalore was used for creating the vacuum of 0.1 mbar and a PIRANI gauge model-VT-AP-11 of the same firm was used for measuring the vacuum. The drying process continued for five days. The dried salt samples were taken at various time intervals for analyzing the moisture content.

2.2.2. Chlorination of LiCl-KCl eutectic salt

Chlorination is considered for the next stage of purification. In order to handle the highly corrosive and lethal chlorine gas, a separate experimental facility, which is compatible with chlorine gas, is required. The experimental facility is made of a leak tight quartz tube (OD-65 mm, length 500 mm) having a Teflon flange at the top to provide the inlet and outlet ports for chlorine gas. Then the vacuum dried reagent grade LiCl and KCl are taken in the proportion 0.59 mole to 0.41 moles and mixed together. A known quantity of the mixture of LiCl and KCl was taken in an alumina crucible (50 mm OD x 46 mm ID x 100 mm height, Naskar Ceramics, Kolkata, India) and placed inside the leak-tight quartz vessel. The chlorination set up used for the purification of the eutectic mixture of LiCl-KCl salt is shown in Fig. 2.2.

The closed quartz vessel was then positioned inside a nichrome resistance furnace (M/s. Bonics control systems, Chennai) and constant temperature was maintained with the help of a PID (Proportional Integral Derivative) temperature controller (M/s. THETA controller). The temperature of the salt was gradually and slowly increased from room temperature to a temperature which is ~50°C above the melting point of the salt taken. The heating operation is carried out in presence of UHP (Ultra High Pure) argon gas, at a heating rate of 3ºC/min, which facilitated the removal of free moisture as well as prevented the cracking of the alumina crucible. Pure dry chlorine gas (bubbled through H_2SO_4 drying column) was bubbled through the melt for about twenty minutes at a flow rate of 50 ml/min. The highly reactive chlorine gas converted all the hydroxides and oxy-chlorides in the melt, if any formed due to absorption of moisture, to the respective chlorides. The excess or unreacted chlorine gas in the melt was removed by bubbling UHP argon gas for about half an hour until complete disappearance of the yellow color (absence of chlorine) inside the vessel. The free chlorine gas from the outlet was killed by passing it through a series of gas bubblers (chlorine "killing" unit) containing 10% NaOH solution. In this chlorine absorber assembly, the free chlorine gas gets dissolved as chloride or oxy-chlorides in the NaOH solution. In the present study, chlorination of LiCl-KCl eutectic salt was carried out at a melt temperature of 400ºC (mp. of LiCl –KCl eutectic is 350ºC). Chlorination was carried out in small batches for our studies in which about 150 g of as-received LiCl-KCl salt was taken in an alumina crucible and the aforementioned procedure was followed. After cooling the cell, the quartz vessel containing the frozen salt in the alumina crucible was sealed under argon gas and immediately transferred into an argon atmosphere glove box facility. The chlorinated salt containing alumina crucible was retrieved and stored in the argon atmosphere glove box facility with a secondary sealed enclosure until further use. It was interestingly observed that after efficient chlorination, the frozen salt lump never stuck to the alumina crucible and the frozen salt was getting easily detached from the inner walls of the alumina crucible as a single lump.

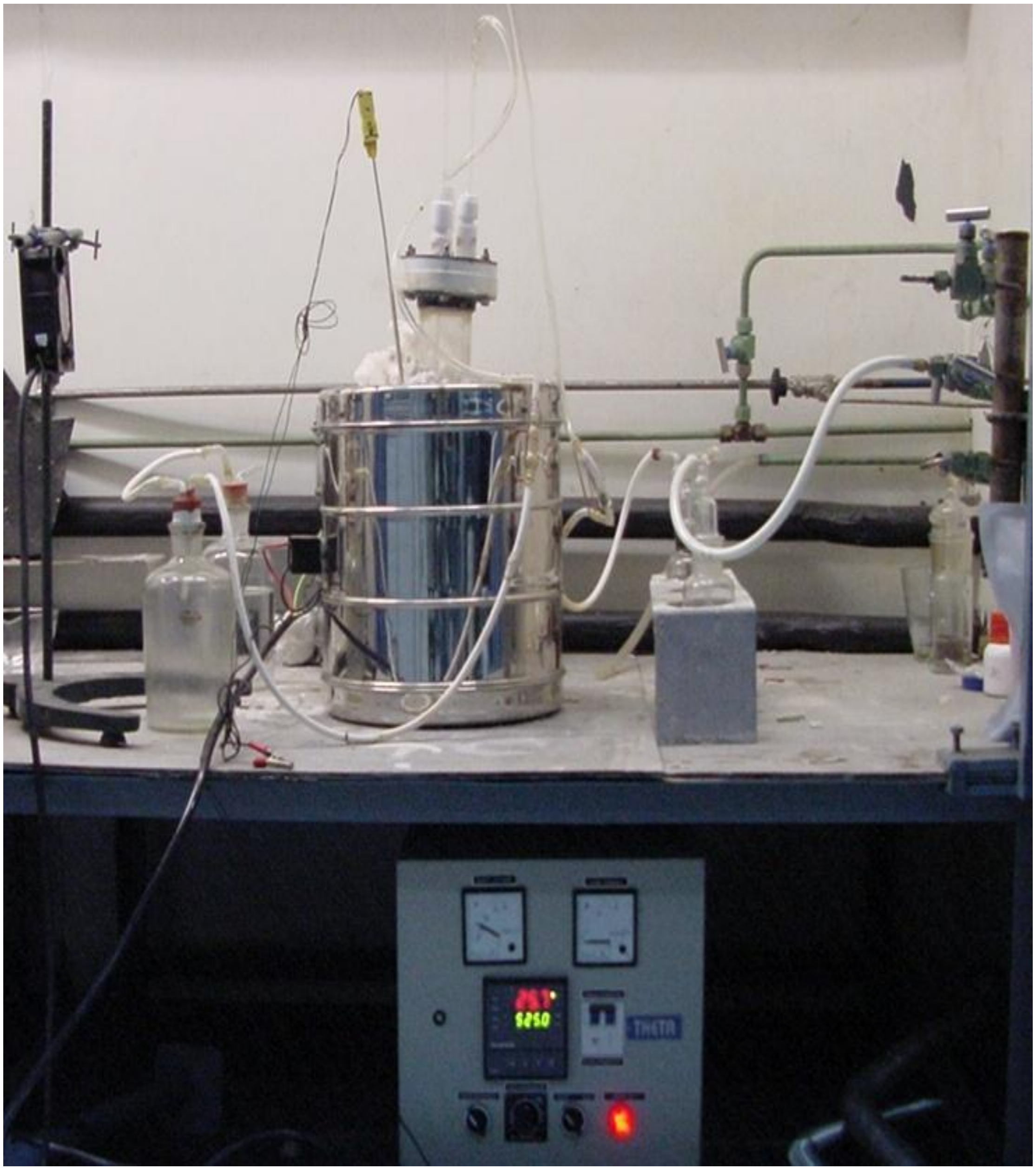

Fig. 2.2. The chlorination set up used for the purification of LiCl –KCl eutectic salt.

2.2.3. Preparation of the LiCl-KCl-UCl_3 electrolyte salt

A known quantity of chlorinated LiCl-KCl eutectic salt was loaded in an alumina crucible, the loaded alumina crucible was placed in a secondary SS crucible and the temperature was slowly increased up to 773 K. Stoichiometric amount of $CdCl_2$ (≥ 99% M/s. Merck, Mumbai) was added to the melt and equilibrated with excess of Uranium metal (from BARC, Mumbai) immersed in the melt in order to form UCl_3 according to the following chemical reaction [34, 69]. Here Uranium metal acts as excess reactant and $CdCl_2$ acts as limiting reactant.

$$2U + 3CdCl_2 \rightarrow 2UCl_3 + 3Cd \qquad (2.1)$$

After 24 to 36 h of operation, a sample of the salt was collected for analysis of the concentration of UCl_3 present in the LiCl-KCl eutectic salt. This process was followed to prepare LiCl-KCl salt containing the required concentration of UCl_3. The clear upper portion of the salt was carefully transferred to a separate SS / ceramic container leaving the unreacted uranium metal and byproduct Cd at the bottom of the alumina crucible. The LiCl-KCl-UCl_3 obtained here was deep dark purple in color as shown in Fig 2.3. The UCl_3 concentration in the sample salt was determined by Davies and Gray method to be 5.0 wt %. The preparation was performed in a glove box filled with a high purity Ar atmosphere (<10 ppm O_2 and <20 ppm H_2O by volume).

Fig. 2.3. Prepared LiCl-KCl-UCl_3 used as the electrolyte salt

2.2.4. Davies and Gray method

The Davies and Gray method is based on a destructive analysis method for quantitative determination of uranium in samples taken from virtually any point in the nuclear fuel cycle. It is widely used in nuclear safeguards for material accountability measurements. A weighed sample is subjected to the titrimetric analysis and the result is the amount of uranium contained in the sample, often reported as a percentage or mass content. Uranium in the aqueous solution which is normally in the VI state is first reduced to U (IV) by the addition of Fe (II) ions and the excess ions are destroyed by oxidation. The U (IV) is titrated against a standard solution of potassium dichromate to U (VI). The end point of the titration is determined through measurement of the electrode potential of the solution. The uranium content is calculated from the amount of dichromate used in the titration. The titration is carried out in phosphoric acid medium in the presence of molybdate ions, the latter acting as a catalyst for the oxidation of Fe (II) by nitric acid. The nitrite formed in the above reaction is removed by sulfamic acid. Vanadyl solution is then added to sharpen the endpoint and the U (IV) is titrated against a standard potassium dichromate solution using a combined platinum electrode.

2.3. Argon atmosphere glove box facility

An argon atmosphere glove box maintained at a positive pressure with respect to ambient pressure was used to handle the air sensitive materials. The LiCl-KCl salt and lanthanide chlorides used in this study are hygroscopic and hence need to be stored in an inert environment in order to prevent the formation of hydroxides due to the interaction with moisture in the air. In addition, when the salt is in molten form, the formation of alkali oxides or rare earth oxides is possible in the presence of significant oxygen. Because of this fact, all electrochemistry work was performed in a glove box maintained at argon atmosphere shown in Fig 2.4. A pressure control system ensures that the pressure inside the glove box was slightly above atmospheric pressure, guaranteeing that any leaks in the glove box would result in argon leaking out of the glove box, rather than air leaking into the glove box. The purification of the argon gas in the glove box was carried out by passing through a tower containing molecular sieves and a copper catalyst to maintain the required levels of moisture and oxygen.

An oxygen analyzer of M/s. NUCON with 4316P sensor was used to monitor the oxygen and a moisture sensor of M/s. SESTECH shown in Fig. 2.5 was used to monitor the moisture concentrations in the glove box. The oxygen and moisture concentrations in the glove box were maintained always below 10 and 20 ppm by volume respectively, while carrying out the experiment. The glove box had an extension port to facilitate the easy handling and transport of the materials in and out of the box without affecting the purity of the inert atmosphere of the glove box. During the transport of materials in/out of the box, a vacuum pump was used to evacuate gas inside the extension port and argon gas was filled from argon cylinder/argon line and these operations were repeated by 3 to 5 times.

2.3.1. Purification tower

The glove box facility needed purification and recirculation of the argon gas in order to control the levels of the impurities, mainly, oxygen and moisture that ingress into the box during normal operation, due to air leaks and air diffusion. It is also possible to maintain the purity in the glove box without purification and recirculation by flushing the box with high purity argon gas, whenever it is being used. But it results in wastage of large volumes of expensive UHP argon gas resulting in large operational costs.

Fig. 2.4. Argon atmosphere Glove box facility

Fig. 2.5. Oxygen and H_2O analyzers

To eliminate the oxygen and moisture present in the gas in the glove box facility, the gas is passed through purification towers filled with purification agents such as molecular sieves and alumina containing highly dispersed metallic copper, called copper catalyst [70]. Molecular sieves are highly porous, synthetic alumino-silicates that can adsorb molecules from gases or liquids that are small enough to enter to their pores. In other words, it can take up in its internal cavities or hold on the surface such molecules by chemisorption. Usually copper used as a catalyst, but here it is not acting as a promoter of reactions in its active sites, but as a chemical absorption agent. Copper is oxidized by oxygen molecules present in the gas stream, forming copper oxide and thus removing oxygen from the gas flow. During the gas purification, copper is oxidized through the following reaction at room temperature

$$Cu_{(s)} + \tfrac{1}{2} O_{2(g)} \rightarrow CuO_{(s)} \qquad \Delta H = -\ 86.7\ \text{kJ/mol} \qquad (2.2)$$

The activation or regeneration of copper catalyst involves chemical reduction of copper oxide to copper in the presence of hydrogen at the temperature of 200^{o}C, as per the following reaction

$$CuO_{(s)} + H_{2(g)} \rightarrow Cu_{(s)} + H_2O_{(g)} \qquad \Delta H = -\ 156.3\ \text{kJ/mol} \qquad (2.3)$$

The theoretical capacity of 1 kg catalyst to absorb oxygen is 60g.

2.4. Electrochemical cell

The LiCl-KCl-UCl_3 salt was contained in a SS 430 crucible which was placed in another SS 304 container. A split type resistance furnace was provided to heat the crucible. A thermal shield made of the ceramic material, pyrophillite in the form of a disc is above the crucible and the holes in the shield are used to position electrodes and thermocouples in the cell. SS 430 crucible was chosen for its high temperature resistance, high corrosion resistance and low thermal resistance. A pyrophillite cup was used to hold the SS 430 crucible so as to prevent the molten salt from contacting the heater insulation, in case of any leaks from the SS 430 crucible. The electrochemical cell and all the components of the electrochemical cell are shown in Fig. 2.6. The electrochemical cell used for this work utilized three electrodes: a working electrode, a counter electrode and a reference electrode. Table 2.2 lists the electrode materials used for this research.

Working electrode: The working electrode is the electrode of interest where the electrochemical measurements are made.

Counter electrode: The counter electrode serves to complete the circuit of the electrochemical cell.

Reference electrode: The reference electrode is used to accurately measure the potential of the working electrode. This is possible because the reference electrode has a stable electrode potential which is constant with reference to which the potential of the working electrode is measured.

Table 2.2. Electrode materials and description.

Electrode	Material/Description
Working electrode (WE)	SS430/Tungsten rod
Counter electrode (CE)	SS430 perforated anode basket/Cd anode
Reference electrode (RE)	1.0 mm silver wire in 1 wt% Ag/AgCl in LiCl-KCl

Fig. 2.6. The components of the electrorefiner (i) Thermal shield with holes for positioning electrodes (ii) Top flange of the outer vessel with connections (iii) Electrorefiner cell assembly without flange (iv) Perforated anode basket (v) SS 430 solid rod cathode (vi) 120 mm dia SS crucible assembled with pyrophillite cup & SS holder.

2.5. Electrodeposition/Electrolysis experiments

All the three terms, namely, electrodeposition or electrolysis or electrowinning nearly give the same meaning and involve the transfer of electrons between electrodes to the ions dissolved in the electrolytic solution. The electrodeposition of materials (metals, metal oxides etc.) involves the reduction of the corresponding ions at the electrode in aqueous or non-aqueous electrolytes [71 - 73]. For instance, the reduction of metal ion $\mathrm{M}^{\mathrm{n}+}$ to metal $\mathbf{M}$ is represented as below

$$\mathrm{M}^{\mathrm{n}+} + \mathrm{ne}^{-} \rightarrow \mathrm{M} \qquad (2.4)$$

where "n" is the number of electrons involved in the reduction. The complete electrodeposition involves, as in all other voltammetric techniques, a number of steps which include mass transport, charge transfer, chemical reaction and crystallization. The electrodeposition experiments are basically related to the Faraday's laws that give the relation between the amount of electricity passed through the system and the amount (mass) of deposit formed at the electrode. The quantity of electricity in coulombs equals the number of electrons (n) involved in the reaction multiplied by the Faraday's constant (F) and the number of moles of material reacted (Δm)

$$Q = nF\Delta m \qquad (2.5)$$

The quantity of electricity in coulombs that passes through a conductor is proportional to both the current and the length of time for which it flows. If one assumes 100% current efficiency and a constant current passed through the system for a period of time then the material deposited is given as Faraday's law

$$\Delta m = \frac{i.\Delta t}{nF} \qquad (2.6)$$

where Δm is number of moles of material deposited, i is the current in amperes, Δt is time in seconds, n is valency of the metal (number of electrons) and F is the Faraday's constant (96500 C.mol^{-1}). In the electrodeposition or electrolysis experiment, if the current efficiency is not exactly 100%, then the above Equation 8 becomes

$$\Delta \mathrm{m} = \frac{\mathrm{i}.\Delta \mathrm{t}}{\mathrm{nF}}.\eta \qquad (2.7)$$

where η is the current efficiency (%). The current efficiency is defined as the ratio between the actual amounts of material deposited to that expected theoretically from Faraday's law [74]. The electrodeposition experiments can be carried out by potentiostatic (constant potential) or galvanostatic (constant current) modes.

2.6. Mathematical Model

COMSOL Multiphysics (known as FEMLAB before 2005) is a commercial finite element software package designed to address a wide range of physical phenomena. It provides a powerful interactive environment for modeling and solving all kinds of scientific and engineering problems. It also provides a powerful integrated desktop environment with a model builder where one can get full overview of the model and access to all functionality. With COMSOL Multiphysics [75] one can easily extend the conventional models for one type of physics into Multiphysics models that solve coupled physics phenomena. COMSOL Multiphysics can be accessed as a standalone product through a flexible graphical user interface (GUI) or by script programming in Java or the MATLAB® language (requires the COMSOL Live Link for MATLAB).

Using the physics interfaces, one can perform various types of studies including:

- ✓ Stationary and time-dependent (transient) studies
- ✓ Linear and nonlinear studies
- ✓ Eigen frequency, modal, and frequency response studies

In the present work, electrochemistry, Chemical Species Transport and Mathematics modules were used to develop the model. Electrochemistry module deals with the current distributions like primary, secondary and tertiary current distributions, electro analytical studies like voltammetry analysis, electrochemical impedance analysis etc., and electrodeposition studies etc. Chemical species transport module includes transport of diluted species, transport of concentrated species, reaction engineering, reacting flow in porous media etc. Mathematical module deals with the PDE interfaces, ODE interfaces, optimization and sensitivity, moving interfaces etc. To achieve the central goal of this project the secondary current distribution (siec) of electrochemistry module is used for simulating electrochemical reactions and the potential and current distributions in the electrochemical cell. The transport of the diluted species (tds) of the chemical species transport module is used for simulation of mass transfer of each species through the diffusion layer and the general form of ODE (g) in ODE interfaces of mathematical module is used for solving the material balance equation for each species. The three modules are coupled to each other and solved simultaneously for some of the problems where ever needed. Individual modules were also applied as per the requirement and developed the model. Here we discuss briefly the fundamentals of modules used in this study and the methods implemented by COMSOL Multiphysics which are useful to achieve the central goal of this project.

2.6.1. Theory for the current distribution interfaces

In this interface some of the following terms are discussed

- ✓ The Nernst-Planck equations
- ✓ Domain equations for primary and secondary current distributions
- ✓ Electrochemical reactions and the difference between a primary and a secondary current distribution
- ✓ Domain equations for tertiary current distributions using the Nernst Planck equations and electroneutrality

2.6.1.1. The Nernst-Planck equations

The following general mass balance equation described briefly for the diluted species in an electrolyte for each species is

$$(\partial c_i)/\partial \mathrm{t} = -\nabla . \mathrm{N_i} \qquad (2.8)$$

Where

$\mathrm{N_i}$ is the flux (mol/m^2.s) of species i,

c_i represents the concentration (mol/m^3) of the species i,

t is the reaction time (s).

The flux in an electrolyte is described by the Nernst-Planck equations and accounts for the flux of charged solute species (ions) by diffusion, migration and convection; these are the first, second and third terms respectively on the right hand side in the equation below

$$\mathrm{N_i} = -D_i \nabla c_i - z_i u_{m,i} \mathrm{F} c_i \nabla \phi_l + c_i \mathrm{u} \qquad (2.9)$$

Where

D_i = Diffusion coefficient (m^2/s) of species i,

z_i = Number of electrons participated in the reaction of species i,

$u_{m,i}$ = Mobility (s. mol/kg),

F = Faraday constant (C/mol),

$\emptyset_l$ = Electrolyte potential (V),

u = velocity vector (m/s).

The net current density can be described using the sum of all species fluxes

$$i_l = F \sum z_i N_i \qquad (2.10)$$

Where i_l denotes the current density vector (A/m^2) in the electrolyte

2.6.1.2. Primary and secondary current distributions

Primary and secondary current distributions were applied in the present study. Some of the valid assumptions made are:

- ✓ electroneutrality condition which cancels out the convection term on the right hand side of the equation (2.9)
- ✓ Assuming negligible concentration gradients of the current carrying species which cancels out the diffusion term on the right hand side of the equation (2.9)

From the equations 2.9 and 2.10

$$i_l = F\,[\Sigma - z_i D_i \nabla c_i + u\,\Sigma z_i c_i - \nabla \phi_l \Sigma\,(z_i)^2\,m_i\,F c_i\,] \qquad (2.11)$$

According to electroneutrality condition, sum of the net charges equal to zero i.e. $\Sigma z_i c_i = 0$,

$$\text{So,} \quad i_l = F\,[\Sigma - z_i D_i \nabla c_i - \nabla \phi_l \Sigma\,(z_i)^2\,m_i\,F c_i] \qquad (2.12)$$

In the electrorefining or electrodeposition process, concentration gradient exists between electrode/electrolyte interfaces due to the diffusion layer. Concentration gradient negligible that means formation of diffusion layer is very small and can be due to perfectly mixing. So, flux and current density can be written as

$$\mathrm{N_i} = - z_i u_{m,i} \mathrm{F} c_i \nabla \phi_l \qquad (2.13)$$

$$i_l = - \mathrm{F}^2 \sum z_i{}^2 \, u_{m,i} c_i \, \nabla \phi_l \qquad (2.14)$$

Further assuming approximately constant consumption of charge carriers, we can define constant electrolyte conductivity as

$$\sigma_l = \mathrm{F}^2 \sum z_i{}^2 \, u_{m,i} c_i \qquad (2.15)$$

So, the current density in the electrolyte can be written as

$$i_l = - \sigma_l \, \nabla \phi_l \qquad (2.16)$$

The above equation considers the same form as Ohm's law in an electrolyte and the charge transport is Ohmic, subject to the above assumptions i.e., all other resistances are negligible for primary current density distribution.

The primary and secondary current distribution interfaces define two dependent variables: One for the potential in the electrolyte and one for the electric potential in the electrode. The conduction of current in the electrolyte is assumed to take place through transport of ions, while electrons conduct the current in the electrode.

2.6.1.3. Difference between a primary and secondary current distribution

Both the primary and secondary current distribution models assume an electrolyte that conducts current according to Ohm's law, with a constant conductivity. The difference between primary and secondary current distribution lies in the description of the electrochemical charge transfer reaction at the interface between an electrolyte and an electrode. The charge transfer reactions can be defined as the boundary conditions, or as sources or sinks in a domain for the case of porous electrodes.

The rate of the electrochemical reactions can be described by relating the reaction rate to the activation overpotential. For an electrode reaction, with index m, the activation overpotential, denoted η_m, is the following

$$\eta_m = \phi_s - \phi_l - E_{eq,m} \qquad (2.17)$$

Where $E_{eq,m}$ denotes the equilibrium potential also known as reduction potential for reaction m. In the primary current distribution interface, the electrochemical reactions are assumed to be fast enough that their kinetics has negligible influence on the cell voltage. Consequently, the activation overpotential, η_m, in this interface is equal to zero. The difference between the electrode and the electrolyte potentials is always equal to the equilibrium potential, $E_{eq,m}$. This condition was implemented as the following constraint on boundaries between the electrodes and electrolyte domains

$$\phi_l = \phi_s - E_{eq,m} \qquad (2.18)$$

In the secondary current distribution interface, the electrochemical reactions are described as a function of the overpotential. The interface uses several relations for the charge transfer current density and the overpotential, such as Butler-Volmer and Tafel expressions. The most general expression of Butler-Volmer is

$$i_{loc,m} = i_0 \left(\exp\left(\frac{\alpha_a F\eta}{RT}\right) - \exp\left(\frac{-\alpha_c F\eta}{RT}\right)\right) \qquad (2.19)$$

where

$i_{loc,m}$ = Local charge transfer current density (A/m^2) for reaction m,

i_0 = Exchange current density (A/m^2),

α_a = Anodic charge transfer coefficient

α_c = Cathodic charge transfer coefficient,

R = Universal gas constant

It is possible to expand the above expression to include the dependence of kinetics on concentration.

2.6.1.4. Tertiary current distribution

The material balance equation for the species, i in the electrolyte is given by the continuity equation and flux is given by the Nernst Planck equation. So we can write the following overall equation as

$$\frac{\partial c_i}{\partial t} = \nabla.(- D_i\nabla c_i - z_i u_{m,i} F c_i \nabla\phi_l + c_i u) \qquad (2.20)$$

The current balance includes the sum of the fluxes of all charged species, which yields the current density in the electrolyte

$$i_l = F\sum_{i=1}^{n} z_i(- D_i\nabla c_i - z_i u_{m,i} F c_i \nabla\phi_l) \qquad (2.21)$$

In the tertiary current distribution, the concentration gradients are not assumed to be negligible. So, the contribution of species diffusion to overall current density may be nonzero. In the above equation i_l denotes the current density vector in the electrolyte. The current balance in the electrolyte then becomes

$$\nabla . i_l = Q_l \qquad (2.22)$$

where Q_l can be a source or sink. By solving the current balance and material balance equations combinedly gives the concentration of unknown species concentration. However, there is still one more unknown parameter that is the electrolyte potential which requires an additional equation. This equation is called electroneutrality condition [76] which follows from the dimensionless analysis of Gauss's law and which applies on scales larger than nanometers.

$$\sum z_i \, c_i = 0 \qquad (2.23)$$

The equations for calculating the charge transfer current density and the overpotential were the same as above used equations for secondary current distribution except that in Butler-Volmer equation the concentration terms should be included. The modified Butler-Volmer equation for tertiary current distribution is following

$$i_{loc,m} = i_0 \left(C_R \exp\left(\frac{\alpha_a F\eta}{RT}\right) - C_O \exp\left(\frac{-\alpha_c F\eta}{RT}\right)\right) \qquad (2.24)$$

where C_R and C_O are dimensionless expressions, that are dependent on reduced and oxidized species in the reaction respectively.

2.6.2. The Transport of Diluted Species Interface

The Transport of Diluted Species Interface (tds) is found under the Chemical Species Transport branch in the model wizard of Chemical Reaction Engineering Module of COMSOL Multiphysics. This interface has equations, boundary conditions and rate expression terms for modeling mass transport of diluted species in mixtures, solutions and solids for solving the concentrations of species. The tds enables the study of the evolution of chemical species transported by diffusion and convection. The interface assumes that all the species present are dilute; that is, that their concentrations are small compared to a solvent fluid or solid. As a rule of thumb, a mixture containing several species can be considered dilute, when the concentration of the solvent is more than 90 mol%. Due to the dilution, the properties of mixture such as density and viscosity can be assumed to correspond to those of the solvent.

This physics interface supports simulation of transport by convection and diffusion in 1D, 2D, 3D as well as for axisymmetric models in 1D and 2D. The dependent variable is the molar concentration. Fick's law governs the diffusion of the solutes, dilute mixtures or solutions.

2.6.2.1. Mass Balance Equation

The Transport of Diluted Species Interface assumes the transport of chemical species through diffusion and convection and implements the mass balance equation

$$\frac{\partial \mathrm{c_i}}{\partial \mathrm{t}} + u.\nabla c = \nabla.(D\nabla c) + \mathrm{R} \qquad (2.25)$$

where

c = concentration of the species (mol/m^3),

D = diffusion coefficient (m^2/s),

R = Reaction rate expression for the species (mol/ (m^3·s)),

u = velocity vector (m/s).

The first term on the left-hand side of mass balance (Equation 2.25) equation corresponds to the accumulation of the species. The second term accounts for the convective transport due to a velocity field. This field can be expressed analytically or be obtained from coupling this physics interface to one that describes fluid flow (momentum balance). On the right-hand side of the mass balance equation (Equation 2.25), the first term describes the diffusion transport, accounting for the interaction between the dilute species and the solvent. Finally, the second terms on the right-hand side of equation 2.25 represents a source or sink term, typically due to a chemical reaction. In order for the chemical reaction to be specified, another node must be added to the Transport of Diluted Species interface, the Reaction node, which has a field to specify a reaction equation using the variable names of all participating species. In the present model, only diffusion terms were solved using this module.

2.6.2.2. Solving a Diffusion Equation

In the present model, transport of species is assumed to be through diffusion in the diffusion layer only and the mass transfer is controlled by diffusion only. Hence the second term on the left hand side of the mass balance equation 2.25 is neglected.

$$\frac{\partial c_i}{\partial t} = \nabla . (D \nabla c) + R \qquad (2.26)$$

Chapter 3

Modeling the Molten Salt Electrorefining Process for Spent Metal fuel using COMSOL and its validation using the experimental data from literature

3.1. Introduction

As was discussed in Chapter 1, molten salt electrorefining is one of the key steps of the pyrochemical reprocessing flow sheet for the spent metallic fuel from fast reactors and development of pyrochemical reprocessing for spent metal fuels from the future fast reactors through experiments [30, 35] as well as modeling is in progress at the Indira Gandhi Centre for Atomic Research (IGCAR) for the past several years. Thermodynamic and electrokinetic models have been developed earlier [29, 33]. In the present study, another kinetic model based on the diffusion control using COMSOL Multiphysics software has been developed. Earlier, Tomczuk et al. of ANL studied the recovery of pure uranium from liquid cadmium anode by electrotransport through molten LiCl-KCl eutectic salt to solid cathode over a range of $PuCl_3/UCl_3$ ratios in the electrolyte [48]. The results of the present model based on COMSOL Multiphysics were validated using the results of Tomczuk et al. [48] and these are discussed in this chapter.

3.2. Mathematical model

The present mathematical model for molten salt electrorefining process is based on the following important assumptions:

i. The molten salt phase and liquid cadmium phase are thoroughly mixed and there is no concentration gradient of any metal ions/metal in each of the phases.

ii. The thickness of each of the diffusion layer is constant and same for each of the metal ions. There is one diffusion layer at the solid rod cathode/ molten salt interface and one each on the cadmium side and the salt side of the liquid cadmium anode/ salt interface.

iii. Most of the concentration gradients of metal ions/ metal lie in the diffusion layer.

iv. The mass transfer of metal ions/ metal in the diffusion layer is due to diffusion only and mass transfer due to convection and migration are neglected.

Figure 3.1 shows the schematic diagram of the ANL laboratory scale electrorefiner [48] and Fig. 3.2 that of its 2D-axis symmetric model.

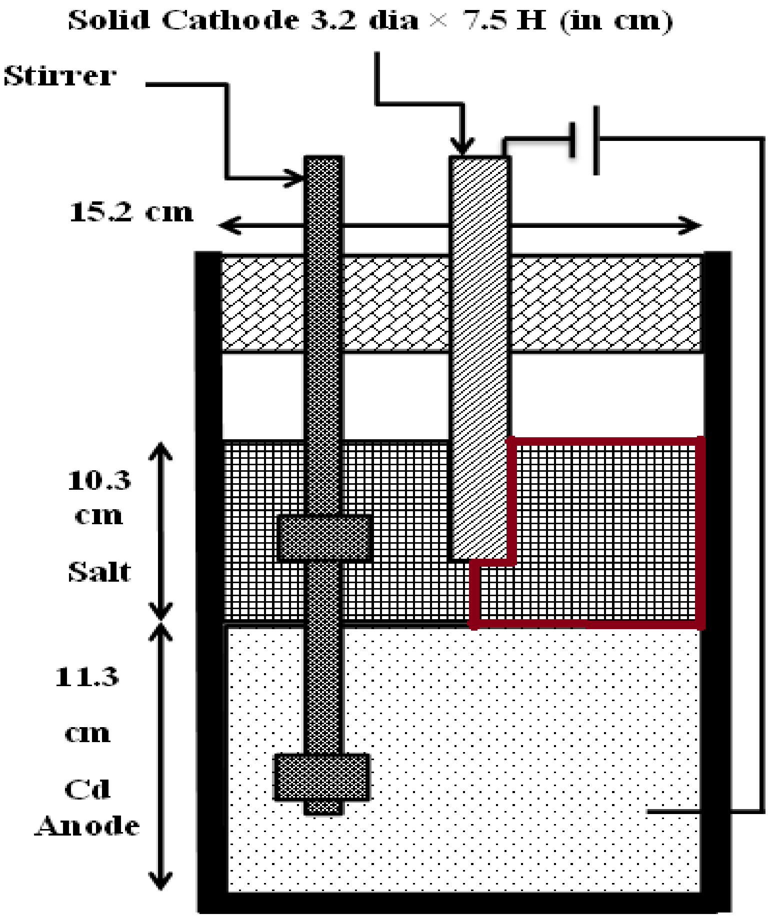

Fig. 3.1. ANL laboratory scale Electrorefiner. Colored portion is used for 2D axis-symmetrical model as shown in Fig. 3.2

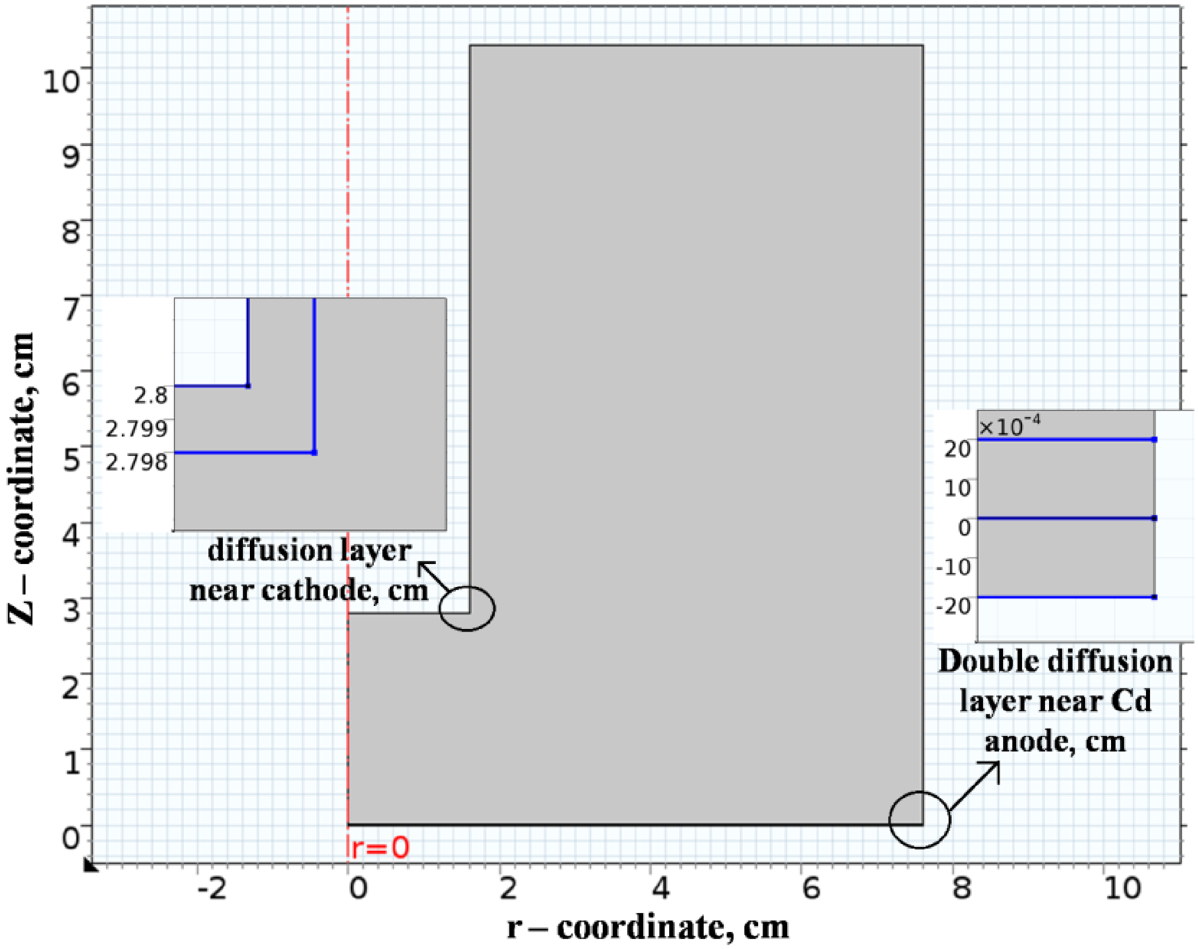

Fig. 3.2. 2D axis-symmetrical electrorefiner model. The magnified region shows the diffusion layers (units in cm) (i) salt side of the diffusion layer near solid cathode (2.798 to 2.8 cm i.e. 0.002 cm) (ii) Double diffusion layer one at salt side (0 to 20 $\times 10^{-4}$ cm) another at Cd side near liquid Cd anode (0 to -20 $\times 10^{-4}$ cm).

In the electrorefiner, Uranium and Plutonium get oxidized at the liquid cadmium anode and are reduced at the solid cathode, as per the following half-cell electrochemical reactions:

$$\mathrm{U} \rightarrow \mathrm{U}^{3+} + 3\mathrm{e}^- \quad \mathrm{E}_{\mathrm{U}}^{0} = -1.10 \text{ V vs Ag/1 wt\%AgCl} \quad \text{(anode)} \quad (3.1)$$

$$\mathrm{Pu} \rightarrow \mathrm{Pu}^{3+} + 3\mathrm{e}^- \quad \mathrm{E}_{\mathrm{Pu}}^{0} = -1.40 \text{ V vs Ag/1 wt\%AgCl} \quad \text{(anode)} \quad (3.2)$$

$$\mathrm{U}^{3+} + 3\mathrm{e}^- \rightarrow \mathrm{U} \quad \mathrm{E}_{\mathrm{U}}^{0} = -1.10 \text{ V vs Ag/1 wt\%AgCl} \quad \text{(cathode)} \quad (3.3)$$

$$\mathrm{Pu}^{3+} + 3\mathrm{e}^- \rightarrow \mathrm{Pu} \quad \mathrm{E}_{\mathrm{Pu}}^{0} = -1.40 \text{ V vs Ag/1 wt\%AgCl} \quad \text{(cathode)} \quad (3.4)$$

The mass transfer is mathematically given by equation (3.5).

$$\frac{\partial c_j}{\partial t} = -\nabla . N_j \qquad (3.5)$$

where C_j is the concentration of j^{th} metal ion in mol/m^3 and N_j, the molar flux (mol/m^{2}s) of species j is given by equation (3.6).

$$N_j = -z_j u_j F c_j \nabla \emptyset - D_j \nabla c_j + c_j v \qquad (3.6)$$

where z is the charge number, u_j is the mobility (s mol/kg) of species j, D_j the diffusion coefficient (m^2/s) of species j, v the velocity (m/s), and F the Faraday's constant (96485 C/mole). The first term on the right-hand side is the flux due to electrical migration, the second term is the flux due to diffusion, and the last term is the flux due to convection. Since in the diffusion layer, the mass transfer is controlled by diffusion only, the first and third terms are neglected. Thus the flux of the species, j given by

$$N_j = -D_j \nabla C_j \qquad (3.7)$$

In each of the diffusion layers, the concentration of the species in the surface that is facing the bulk of the fluid will be the same as the concentration of the species in the bulk. So, the boundary condition in the surface of the diffusion layer is imposed as:

$$C_j = C_{b,j} \tag{3.8}$$

where $C_{b,j}$ is the concentration of the species *j* in the bulk. On the electrode surfaces, the flux of the species *j* depends on the local current density of the species *j* arising due to electrochemical reaction. So the boundary condition on the surface of the electrode is given as:

$$N_j = \frac{i_{loc,j}}{zF} \tag{3.9}$$

where $i_{loc,j}$ is the local current density (A/m^2) of the species *j* at the electrode surface. The local current of the species at the electrode surface is given by the concentration dependent Butler Volmer equation shown below.

$$i_{loc,j} = i_{o,j}\left(\frac{C^*_{Ox,j}}{C_{Ox,b,j}} exp\left(\frac{\alpha F\eta_j}{RT}\right) - \frac{C^*_{Red,j}}{C_{Red,b,j}} exp\left(-\frac{(1-\alpha)F\eta_j}{RT}\right)\right) \tag{3.10}$$

where $i_{o,j}$ is the exchange current density of the species *j*, Ox and Red subscripts indicate reduced and oxidized forms of the species *j, α* is the transfer coefficient and η_j is the overpotential (V) for species *j* at the electrode surface.

The exchange current density is defined in the form of normalized current density as given by Riley Cumberland et.al [64, 65] and the expression is given below:

$$i_{o,norm} = \frac{i_0}{[C_j]^\alpha} \tag{3.11}$$

The model is sensitive to the exchange current density of the species and its proper determination using experiments is essential to predict the results more accurately. Also there are no literature data available for exchange current density for liquid cadmium electrode. In this model the exchange current density of liquid cadmium anode is taken to be the same as that at the solid electrode. The overpotential of the electrode for species j is given as:

$$\eta_j = \emptyset_s - \emptyset_l - E_{eq,j} \qquad (3.12)$$

where $\emptyset_s$ is the electric potential of the electrode (V), $\emptyset_l$ is the electrolyte potential (V) adjacent to the electrode and E_{eq}, the equilibrium potential (V) of the species *j* at the electrode surface. The difference between $\emptyset_s$ and $\emptyset_l$ gives the electrode potential of the electrode, as if it is measured with respect to a reference electrode placed close to it. The equilibrium potential $E_{eq,j}$ of the species *j* at the electrodes surface is calculated by the Nernst equation. For the liquid cadmium anode and the solid cathode, the Nernst equations are given by equations 3.13 and 3.14, respectively:

$$E_{eq,j} = E^o_{red,j} + \frac{RT}{zF} ln\left(\frac{\gamma_j^{salt} C^*_{Ox,j}}{\gamma_j^{Cd} C^*_{Red,j}}\right) \qquad (3.13)$$

$$\mathrm{E_{eq,j}} = \mathrm{E^o_{red,j}} + \frac{\mathrm{RT}}{\mathrm{zF}} \ln\left(\gamma_\mathrm{j}^\mathrm{salt} \mathrm{C_{Ox,j}}\right) \qquad (3.14)$$

where $E^o_{red,j}$ is the standard potential (V) of species *j*, *R* = 8.314 J/(mol K) is the gas constant, *T* is the temperature (K), *z* is the number of equivalents per mole of species *j*, γ_j^{salt} is the activity coefficient of the species *j* in salt, γ_j^{Cd} is the activity coefficient of the species *j* in cadmium. In equation (3.13), $C^*_{Ox,j}$ is the concentration of species *j* at the salt side of the cadmium-salt interface and $C^*_{Red,j}$ is the concentration of species *j* at the cadmium side of the cadmium – salt interface. In equation (3.14), $C_{Ox,j}$ is the concentration of *j* at the salt side of the solid electrode-salt interface. The cell potential is defined by two dependent variables, namely, the potential in the electrolyte ($\emptyset_l$) and the electric potential in the electrode ($\emptyset_s$). Conduction of current in the electrolyte is assumed to take place through the transport of ions, while electrons conduct the current in the electrode. The current density vectors in the electrode and electrolyte are defined by a general equation shown below:

$$i_k = -\sigma_k \nabla \emptyset_k \qquad (3.15)$$

where σ_k denotes the conductivity, $\emptyset_\mathrm{k}$ denotes the potential and k denotes an index that is l for electrolyte and *s* for the electrode. The general charge balance equation for the electrolyte and electrode domains with no general source term is given as:

$$\nabla . i_k = 0 \qquad (3.16)$$

The charge transfer reaction at the interface between the electrolyte and electrode imposes the relationship between the two potential$s, \emptyset_l$ and $\emptyset_s$ by equation (3.12). The rate of the electrochemical reaction can be described by relating it to the overpotential by equation (3.12). In this model, the cadmium electrode acts as the anode and the external electric potential of this electrode is kept at ground potential i.e.

$$\emptyset_s = 0 \qquad (3.17)$$

The solid electrode acts as cathode and the total current of $-I_{app}$ is imposed as the boundary condition. The sum of all the electrode reaction currents arising due to multiple electrochemical reactions at the electrode surfaces must be equal to the total current at the electrode surface. This condition is imposed by following constraints equation:

$$I_{app}/A = \sum_{j=1}^{n} i_{loc,j} \qquad (3.18)$$

where 'I_{app}' is the total current (Amperes) at the electrode surface, A is the electrode surface area (m^2) and $i_{loc,j}$ is the local current density (A/m^2) contributed due to oxidation or reduction reaction of species *j*. The changes in the bulk concentrations of the species, j in the molten salt and also in the liquid cadmium anode were evaluated by using the ODE interface of the mathematical module of COMSOL Multiphysics by coupling it with the secondary current distribution module. The change in bulk concentration of species *j* in molten salt is determined using the material balance equation (3.19) shown below:

$$V_{salt}\frac{dC_{b,j}^{salt}}{dt} = \left(\frac{i_{loc,j}}{zF}\right)_{anode} - \left(\frac{i_{loc,j}}{zF}\right)_{cathode} \quad (3.19)$$

where V_{salt} is the molten salt volume (m^3) and $C_{b,j}^{salt}$ is the bulk concentration of species *j* in the molten salt (mol/m^3). The first and second terms on the right hand side of the equation (3.19) denote the input and output of species *j*. The input parameters for solving the equation (3.19) are V_{salt}, $C_{b,j}^{salt}$ and the local current of the species j, $i_{loc,j}$ which are derived by solving the equation (3.10) of secondary current distribution module. Similarly, the change in concentration of species *j* in liquid cadmium anode is determined with the help of material balance equation (3.20) shown below:

$$V_{cd}\frac{dC_{b,j}^{Cd}}{dt} = -\left(\frac{i_{loc,j}}{zF}\right)_{anode} \quad (3.20)$$

where V_{Cd} is the volume of cadmium (m^3) and $C_{b,j}^{Cd}$ is the bulk concentration of species *j* in cadmium (mol/m^3). The first term on the right hand side of the equation (3.20) denotes the output of species *j*.

3.2.1. COMSOL simulation

The electrochemistry module, the chemical species transport module and the mathematics module of the COMSOL Multiphysics package [67] are used for this simulation. The secondary current distribution (siec) of electrochemistry module is used for simulating electrochemical reactions and the potential and current distributions in the electrochemical cell. The transport of the diluted species (chds) of the chemical species transport module is used for simulation of mass transfer of each species through the diffusion layer and the general form of ODE (g) in ODE interfaces of mathematical module is used for solving the material balance equation for each species. The three modules are coupled to each other and solved simultaneously.

The simulation is of transient type and proper initial condition for each variable such as current, potential and concentration of each species is required to simulate the actual results. The total simulation time required for the model is 397 seconds.

Figure 3.3 shows the meshed geometry of the 2-D axis symmetric model of the electrorefiner developed in COMSOL. Mapped mesh (user-controlled mesh) is used in the diffusion layer region whereas triangular mesh is used in the other regions. The number of mesh elements was varied in the range of 12213 to 139633 (12213, 18278, 105465 and 139633). It was observed that there was no change in the concentrations of species in the molten salt and liquid cadmium anode. However, the time required for solving was found to be higher by 300% with physics controlled mesh elements of 105465 compared to that with the mapped 12213.

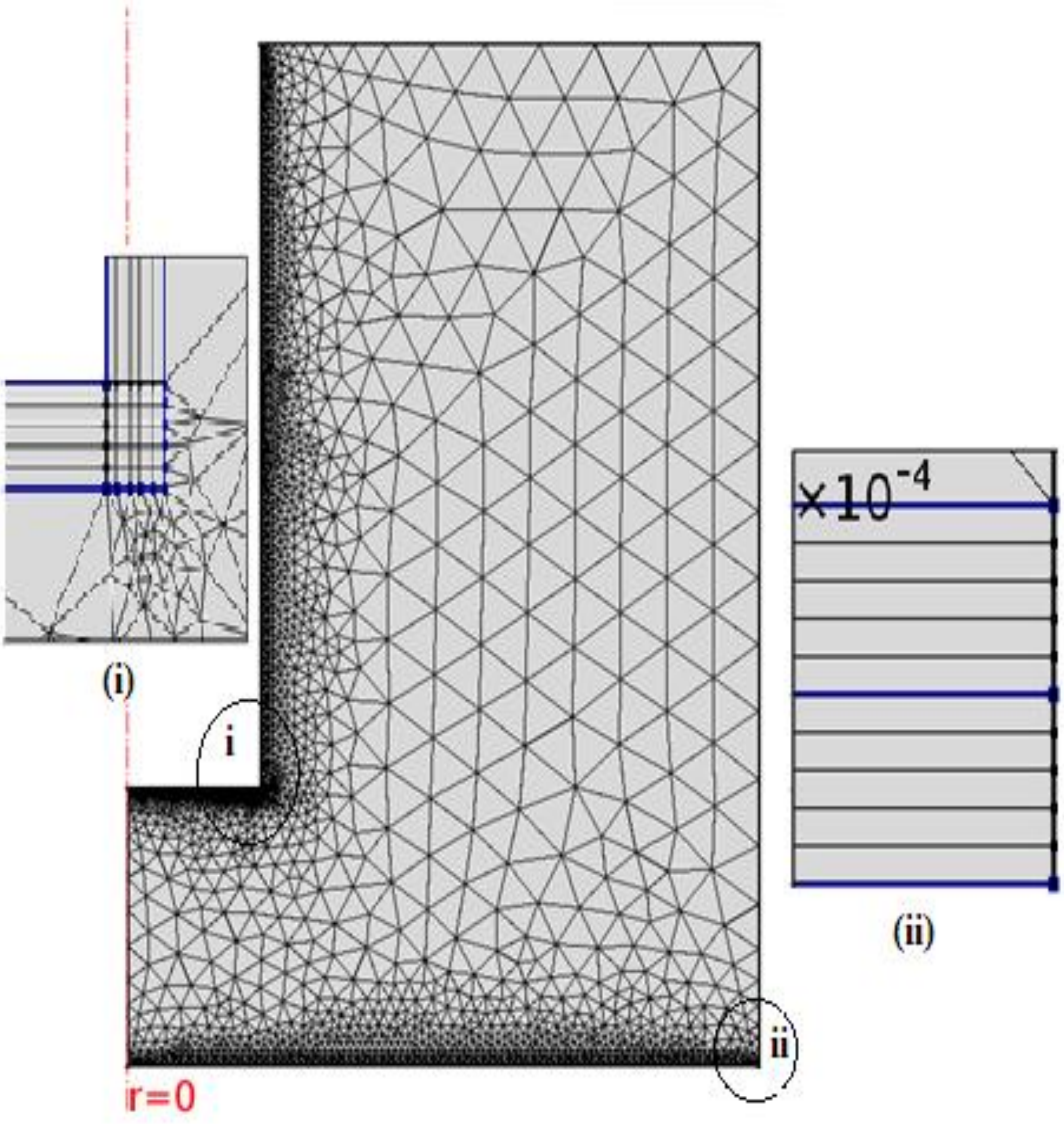

Fig. 3.3. Mesh used for the simulation. The magnified area shows the mapped mesh in the diffusion layer region. In the remaining regions, triangular mesh was used.

3.3. Results and discussion

As mentioned earlier, the electrotransport of U and Pu from liquid cadmium anode to solid cathode and their subsequent deposition on the solid cathode was modeled and validated. The operating conditions and the initial concentrations of U and Pu in the electrolyte salt and in the liquid cadmium anode, used by Tomczuk et al [48], are summarized in Table3.1. The input parameters and thermodynamic data used in model calculation are summarized in Table 3.2. The current applied by Tomczuk et al. in their experiments varied in the range of 1–2 A. For the model calculations, an average value of 1.45 A was used based on deposition rate reported.

Table 3.1 Initial operating conditions [48]

Parameter	Value
U in Cd pool, wt.%	1.01
Pu in Cd pool, wt.%	0.59
U in electrolyte salt, wt.%	1.61
Pu in electrolyte salt, wt.%	1.82
Current, A	1.45
Temperature, K	773

Figures 3.4-3.6 present the validation of the model with experimental data reported in the literature by Tomczuk et al. The variation of concentration of U and Pu in the molten salt with time could be predicted by the model as shown in Fig. 3.4. As can be seen, the values as well as the rates of increase of the concentration of Pu in the molten salt predicted by the model are in god agreement with the experimental data. Similarly the values and rates of decrease of the concentration of U in the molten salt predicted by the model are in good agreement with the experimental data.

Table 3.2 Parameters and thermodynamic data used in model calculation [42, 47, 48, 64, 65, 77 - 82]

Parameter	Expression	Value	Reference
Faraday constant, (C/mol)	F	96485	-
Universal gas Constant, (J / (mol K))	R	8.314	-
Standard potential of U, (V) vs Ag/0.1%AgCl	$E^{o}_{red,U}$	-1.1	[81]
Standard potential of Pu, (V) vs Ag/0.1%AgCl	$E^{o}_{red,Pu}$	-1.4	[47]
Diffusion layer thickness in molten salt and cadmium, (cm)	Δ	0.002	[47]
Activity coefficient of U in molten salt	γ_{U}^{salt}	5.79×10^{-3}	[82]
Activity coefficient of Pu in molten salt	γ_{Pu}^{salt}	6.62×10^{-3}	[82]
Activity coefficient of U in cadmium	γ_{U}^{Cd}	88.7	[80, 81]
Activity coefficient of Pu in cadmium	γ_{Pu}^{Cd}	2.32×10^{-4}	[80, 81]
Diffusion coefficient of U in molten salt, (cm^2 / s)	D_{U}^{salt}	1.4×10^{-5}	[78, 79]
Diffusion coefficient of Pu in molten salt, (cm^2/s)	D_{Pu}^{salt}	1.08×10^{-5}	[79]
Diffusion coefficient of U in Cadmium pool, (cm^2/s)	D_{U}^{Cd}	1.51×10^{-5}	[42]
Diffusion coefficient of Pu in Cadmium pool, (cm^2/s)	D_{Pu}^{Cd}	1.51×10^{-5}	[42]
Molten salt volume, (ml)	V_{salt}	1808	[47, 48]
Cadmium Volume, (ml)	V_{Cd}	2050	[47, 48]
Molten salt weight, (g)	W_{salt}	3680	[48]
Cadmium weight, (g)	W_{Cd}	16500	[48]
Transfer coefficient for U	α_{U}	0.5	[64]
Transfer coefficient for Pu	α_{Pu}	0.5	[64]

Molten salt conductivity, (S/m)	σ_{salt}	1.9	[77]
Normalized exchange current density for Uranium, (A/m^2)	$i_{u,o,norm}$	100	[64, 65]
Normalized exchange current density for Plutonium, (A/m^2)	$i_{Pu,o,norm}$	100	[64, 65]
Charge number	z	3	-

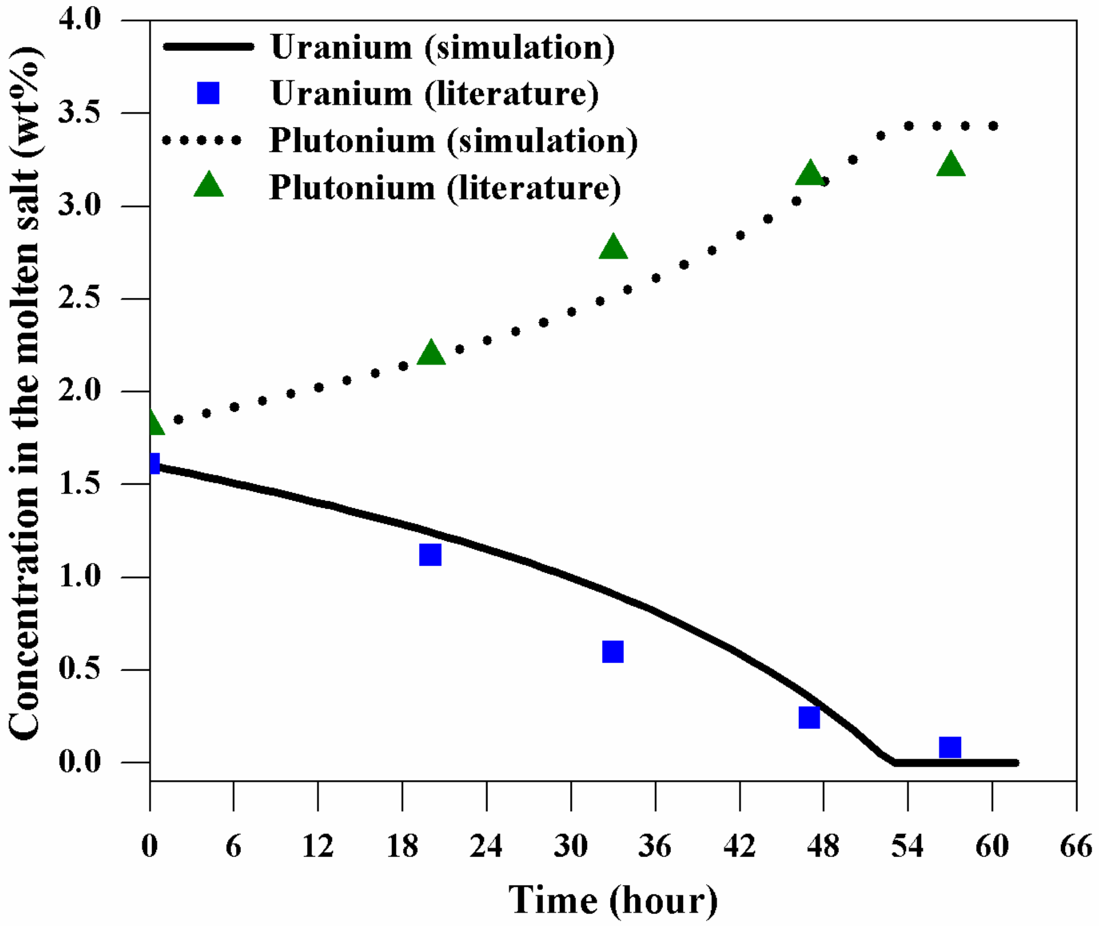

Fig. 3.4. Concentration of uranium and plutonium in the molten salt - model validation with experimental data from literature [48].

Figure 3.5 shows the variation in concentration of U and Pu in the liquid cadmium anode. The concentration of uranium was higher than that of Pu in the initial stages and as the deposition of U on the cathode proceeded, the U concentration became lower in the later stages. The rate of decrease of U concentration in the anode was almost the same until more than 98% of it got deposited. At this point, Pu also gets deposited and hence the rate of decrease of Pu in the anode becomes higher after that stage. The results from COMSOL model are in general in good agreement with the experimental data, as can be seen from Fig. 3.4 and 3.5.

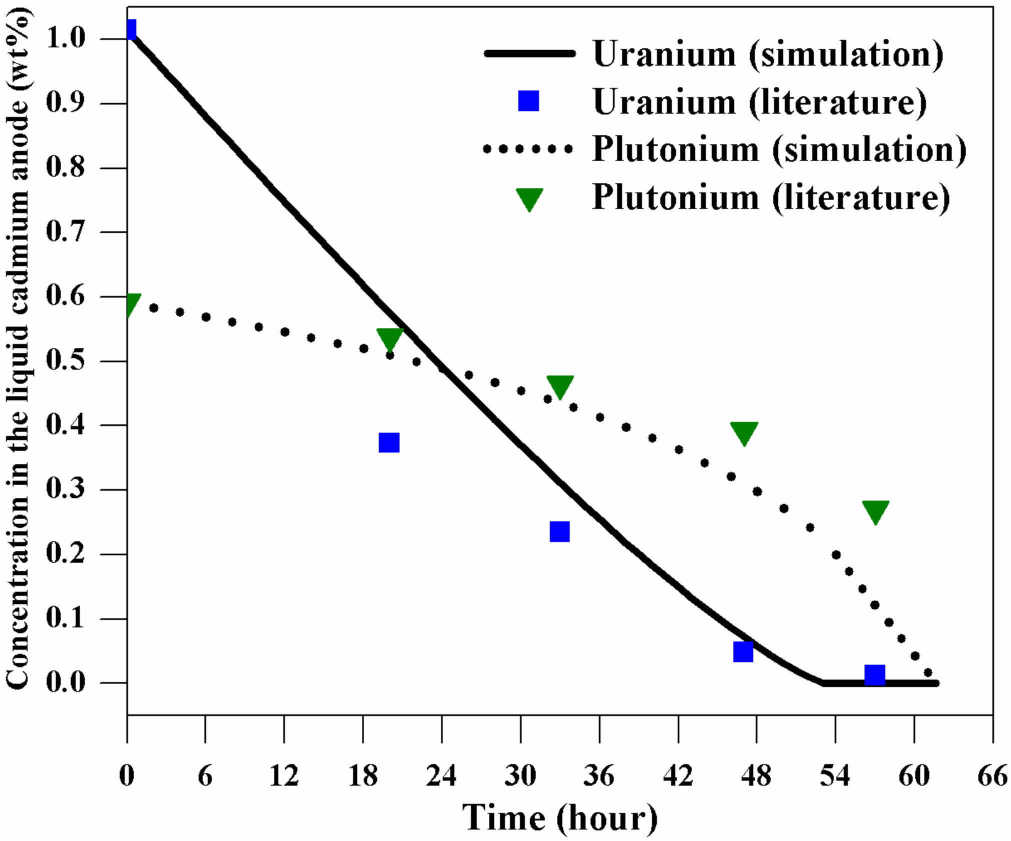

Fig. 3.5. Concentration of uranium and plutonium in the liquid cadmium anode - model validation with experimental data [48].

Figure 3.6 shows the amounts of U and Pu deposited on the solid cathode with the progress of electrorefining. U deposition on the solid cathode increased linearly with time until 52 hours and there is no further deposition. There is no Pu deposition on the solid cathode until 52 hours, as $PuCl_3$ is more stable compared to UCl_3. After 52 hours, there is a sudden increase in the Pu to U ratio in the molten salt, which results in Pu deposition as shown in Fig. 3.7. Increases of Pu to U ratio in the molten salt as well as in the liquid cadmium anode with the progress of electrorefining are shown in Fig. 3.8.

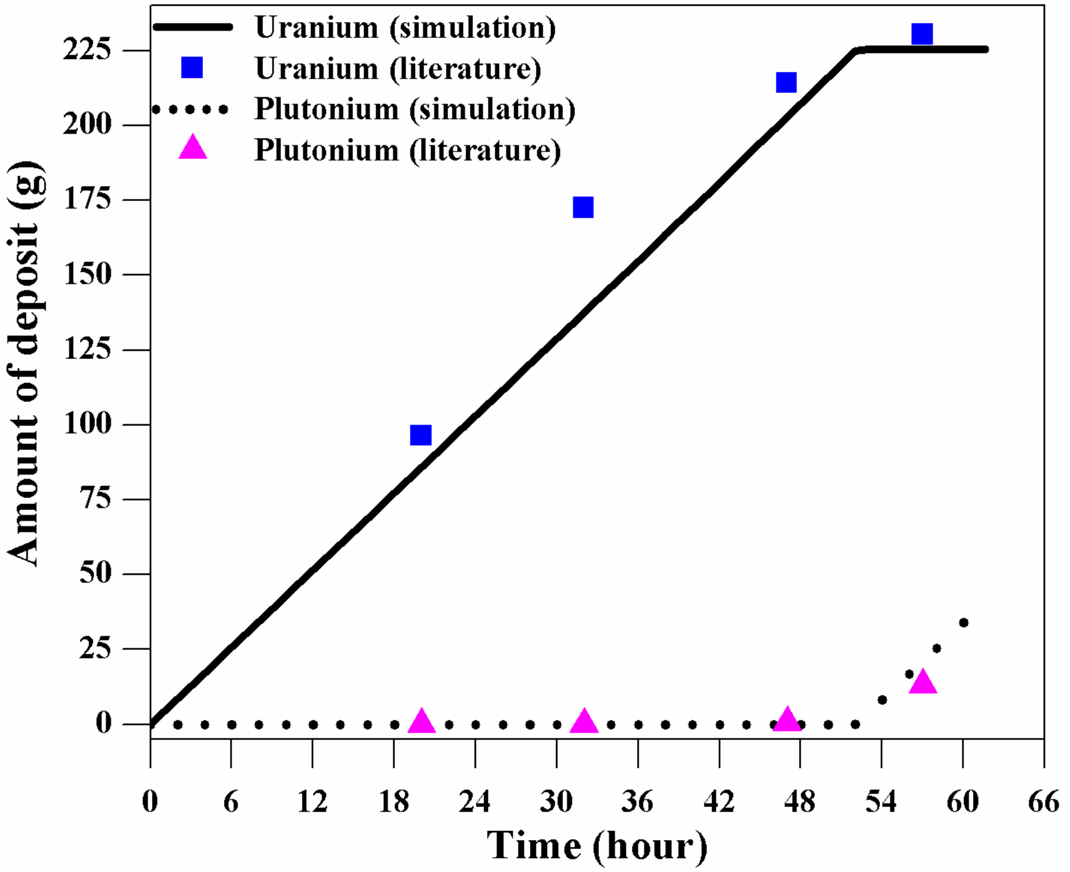

Fig. 3.6. Deposition histories of uranium and plutonium on the solid cathode - model validation with experimental data [48].

Up to 52 hours of operation, there was a slow increase in the Pu/U ratio in the salt reaching a value of more or less 66. At this point there is a sudden increase in Pu/U, the ratio reaching to 1.1×10^6 at 54 hours. As per the thermodynamic data, a Pu/U ratio of $>10^5$ is required for Pu deposition on the solid cathode and as expected, Pu deposition gets accelerated at this stage. It can be seen from Fig. 3.5 that Pu concentration in the anode decreases to a minimum value around 60 hours and after that no further transport of Pu is possible from the anode. In Fig. 3.9 the computed cell voltage is compared with literature data. It is seen that there is sudden increase in the cell voltage, when plutonium starts to deposit at the cathode due to difference in deposition potentials of uranium and plutonium. This model reproduced the trend of increase in cell voltage as in the reported data [47] due to the deposition of plutonium.

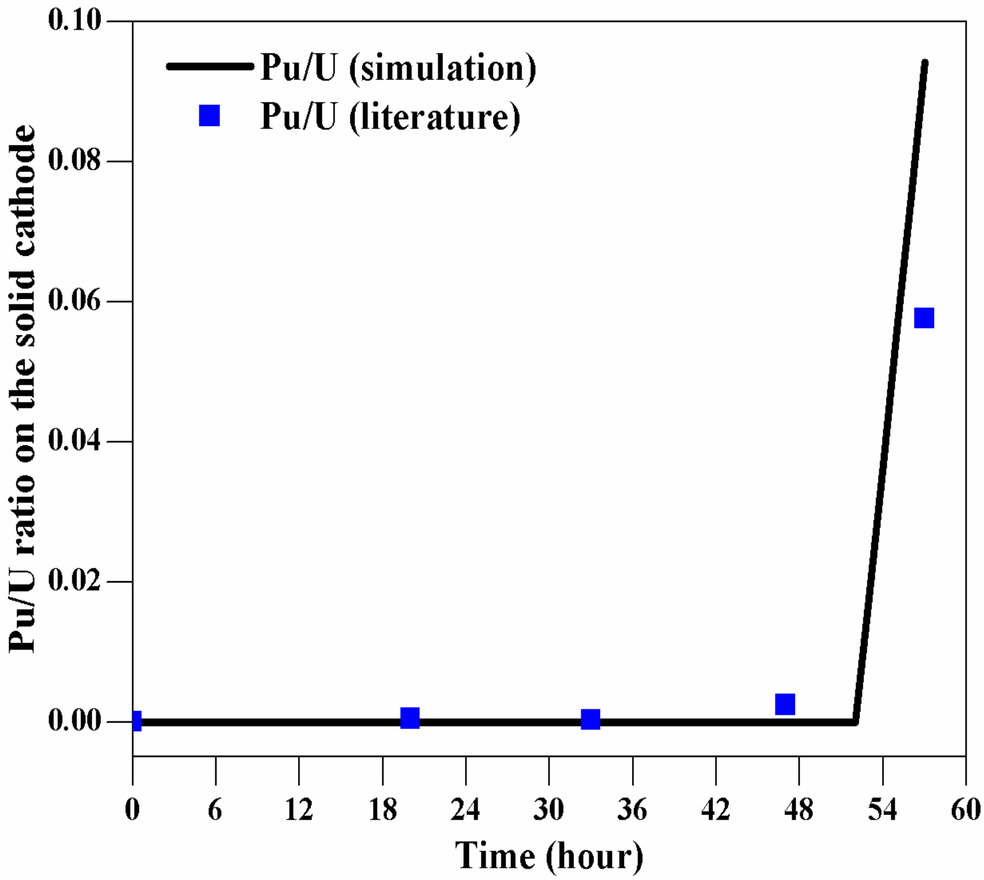

Fig. 3.7. Pu/U ratio on the solid cathode - model validation with experimental data [48].

Even the small variation of the predicted values from the experimental ones, as seen from the above figures, is mainly due to two factors. As explained above in mathematical model section, the exchange current density of liquid cadmium anode is taken same as solid electrode, in the absence of experimental data. Secondly, an average value of 1.45 Amperes is taken for computation, where as the current was varied between 1 and 2 Amperes in the experiments. The present model is also capable of predicting the effect of electrode geometry and this aspect of the model will be validated by bench scale experiments being planned in our laboratory, in addition to other aspects.

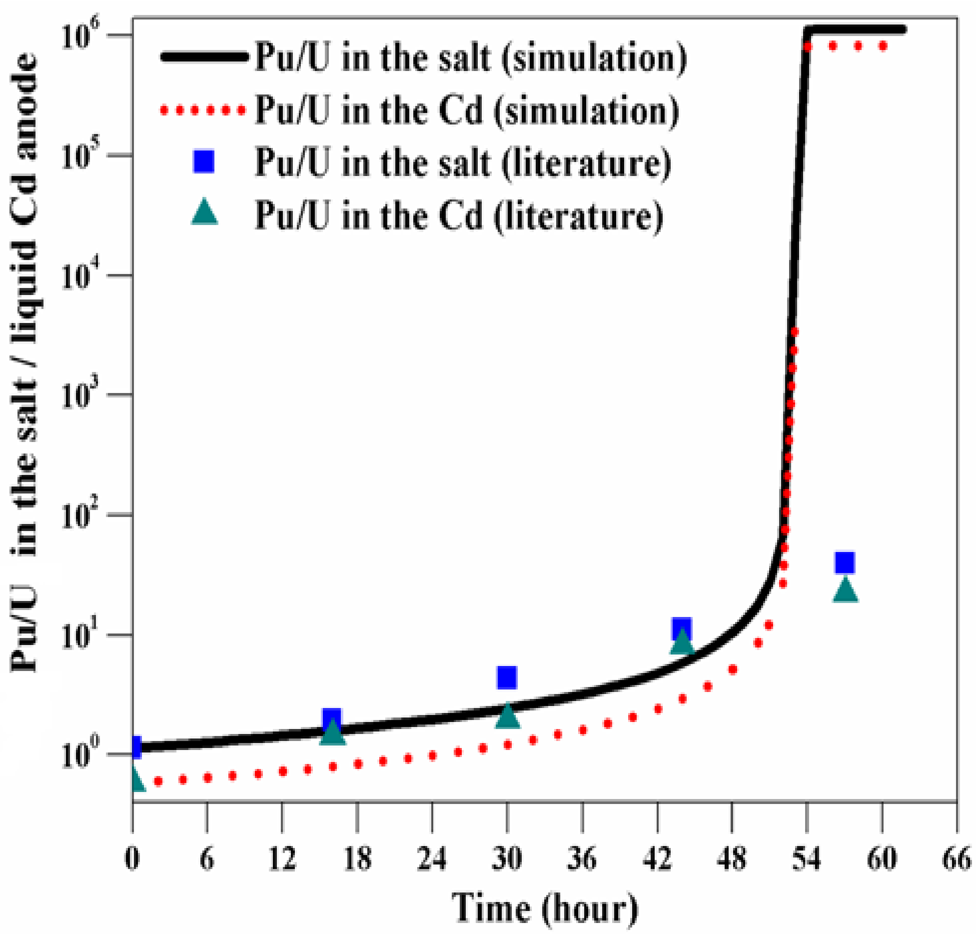

Fig. 3.8. Pu/U ratio in the molten salt / liquid cadmium anode - model validation with experimental data [48].

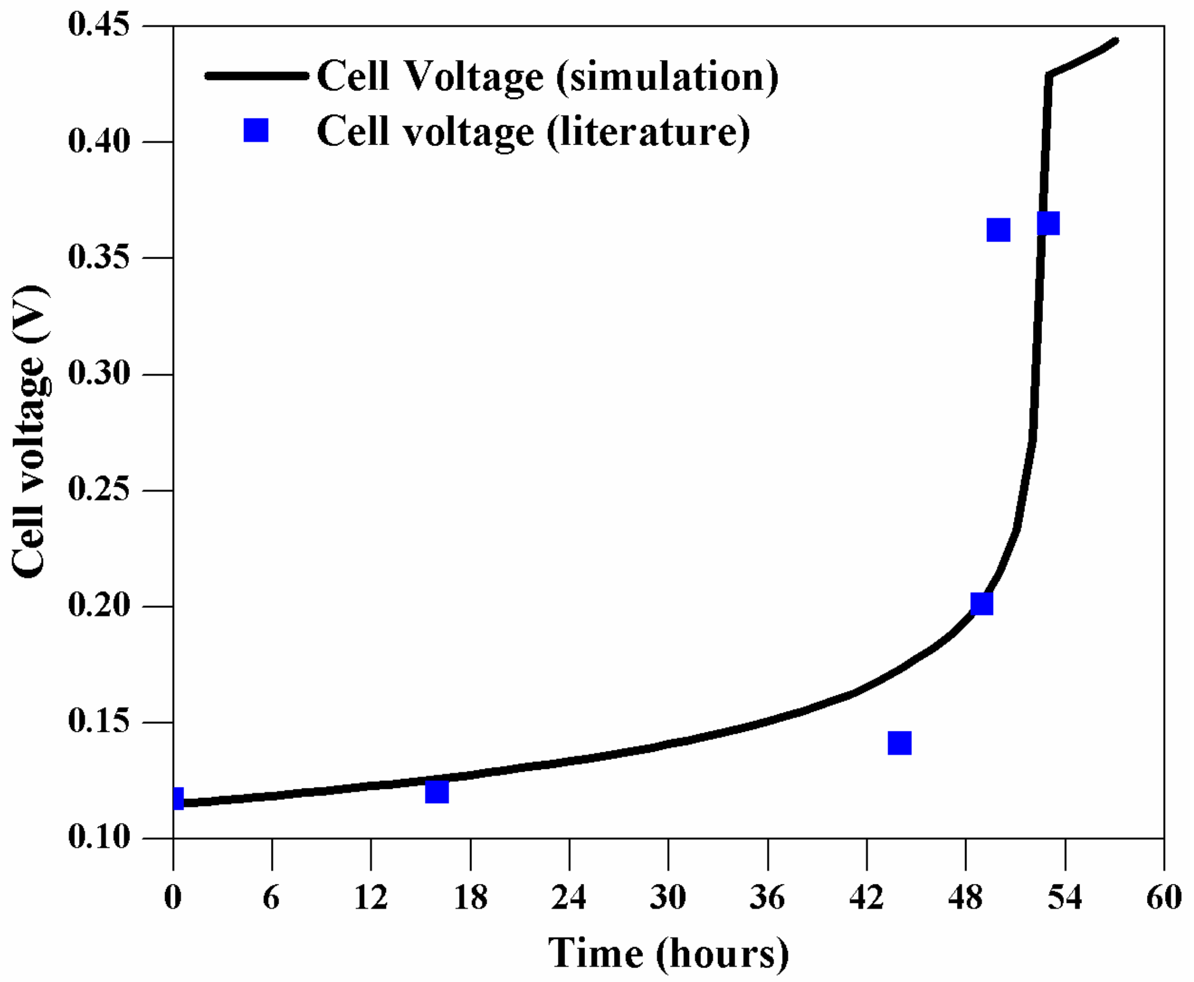

Fig. 3.9. Cell voltage in the electrolytic cell - model validation with literature data [47].

3.4. Conclusion

A kinetic model for the electrorefining process has been developed using the various modules of COMSOL Multiphysics. The model employs the secondary current distribution as well as the transport of diluted species within the diffusion layer and also considers the variation of concentration in the molten salt and liquid cadmium anode as well as the amount of deposit on the solid cathode. The ODE interface of mathematical module was also included to solve the material balance equation. The model was validated with the experimental results of Tomczuk et al. and the results show good agreement, the variation being less than 10% for the U and Pu concentration changes in liquid Cd anode and molten salt, and U deposit on solid cathode. This model can be used effectively to predict the performance of electrorefining process of similar electrode configurations. In the future, it is hoped to develop the model with actual compositions of the spent fuel of the fast reactor. Work will also be done to experimentally determine the exchange current density. It is also necessary to determine how the anodic and cathodic surface area (in the case of solid cathode and perforated basket as anode) may differ for each species during electrorefining process. In addition, it is also desired to determine the shape (i.e. dendritic) of the deposit on the solid cathode. Also, work will also be done to determine how both the mass transfer coefficients and surface areas change with respect to coulombs passed through the electrorefiner and not firmly with time.

Chapter4

Development of code for the optimization of electrode configuration in a molten salt electrorefiner and its validation

4.1. Introduction

COMSOL Multiphysics was used to develop a code to study the effect of the electrode configuration on the performance of the electrorefiner and it was validated using electrorefining experiments. The effects of the following electrode configurations were studied: (i) providing an insulation disc at the bottom of the solid cathode, (ii) variation in the distance between the electrodes, (iii) variation in the elevations of the liquid cadmium cathode, and (iv) the surface area of the solid cathode. Further, the effect of arranging a pair of solid cathodes and a pair of perforated anode baskets in parallel and staggered configurations was also studied. The details of the studies and the results are discussed in this chapter.

4.2. Experimental

4.2.1. Experimental procedure and equipment

The electrorefining apparatus used in this study for validating the code is shown schematically in Fig. 4.1. A SS430 crucible of 120 mm ID, 3 mm wall thickness and 190 mm height served as the electrochemical cell. LiCl-KCl electrolyte salt with 5 wt. % UCl_3 and the liquid cadmium pool taken at the bottom of the cell occupied a height of 80 mm and 30 mm, respectively. The purpose of the liquid cadmium pool was to collect any uranium metal deposit that may fall from the solid cathode. In some experiments, this liquid cadmium pool was used as the anode. In those experiments the concentration of uranium in liquid cadmium was maintained to be approximately 2 wt. %. The details of the electrodes and equipment used in these experimental studies were described earlier in the chapter 2. The vessel was heated using a split furnace. A PID controller was used for controlling the temperature. A glass tube containing Ag/1wt% AgCl in LiCl-KCl eutectic salt was used as the reference electrode.

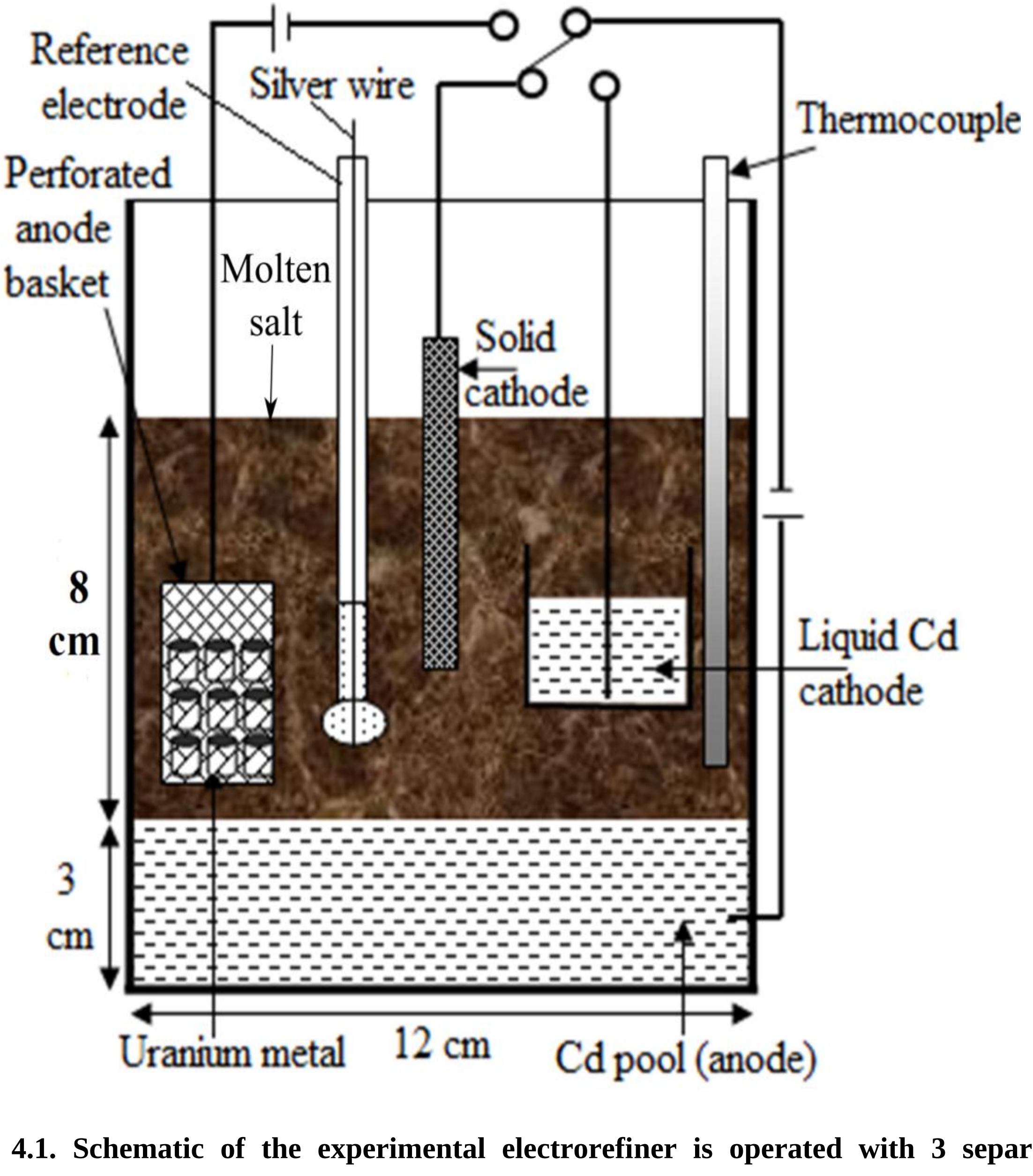

Fig. 4.1. Schematic of the experimental electrorefiner is operated with 3 separate arrangements (a) Cd pool anode – solid cathode (b) Cd pool anode -liquid Cd cathode (c) Perforated anode basket – solid cathode.

4.3. Model calculation

In the present study, a 2D/2D axisymmetric model was developed for the electrotransport of uranium from liquid Cd/perforated basket anode to solid/Cd cathode and the current density distribution profile was computed using COMSOL Multiphysics [67].

The current distribution in an electrolyte is dictated by the transport of charged ions in the electrolyte of uniform composition and that in an electrode is computed using ohm's law in combination with a charge balance. Using this interface, the ohmic losses were estimated using simplified models of electrochemistry and the interface yields a good estimate of the current and potential distribution in a cell showing that the activation and mass transport losses are very small compared to the ohmic losses. The general equation for primary current distribution interface model is given as:

$$\nabla . i_k = Q_k \quad \text{and} \quad i_k = - \ \sigma_k \nabla \emptyset_k \qquad (4.1)$$

where, Q_k denotes a general source term, k denotes an index that is l for the electrolyte or s for the electrode, σ_k denotes the conductivity (SI unit: S/m) and $\emptyset_k$ the potential (SI unit: V).

The interfaces define two dependent variables, one for the potential in the electrolyte and one for the electric potential in the electrode. The conduction of current in the electrolyte is assumed to take place through transport of ions, while electrons conduct the current in the electrode. For an electrolyte of uniform composition, the sum of the fluxes of all charged species yields the following expression for the current density vector:

$$i_l = - \ \sigma_l \nabla \emptyset_l \qquad (4.2)$$

where σ_l , denotes the electrolyte conductivity and $\emptyset_l$, the potential in the electrolyte. An analogous equation is defined by the interfaces for current conduction in the electrodes:

$$i_s = - \sigma_s \nabla \emptyset_s \tag{4.3}$$

The difference between the interfaces lies in the description of the electrochemical reactions. The rate of electrochemical reactions can be described by relating it to the activation overpotential. For an electrode reaction with index *m*, the activation overpotential, denoted $\eta_{m,}$ is the following:

$$\eta_m = \phi_s - \phi_l - E_{eq,m} \tag{4.4}$$

where, $E_{eq,m}$denotes the equilibrium potential for the reaction *m*. In the primary current distribution interface, the electrochemical reactions are assumed to be fast enough so that their influences on the losses in the cell are negligible. Consequently, the activation overpotential, η_m, in this interface is equal to zero. Therefore, the difference between the potentials of the electrolyte and the electrode, measured against a reference, is always equal to unity at equilibrium, $E_{eq,\,m}$. The total current I is calculated by integrating the current density i. The cell resistance R is calculated from the total current and applied cell voltage V as follows

$$R = V/I \tag{4.5}$$

4. 4. Results and discussion

In the present study, the effect of electrode configuration on the potential and current distribution in a molten salt electrorefiner was studied for uranium electrorefining.

4.4.1. Parallel and staggered arrangements of electrodes

A perforated anode basket loaded with uranium rod pieces and a SS 430 solid rod were used as anode and solid cathode respectively. The basket was dipped in the electrolyte such that uranium rods in the basket were fully immersed. The diameter and the height of the uranium rods in the electrolyte were 2 cm each. The area of the uranium rods, rather than that of the perforated anode basket were taken as the surface area of anode. The diameter and the height of the solid cathode immersed in the electrolyte were 0.8 and 2 cm respectively.

In this study, a pair of perforated anode baskets and a pair of solid cathodes were configured in two different arrangements (parallel and staggered) to study the effect of these configurations on the potential and current profiles in the electrorefiner. As mentioned earlier, the dimensions of the two anodes were similar, as were those of the two cathodes. The centre to centre distance between the four electrodes in each direction was maintained at 42 mm in both the parallel and staggered arrangements. A 2D geometry was created for the electrotransport of uranium from the perforated anode basket to the solid cathode and the primary current distribution was computed. The value of the potential at the surface of the perforated anode basket was arbitrarily set to be -1.2 V, the value measured for a U/U^{3+} electrode usually with respect to an $Ag/Ag+$ reference electrode. A cell voltage of 0.2 V was imposed by setting the cathode potential to be -1.4 V. The potential and current density distributions were evaluated for both the electrode configurations. The potential distributions from anode to cathode for the two arrangements are shown in Fig. 4.2. It can be seen that in the parallel arrangement, only one side of the electrodes is effective, whereas in the staggered arrangement, two sides of the electrodes are effective. In the parallel arrangement of electrodes, the potential was distributed only in the space between the electrodes and electrodeposition occurred only on one face of the cathodes. The current distribution was also observed between one anode and one cathode facing each other in the parallel arrangement as shown in Fig. 4.3, whereas for the staggered arrangement, current distribution was observed from all the four faces of the anodes to all the sides of the two cathodes. The calculated cell resistance was 0.33 ohm/cm for the parallel arrangement and it dropped to 0.18 ohm/cm for the staggered arrangement which can be expected from the differences in the current distribution patterns for the two configurations. The cell resistances were calculated using the model and compared with the present experimental values in Table 4.1.

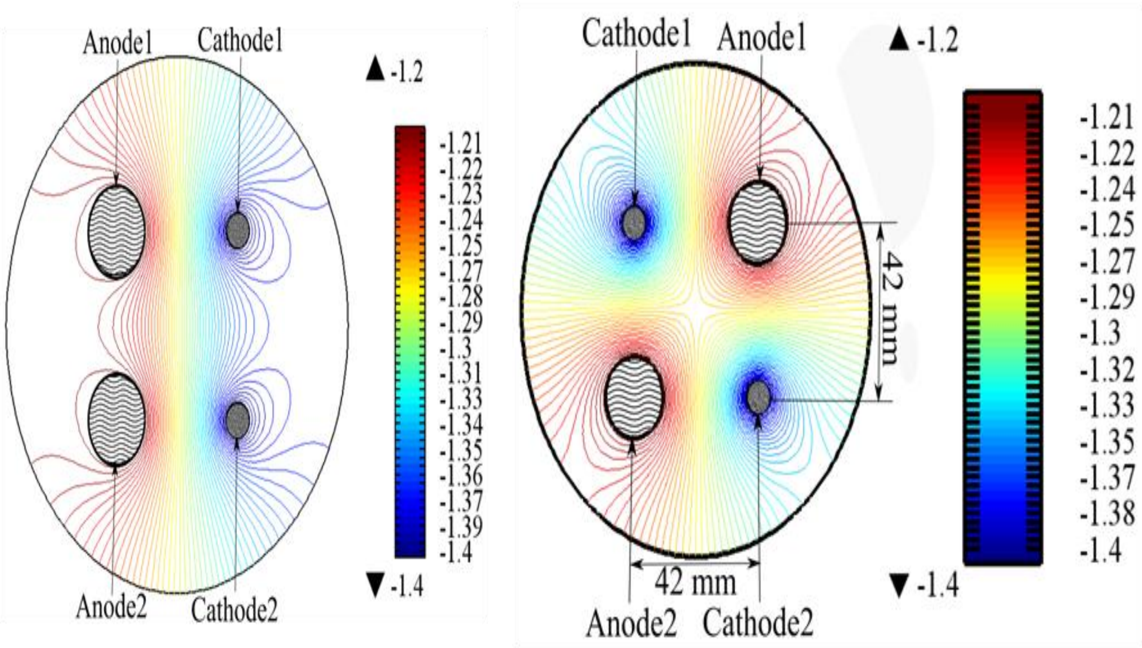

(a) Parallel arrangement **(b) Staggered arrangement**

Fig. 4.2. Potential distributions for the parallel and staggered arrangement of electrodes

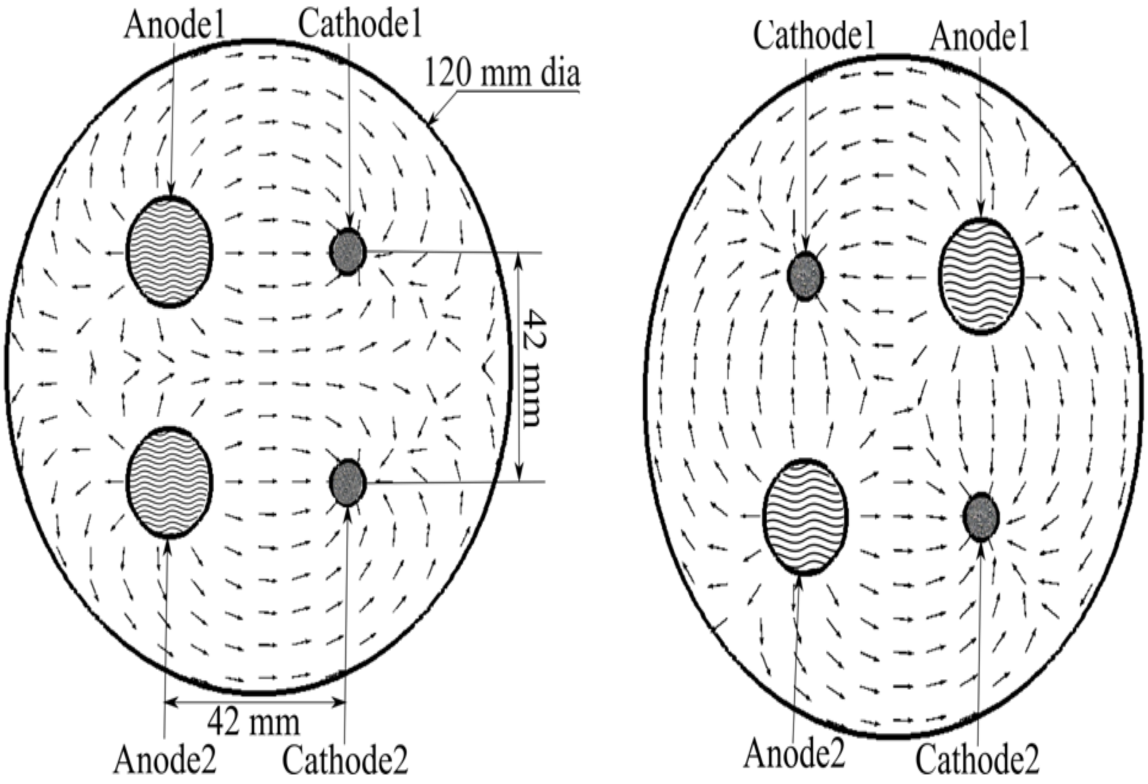

(a) Parallel arrangement **(b) Staggered arrangement**

Fig. 4.3. Current density distributions of parallel and staggered arrangement

As can be seen, both the calculated and experimental values are in good agreement within ~ 10% for the staggered arrangement and ~20% for the parallel arrangement. Computations have been carried out in the present work using COMSOL Multiphysics for the experimental cells of described by Kobayashi et al. [83] for which they have also reported computed values, although using a different modeling approach. The two sets of computed values are compared in Table 4.2. As can be seen, there is good agreement between the two sets of computed values.

Table 4.1. Comparison of experimental cell resistance with the computed values from the present work

Configuration	Parameter	Experimental	Computed
Parallel arrangement	Cell voltage, V	0.2	0.2
	Total current, A	0.49	0.61
	Cell resistance, ohm	0.41	0.33
Staggered arrangement	Cell voltage, V	0.2	0.2
	Total current, A	1.01	1.09
	Cell resistance, ohm	0.20	0.18

Table 4.2. Comparison of present computed values for cell resistance with literature data

Configuration	Parameter	Computed values of Kobayashi et al. [83]	Computed values from present study
Parallel arrangement	Cell voltage, V	0.4	0.4
	Total current, A	2.56	2.54
	Cell resistance, ohm	0.16	0.16
Staggered arrangement	Cell voltage, V	0.4	0.4
	Total current, A	4.24	4.26
	Cell resistance, ohm	0.09	0.09

4.4.2. Effect of variation of the distance between the electrodes

A 2D geometry was created and the primary current distribution for electrotransport of uranium from perforated anode basket to solid cathode was computed with various distances (2-8 cm) of cathode. The value of the potential at the surface of the perforated anode basket was arbitrarily set to be -1.2 V, the value measured usually for U/U^{3+} electrode with respect to a Ag/Ag+ reference electrode. A cell voltage of 0.2 V was imposed by setting the cathode potential to be -1.4 V. The potential and current density distributions were calculated for various center to center distances of cathode from fixed position of anode. The computed potential and current density distributions are shown in Fig. 4.4. As can be seen in the figure, the potential and current distributions were similar to that observed for the parallel arrangement of electrodes discussed in the section 4.1. It is observed from Fig. 4.5 that the cell resistance increased with increase in center to center distance between the electrodes.

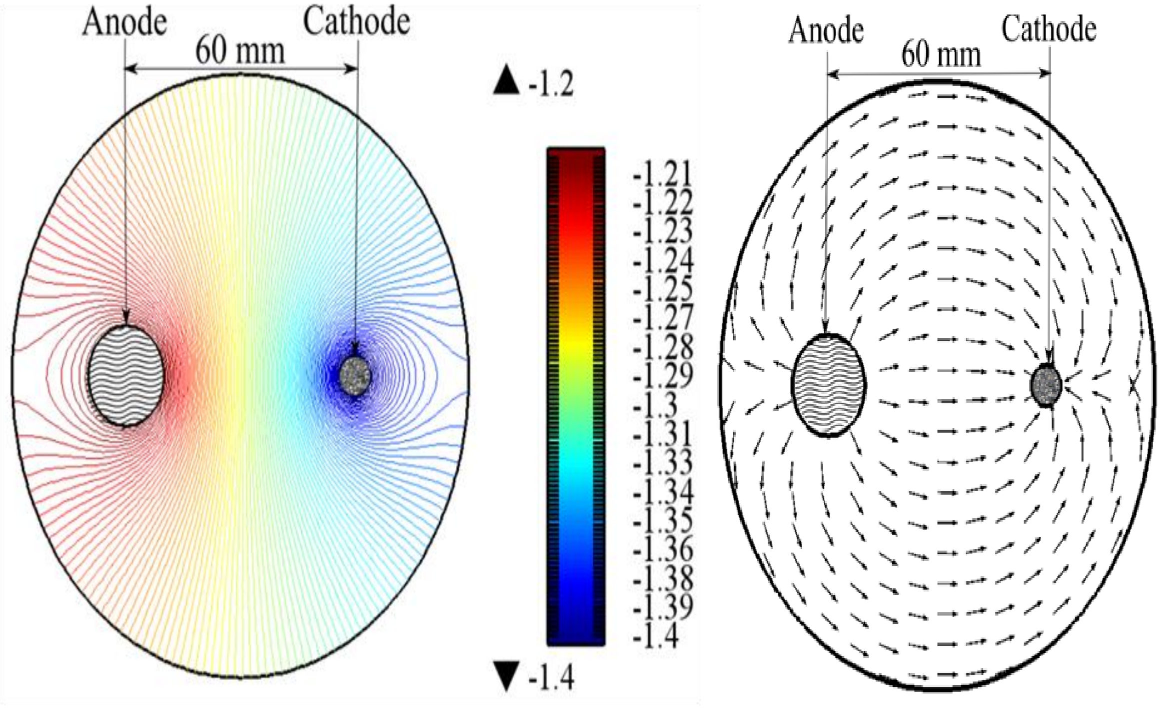

(a) Potential distribution **(b) Current density distribution**

Fig. 4.4. Potential and current density distributions for a distance of 60 mm between the anode and cathode

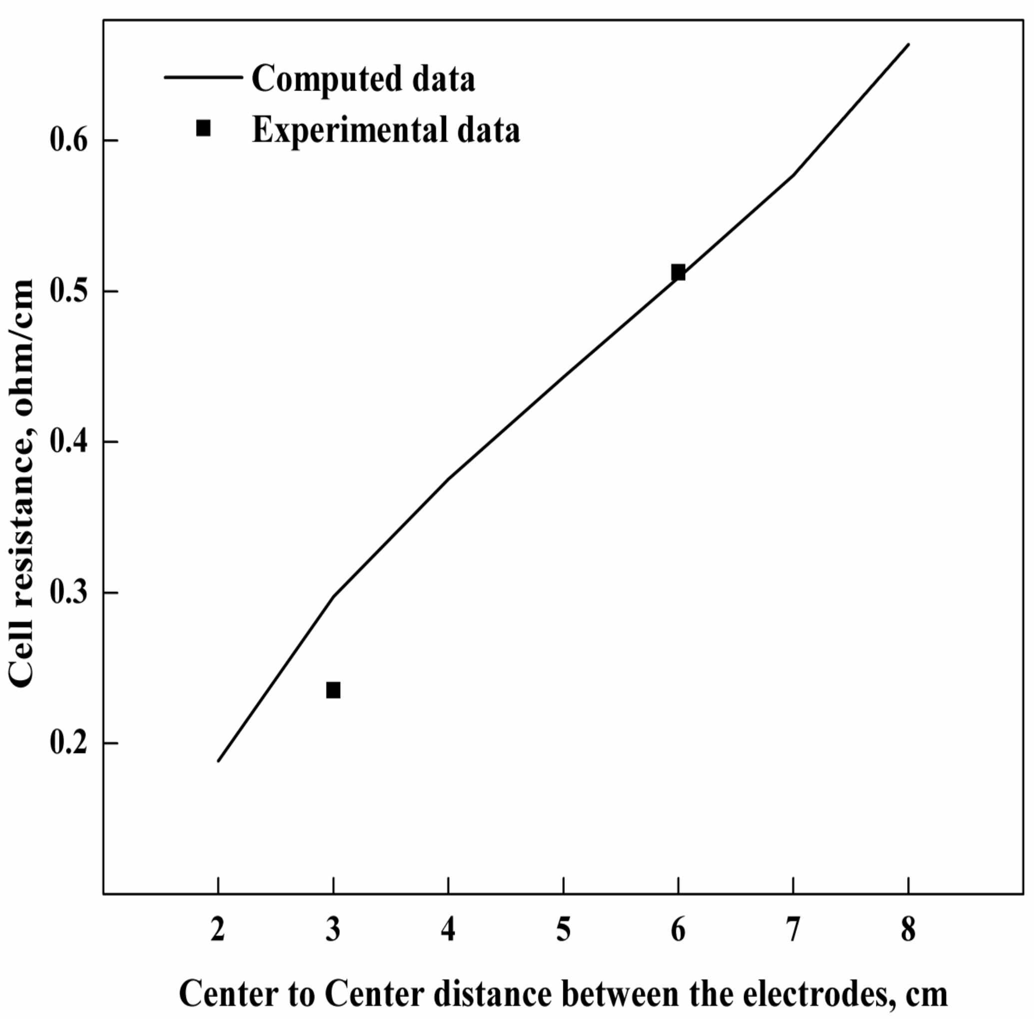

Fig. 4.5. Variation of cell resistance as a function of distance between the electrodes

The distance between the anode and cathode was kept as 3 and 6 cm and the effect of these two distances on the electrodeposition of uranium was also studied experimentally. The diameter and the height of the anode (uranium rods) in the electrolyte region were 2 cm and 2.5 cm respectively. The diameter and the height of the solid cathode in the electrolyte region were 0.8 cm and 2 cm respectively. The computed cell resistance using the model is in very good agreement with the experimentally (present study) determined value in one case and about 30% higher in another case, as shown in Fig. 4.5. No literature data are available for comparing our present results.

4.4.3. Effect of having an insulating disc at the bottom of the solid cathode

Electrodeposition of uranium was also investigated with and without an insulating ceramic disc at the bottom of the solid cathode. In these experiments, liquid cadmium containing a known amount of uranium was used as the anode. The height and diameter of the solid cathode immersed in the electrolyte salt region were 4 and 0.8 cm, respectively. The thickness and diameter of the ceramic disc were 1.2 and 0.3 cm, respectively. The purpose of the insulation is to avoid the growth of the dendrite deposit at the bottom of the solid cathode, which this is likely to fall away from the cathode. Also, the deposit could extend up to the liquid cadmium anode, thus shorting the cell. With these dimensions, a 2D axisymmetric model was developed using COMSOL Multiphysics. Due to the symmetry in the electrochemical cell, a 2D axisymmetric model was chosen. The value of the potential at the surface of the Cd anode was arbitrarily set to be -1.1 V, as it was the value measured usually for a U(Cd)/U^{3+} by an Ag/Ag+ reference electrode. A cell voltage of 0.2 V was imposed by setting the cathode potential to be -1.3 V. The computed potential and current distributions for these two configurations (with and without insulation) of the solid cathode are compared as shown in Fig. 4.6 and Fig. 4.7 respectively. There is no significant difference in the potential and current profiles for the two configurations. The results show that the solid cathode with insulation had an advantage of avoiding uranium dendrites growth towards liquid cadmium anode without any significant loss in the performance, as the increase of cell resistance is only 11 % for the solid cathode with insulation compared to that without insulation. The calculated cell resistances for the solid cathode without insulation were comparable with the experimental results as shown in Table 4.3. The present computed cell resistance values are also compared with the experimental and computed results of

Kobayashi et al. for a cell of similar dimensions. (Table 4.4). As can be seen, both the sets of data are in good agreement with each other.

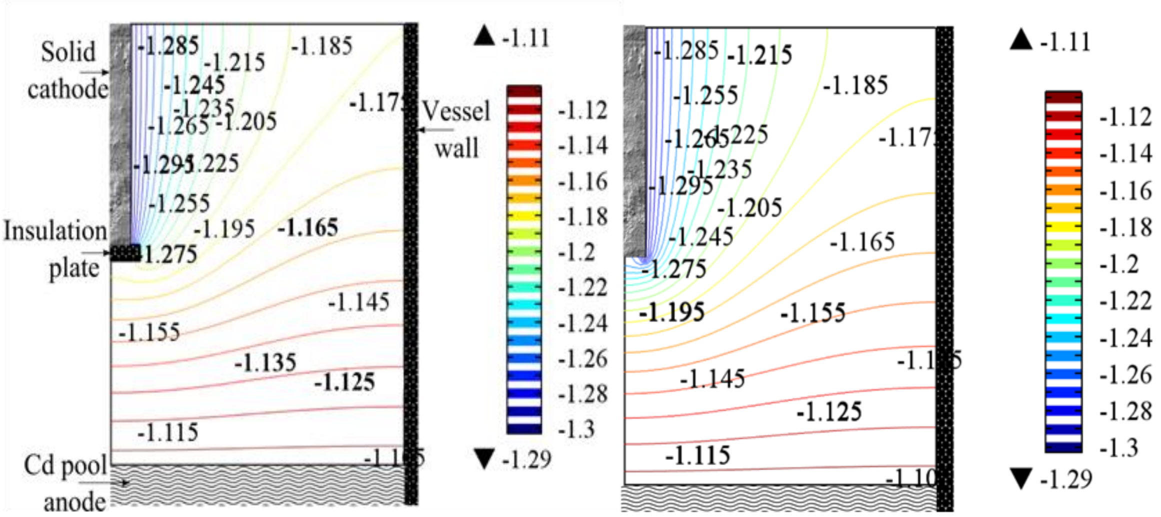

(a) (b)

Fig. 4.6. Potential distributions for the configurations (a) with and (b) without insulation at the bottom of the solid cathode

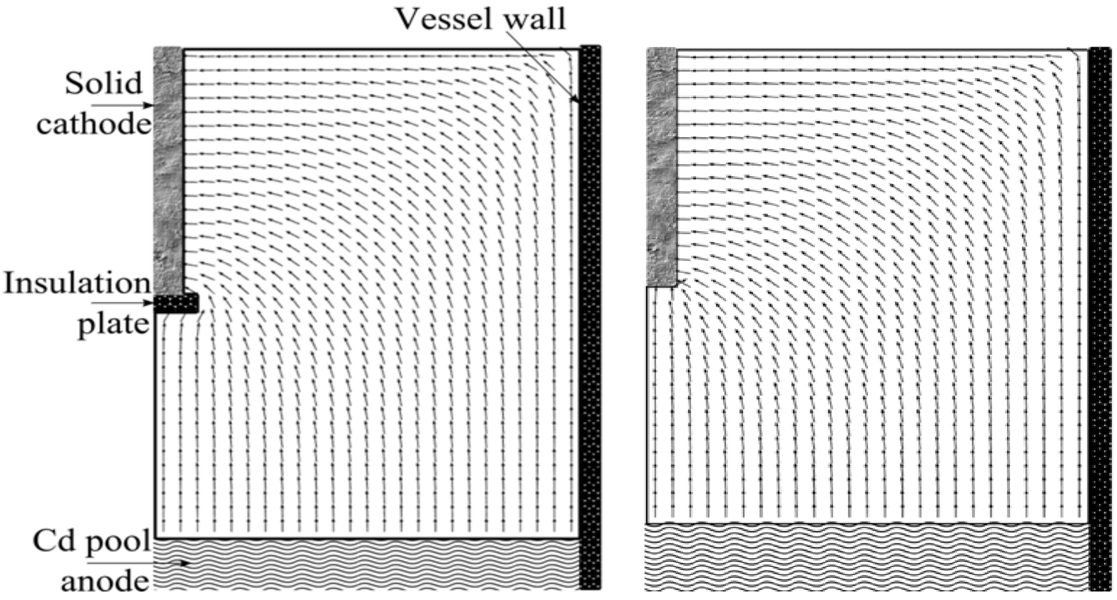

(a) (b)

Fig. 4.7. Current density distributions for the configurations (a) with and (b) without insulation at the bottom of the solid cathode

Table 4.3. Comparison the experimental cell resistance with the computed values from the present work

Configuration	Parameter	Experimental	Computed
Solid cathode without insulation	Cell voltage, V	0.2	0.2
	Total current, A	1.36	1.30
	Cell resistance, ohm	0.15	0.15
Solid cathode with insulation	Cell voltage, V	-	0.2
	Total current, A	-	1.17
	Cell resistance, ohm	-	0.17

Table 4.4 Comparison of computed cell resistance with experimental and computed literature data

Configuration	Parameter	Experimental data from literature [83]	Computed data from literature [83]	Computed data from present work
Solid cathode with insulation	Cell voltage, V	0.4	0.4	0.4
	Total current, A	50	46.89	46.64
	Cell resistance, ohm	0.008	0.0085	0.0085
Solid cathode without insulation	Cell voltage, V	-	0.4	0.4
	Total current, A	-	54.54	52.78
	Cell resistance, ohm	-	0.0073	0.0075

4.4.4. Effect of the design parameters of the Cd cathode

Liquid cadmium taken in an alumina crucible was used as the liquid cadmium cathode and the cadmium pool at the bottom of the electrorefiner was used as the anode, for these experiments. No uranium was added to the Cd cathode. As mentioned above, the concentration of uranium in the liquid cadmium anode was approximately 2 wt. %. Liquid cadmium cathode was immersed in the electrolyte salt up to known height (‘h_1’). The height of the empty space inside the alumina crucible above liquid cadmium was taken as ‘h_2’ and the surface area of the cadmium cathode was ‘S’. The value of the potential at the surface of the Cd anode was arbitrarily set to be -1.1 V, as mentioned above. A cell voltage of 0.2 V was imposed by setting the cathode potential to be -1.3 V. Electrotransport of uranium from liquid Cd anode to liquid Cd cathode was computed by changing the surface area of the Cd cathode for a 2D axisymmetric model developed for the above experimental conditions. The potential and current density distributions were calculated with various surface areas of the Cd cathode. The calculated potential and current density distributions are shown in Fig. 4.8. The cell resistances computed using the present model are compared with the experimental results in Table 4.5 for two sets of values of h_1, h_2 and S. The agreement between the computed and experimental values is very good. Computations were also carried out for the experimental conditions described by Kobayashi et al. and the results are compared in Table 4.6. It can be observed that with increase in the height of the immersed region (h_1) of the crucible, the cell resistance decreased due to the decrease in the distance between the anode and cathode. Increasing the height of empty space of crucible (h_2) resulted in an increase in the cell resistance and increasing the Cd cathode surface area leads to decrease in the cell resistance, as is expected. Further increase in the Cd cathode surface area would lead to polarization of the Cd anode. The 2D axisymmetric model was superimposed to 3D axis model and the computed potential distribution for the 3D axis model is shown in Fig. 4.9. That it can be extrapolated to 3D axis model is an additional advantage of 2D axisymmetric model.

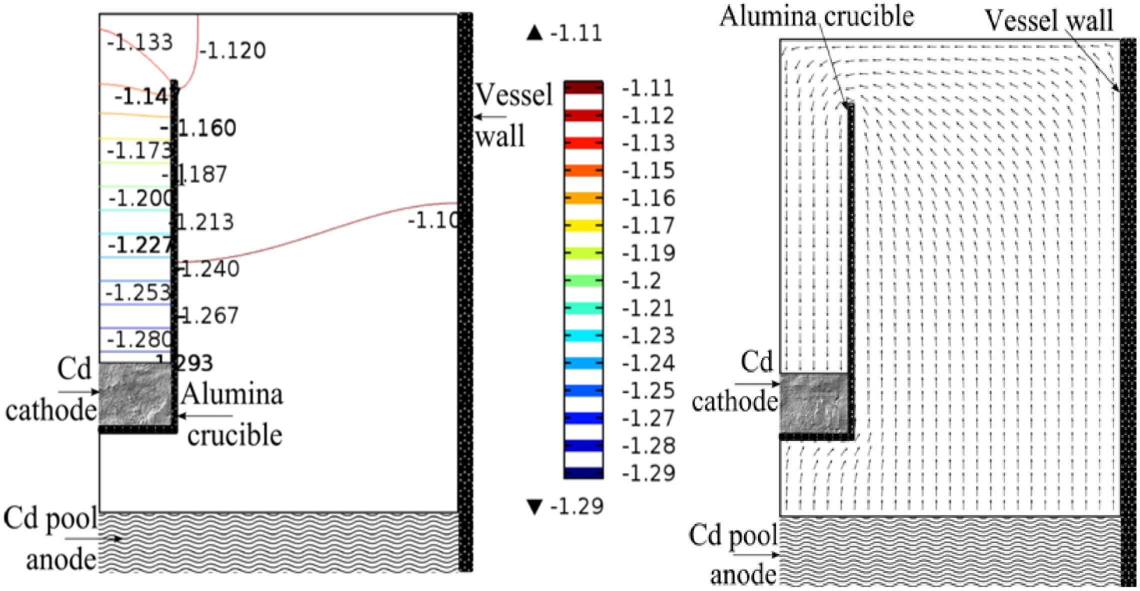

(a) (b)

Fig. 4.8. (a) Potential and (b) current density distributions in electrorefiner in which liquid Cd acts as the cathode and anode

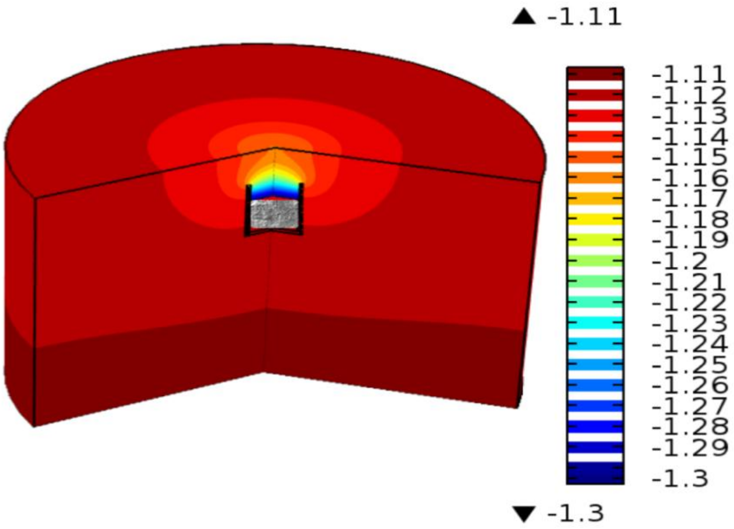

Fig. 4.9. Potential distribution in the electrorefiner with Cd cathode and Cd anode in 3D

Table 4.5. Comparison of experimentally measured cell resistance with computed ones as a function of the parameters of the Cd cathode

h_1,cm	h_2, cm	S, cm^2	Cell Resistance, ohm	
			Experimental	Computed
1	0.55	1.13	0.53	0.47
1	4.25	4.52	0.68	0.63

Table 4.6. **Comparison of cell resistance results for the various elevations of the Cd cathode**

h_1,cm	h_2, cm	S, cm^2	Cell Resistance, ohm		
			Experimental data of Kobayashi [83]	Computed data of Kobayashi [83]	Computed data of present work
1.82	10.67	160.6	4.40E-02	5.50E-02	5.46E-02
2.77	6.99	174.4	3.40E-02	4.01E-02	3.81E-02
5.31	2.54	198.6	2.20E-02	1.95E-02	2.12E-02
7.85	2.54	198.6	1.30E-02	1.77E-02	1.93E-02
1	2.54	198.6	---	2.76E-02	4.10E-02
3	2.54	198.6	---	2.19E-02	2.56E-02
5	2.54	198.6	---	1.97E-02	2.16E-02
7.85	2.54	198.6	---	1.77E-02	1.93E-02
7.85	2.54	198.6	---	1.77E-02	1.93E-02
7.85	5	198.6	---	2.53E-02	2.42E-02
7.85	7.54	198.6	---	3.16E-02	2.94E-02
7.85	10	198.6	---	3.81E-02	3.43E-02
7.85	2.54	50	---	4.78E-02	4.52E-02
7.85	2.54	100	---	2.89E-02	2.87E-02
7.85	2.54	150	---	2.19E-02	2.25E-02
7.85	2.54	198.6	---	1.77E-02	1.93E-02

4.4.5. Effect of solid cathode surface area

Different sizes of solid rods (SS430) were used as solid cathodes to find the effect of cathode surface area on electrodeposition of uranium. Liquid cadmium was used as anode with approximately 2 wt. % of uranium. A 2D axisymmetric model was developed with the same experimental and operating conditions. The potential and current density distributions were evaluated. The measured cell resistances are compared with experimental cell resistances in Fig. 4.10 which shows that the two sets of data are in good agreement except for one value wherein the experimental data is lower by 10%. It can be observed that with increase in the cathode surface area, the cell resistance decreased and current is maximized, which results in high throughput of electrorefiner. But further increase in surface area would lead to polarization of liquid Cd anode and electrotransport would be interrupted [84].

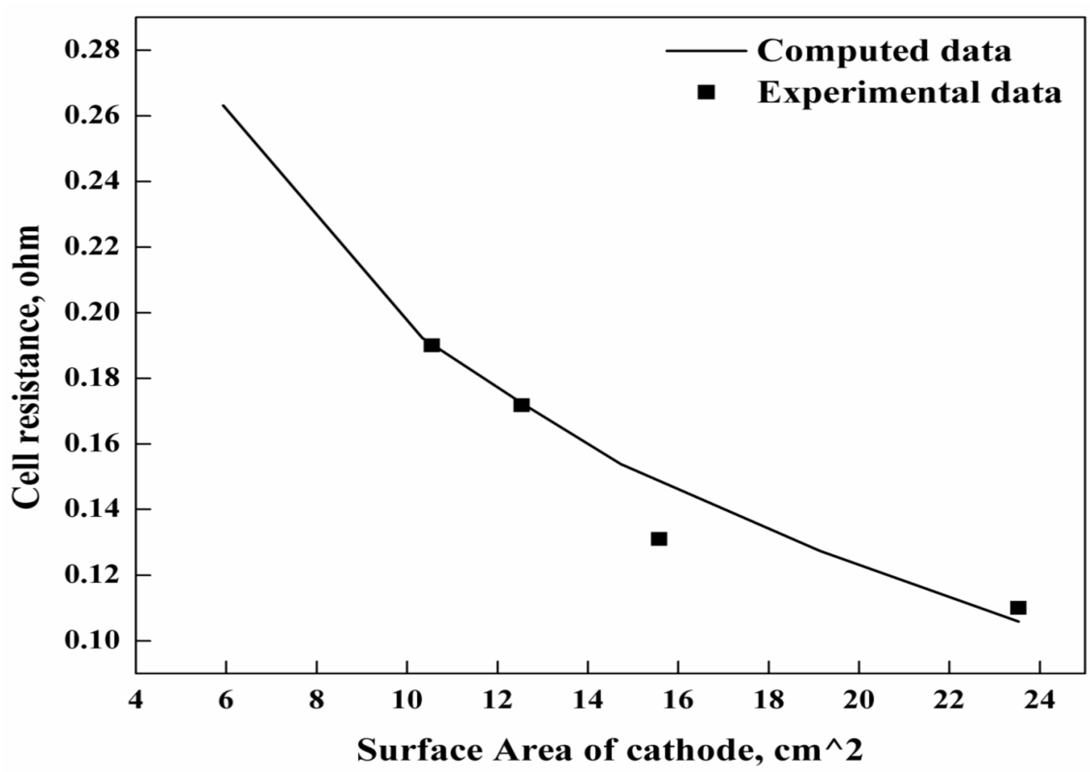

Fig. 4.10. Variation of cell resistance with cathode surface area computed data validated with experimental data

4.4.6. Cell resistance sensitivity study

A sensitivity analysis was performed to determine which of the two parameters, namely, the electrolyte conductivity and the cell resistance more significantly affect the results for the cell resistance. Computations were carried out with the conditions similar to that used in section 4.3 for the solid cathode without insulating disc at the bottom and liquid cadmium as anode. Each parameter was perturbed by ±10%, 20%, 30%, 40% and 50% of its original value and the cell resistance was recalculated for every case. The computed cell resistances are plotted in Fig. 4.11. It is observed that the cell resistance is more sensitive to the electrolyte conductivity and it is not affected by cell voltage.

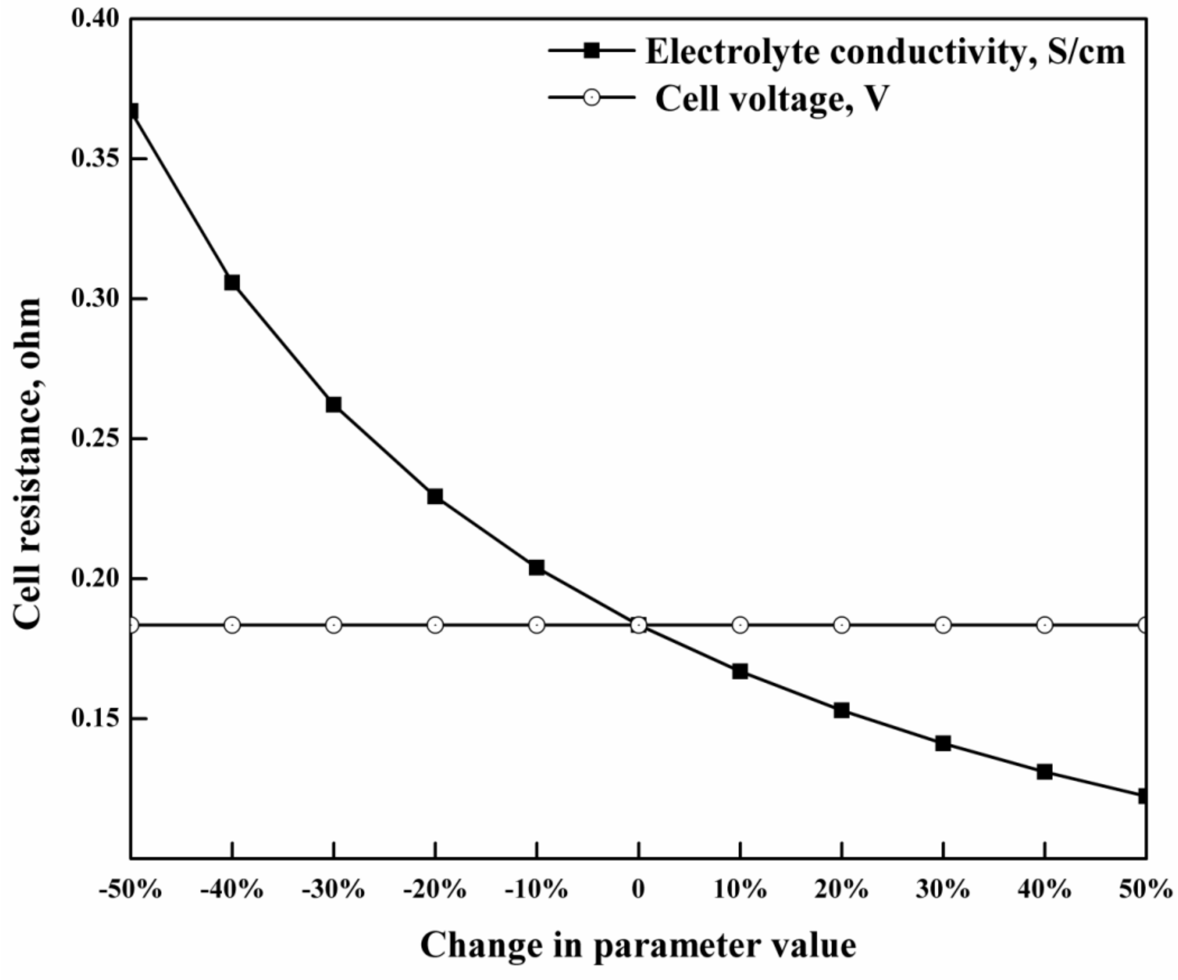

Fig. 4.11 The effect of changes in parameters on Cell resistance

4.5. Conclusions

The potential and current density distributions as well as the cell resistance in a molten salt electrorefiner were evaluated for various electrode configurations using COMSOL Multiphysics. Experiments were also conducted for various electrode configurations. A very good agreement between the experimental values and simulation results was found. The small deviation in the simulation results observed may be due to the assumption of axisymmetry of the electrochemical cell for some of the electrode configurations. The primary current distribution (piec) of electrochemistry module is used for simulating electrochemical reactions and the potential and current distributions in the electrochemical cell to evaluate the performance of molten salt electrorefiner. The cell resistance for a solid cathode having an insulation plate on its bottom was observed to be only 11 % more compared to that of a cathode without insulation. However an insulation plate at the bottom of the solid cathode was shown to be effective for preventing undesired growth of the dendritic uranium deposit. Staggered arrangement of electrodes resulted in broad potential distributions because of the increased effective electrode area compared to parallel arrangement of electrodes. Decrease in cell resistance of 49 % observed for staggered arrangement than that of parallel arrangement. Cell resistance increases with increase in the center to center distance between the electrodes. The cell resistance was evaluated for various elevations of Cd cathode. It was also observed that cell resistance decreases with increase in the solid cathode surface area resulting a high throughput electrorefiner. A sensitivity analysis was also performed to determine the parameter that more significantly affect the results of cell resistance. The two parameters that were varied were the electrolyte conductivity and the cell voltage. It is observed that the cell resistance is more sensitive to the electrolyte conductivity and there is no change in cell resistance with cell voltage. The calculated results from the model developed in this study are also comparable with literature data and found to be useful in interpreting the experimental data for improving the cell design.

Chapter 5

Development of the electrodeposition code using COMSOL Multiphysics for three different shapes of the cathode

5.1. Introduction

In this chapter, a code developed using COMSOL Multiphysics for the electrodeposition of uranium from a solid anode (uranium rods) to a solid cathode (SS430 rod) in an electrorefiner and the results obtained for the computations using three different shapes of cathodes are discussed. Electrorefining exeriments on U were also carried out using a solid anode and a solid cathode with three different shapes of cathodes and the results are comapred. The model was developed using the secondary, electrodeposition interface of electrochemistry module of COMSOL Multiphysics. The amount of uranium deposited ~~of uranium~~ on the three cathodes were computed and the results are compared with the experimentally obtained deposition results. The results are discussed in this chapter.

5.2. Experimental

A three-electrode electrochemical cell was used for all the experimental measurements. The three electrodes of different shapes were made of SS430. A perforated SS430 basket in which uranium was loaded was used as the anode. The three shapes of cathodes were shown in Fig. 5.1:

(1) Cylinder

(2) Rectangular prism

(3) Cruciform type

An Ag/AgCl couple was used as the reference electrode. It consisted of a Pyrex tube with a very thin bottom in which the LiCl–KCl eutectic mixture containing 1wt% AgCl was placed and an Ag wire (dia. = 1.5 mm) was immersed in the salt. A SS430 (ID= 120 mm &

height 190 mm) crucible was used to contain the LiCl–KCl eutectic salt, as mentioned earlier in chapter 2. All the electrochemical experiments were carried out at 773 K in a glove box having high purity Ar atmosphere. The temperature of the molten salt was measured with ±3.0 K accuracy using a calibrated Chromel–Alumel thermocouple.

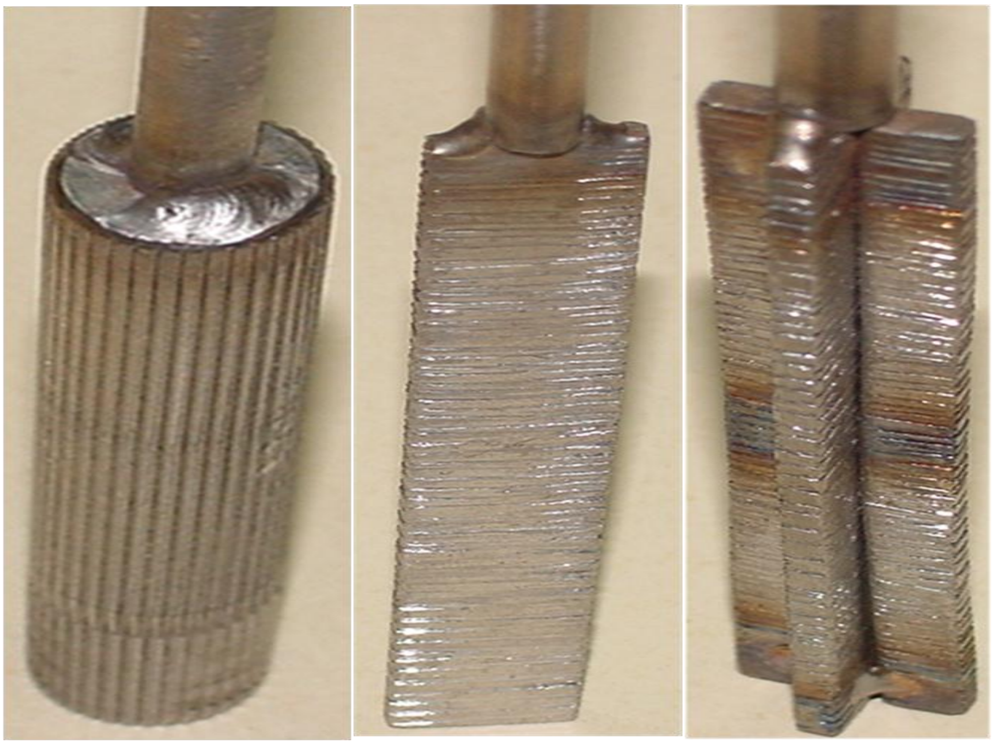

1. Cylindrical shape **2. Rectangular prism** **3. Cruciform shape**

Fig. 5.1. cathodes used for electrorefining

5.3. Results and discussion

In the present study, simulation of the electrotransport of uranium from the perforated anode basket to three cathodes of different shapes were performed using the secondary, electrodeposition interface of electrochemistry module of the COMSOL Multiphysics. At first, three cahodes of diffferent shapes with equal surface area were considered. The immersion heights in the LiCl-KCl electrolyt was varied for the different cathodes , as given in Table 5.1 so as to equalise their surface area. The perforated anode basket in which uranium rods were present was taken as the anode. A 3D geometry was created and the electrotransport of uranium was simulated. The value of the potential at the surface of the perforated anode basket was arbitrarily set to be -1.2 V, as it was the value of the U electrode measured with respect to an Ag/Ag+ reference electrode. A cell voltage of 0.1 V was imposed by setting the cathode potential to be -1.3 V. The potential and current density distributions were calculated for the three cathodes. The input parameters used in this study are also shown in Table 5.1. Multimode electrochemical detection method of DC amperometry was used to perform the electrodeposition experiments under the same conditions used in the simulation. The uranium concentration in the electrolyte salt was measured as 5 wt. % using Davis and Gray method. The potential and the current distribution profiles across the electrorefiner were computed. From the current profile computed, the amount of measured coulombs passed was calculated and assuming 100% current efficiency, the amount of U deposited on each cathode was also calculated. The amounts of coulombs passed and the calculated amounts of deposit on each cathode are also given in Table 5.2. The amounts of coulombs passed, the total amount of deposit (including occluded salt) and the amount of U in the deposit obtained in the electrorefining experiments carried out potentiostatically under similar conditions used for simulation are given in Table 5.3. It was assumed that the deposit contains 30% of salt occluded with uranium. Comparing Table 5.2 and 5.3, it can be seen that the amounts of coulombs passed obtained by computation is only 0.5 to 2% higher than the experimental ones, confirming the efficacy of the simulation. The experimentally determined amount of U deposited is ~ 5-6% less than the calculated ones. The difference between the calculated and experimental results is higher in this case due to the experimental current efficiency being less than 100%, which was assumed for simulation. The deposits on the cathodes from the experimental runs are shown in Fig.5.2.

Table 5.1. Parameters and thermodynamic data used in model calculation

Parameter	Value
Anode potential	-1.2 V vs Ag/AgCl
Cathode potential	-1.3 V vs Ag/AgCl
Electrolyte conductivity	-1.9 S/cm [77]
Exchange Current density	1 A/cm^2 [65]
Anodic transfer Coefficient	0.5 [64]
Cathodic transfer coefficient	0.5 [64]
Operating temperature	773 K [65]
Diffusion coefficient of U in molten salt	$1.4*10^{-5}$ cm^2 / s [78, 79]
Charge number	3
Faraday constant	96485 C / mol
Universal gas Constant	8.314 J / (mol K)
Molten salt (LiCl-KCl) volume	892 ml
Molten salt weight	1445 g

The evaluated potential distributions for the three cathodes are shown in Fig. 5.3. The model also evaluated the change in the thickness of the deposit during electrotransport of uranium. The thicknesses of the cathode deposit along the length of the three cathodes are shown in Fig. 5.4 (a) to (c). More uniform thickness distribution was observed for cylindrical cathode compared to the other two. It was also observed that the thickness was high at the edges which are nearer to the anode surface.

As the second approach, three cathodes of different shapes, but equal equal heights were taken. The suface areas and the immersion heights of the three electrodes are given in Table 5.4. The same exercise as the first approach was carried out. Calculated amounts of coulombs passed during electrotransport of uranium and the amount of U deposited on the cathodes are given in Table 5.4. More deposition was observed for the cruciform cathode compared to the other two. It is in the expected lines, as the available surface area of this cathode is more compared to other two. But the cruciform shaped cathode poses a practical problem by making it more difficult to scrape the deposit.

The potential distribution for cylindrical cathode is shown as a slice surface in Fig. 5.5. Overpotential and normalized current densities during electrodeposition obtained by simulation for the cylindrical cathode are shown in Fig. 5.6 and 5.7. It was observed that overpotential is zero (negligible) for primary current distribution and the secondary and tertiary current distributions show almost equal overpotential along the cathode except at the edges of cathode which are nearer to the anode (was high for tertiary current distribution. In Fig. 5.7, it can be seen that the current density is very uniform along the length except at the edges of the cylindrical cathode surface where current density was significantly high.

Table 5.2. Amount of uranium deposited on three cathodes arrived at by computation

Model	Cathode type	Surface area, mm^2	Immersed height, mm	Charge passed, Coulombs	Uranium deposit, g
Run-1	Cylindrical	1030	20	20524	16.87
Run2	Rectangular prism	1030	29.05	20341	16.72
Run-3	Stirrer shape	1030	17.05	20249	16.65

Table 5.3. Amount of uranium deposited on three different shapes of the cathode with equal surface by experimental results

Experiment	Cathode type	Surface area, mm^2	Immersion height, mm	Charge passed, Coulombs	Uranium deposit with salt, g	Uranium deposit, g (after removal of 30% salt)	Computed amount of Uranium deposit, g
Exp-1	Cylindrical	1030	20	19799	22.77	15.94	16.28
Exp-2	Rectangular prism	1062	30	20225	22.52	15.76	16.63
Exp-3	Stirrer shape	1027	17	20196	22.22	15.55	16.61

Table 5.4. Amounts of uranium deposited on the three cathodes of different shapes but equal height by secondary electrodeposition model

Model	Cathode Shape	Surface area, mm^2	Immersed height, mm	Charge passed, Coulombs	Uranium deposit, g
Run-1	Cylindrical	1030	20	20524	16.87
Run-4	Rectangular prism	722	20	19387	15.94
Run-5	Cruciform	1195	20	22176	18.23

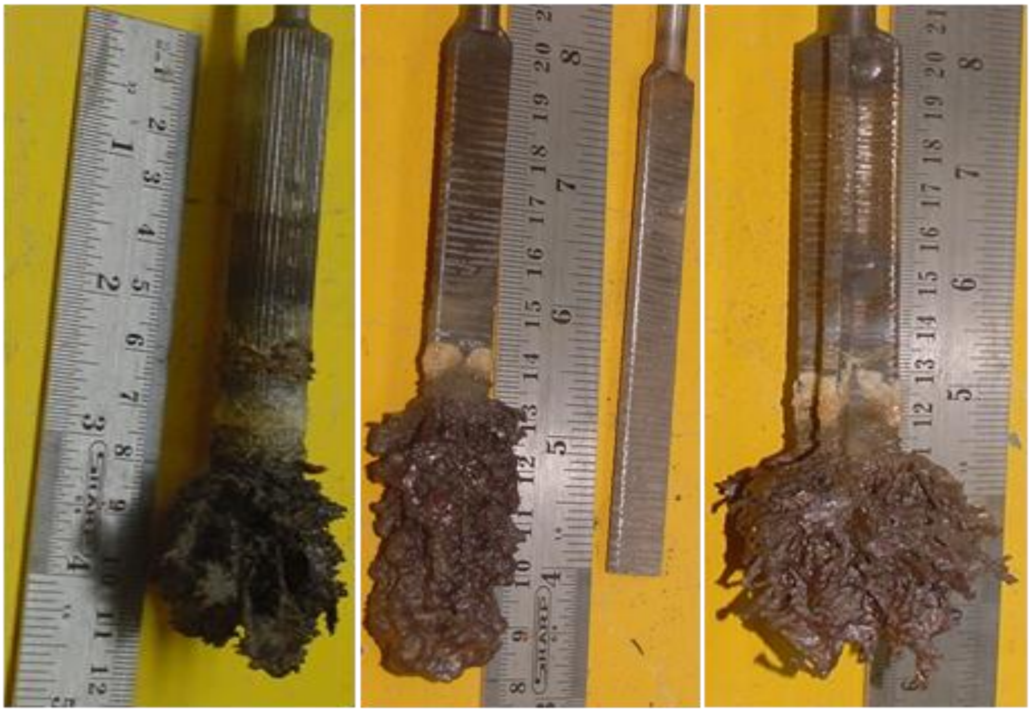

Fig. 5.2. The deposits on the (a) Cylindrical (b) Rectangular prism and (c) Cruciform cathodes

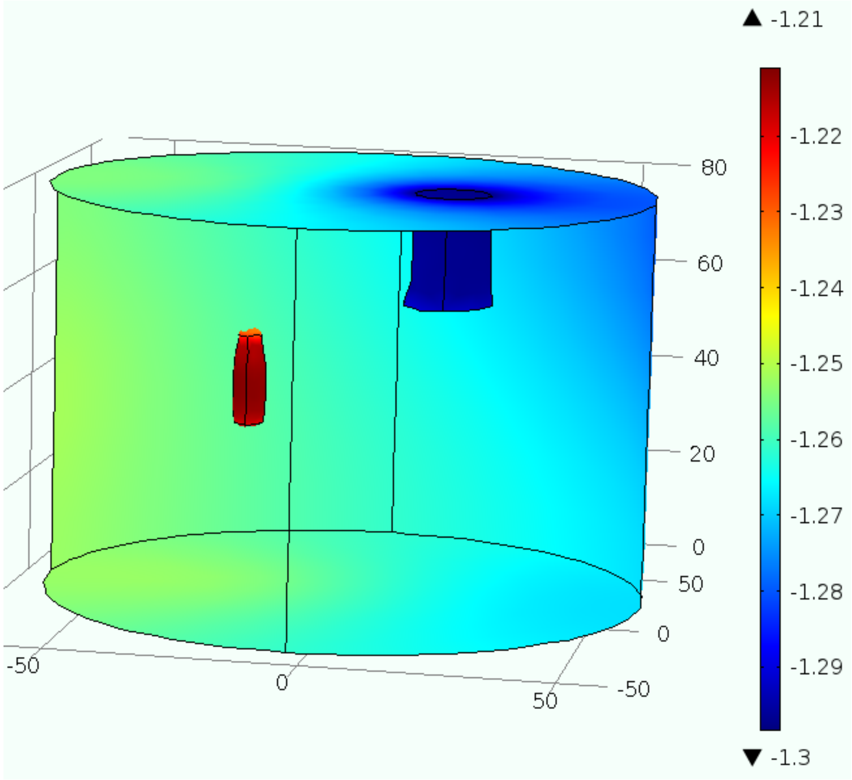

(a) Potential distribution of solid cathode of cylindrical shape

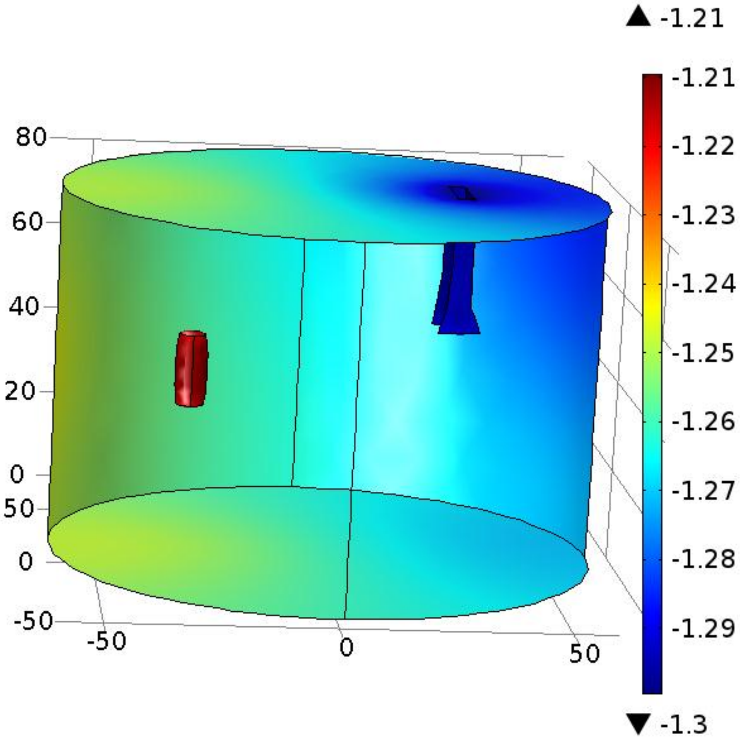

(b) Potential distribution of solid cathode of Rectangular prism

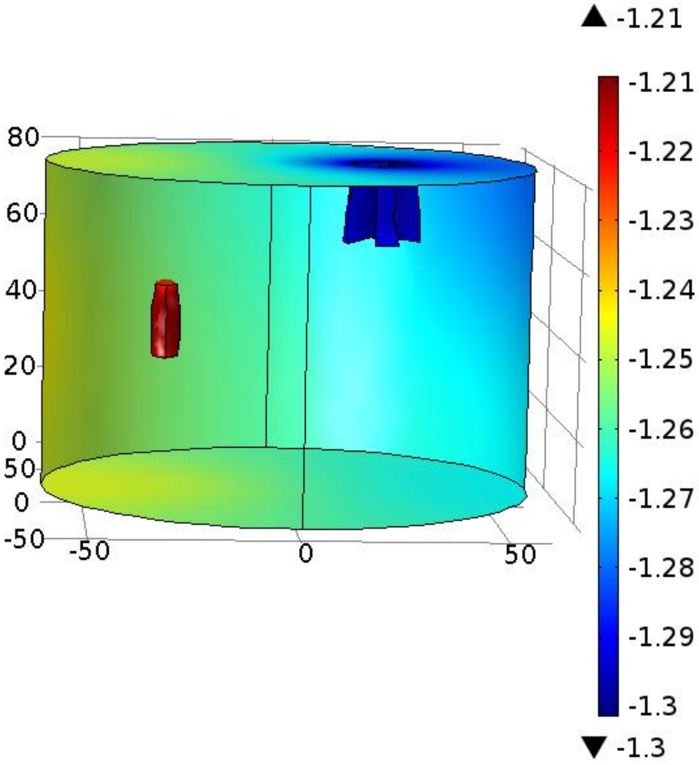

(c) Potential distribution of solid cathode of cruciform shape

Fig. 5.3. Potential distributions along (a) Cylindrical (b) Rectangular prism and (c) Cruciform cathodes

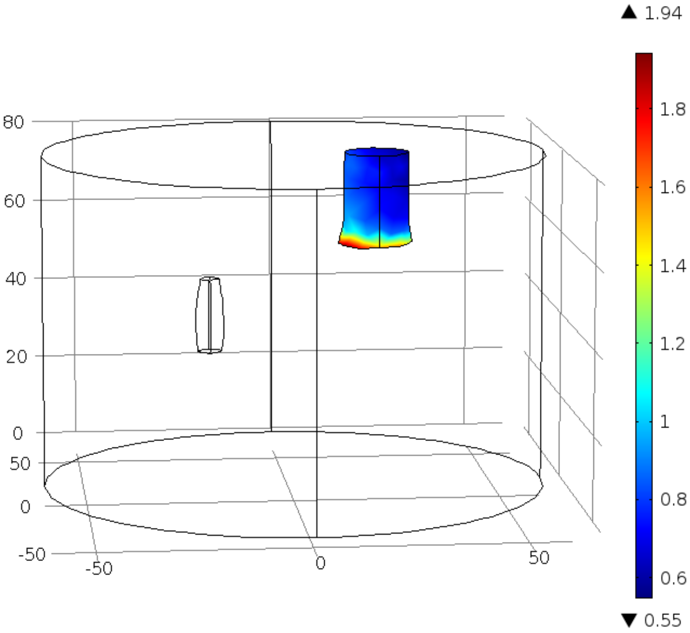

(a) Deposit thickness on the cylindrical cathode

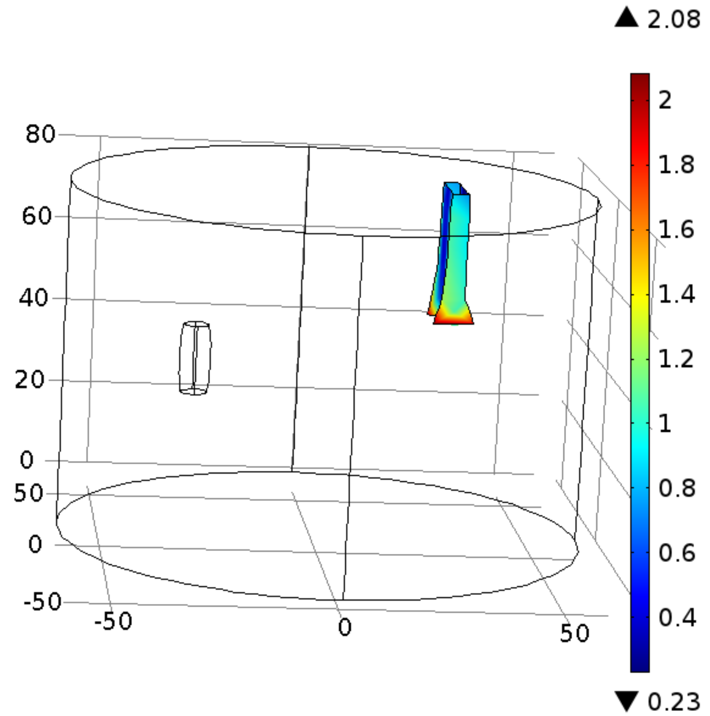

(b) Deposit thickness on the rectangular prism cathode

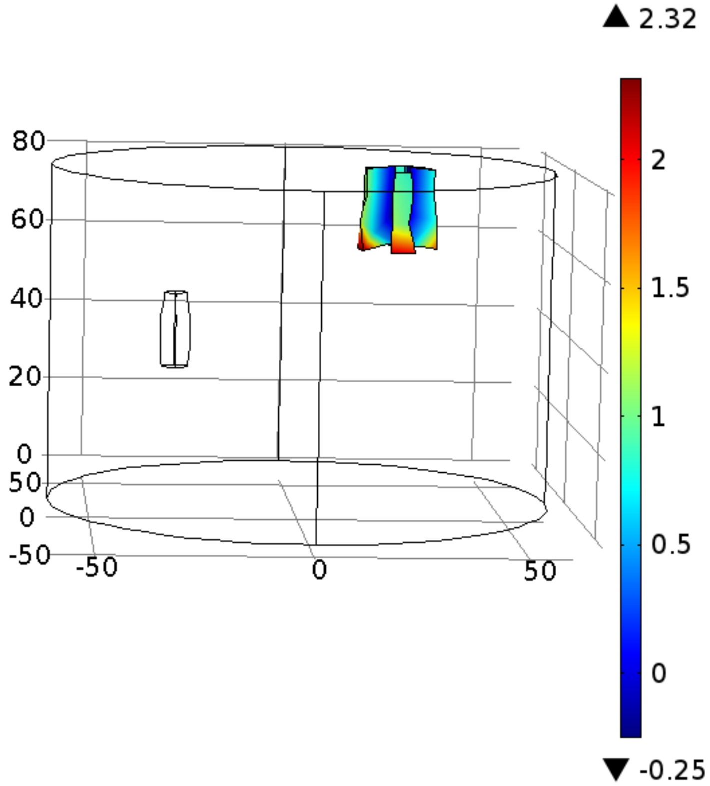

(c) Deposit thickness on cruciform cathode

Fig. 5.4. Deposit thickness of (a) Cylindrical (b) Rectangular prism and (c) Cruciform cathodes

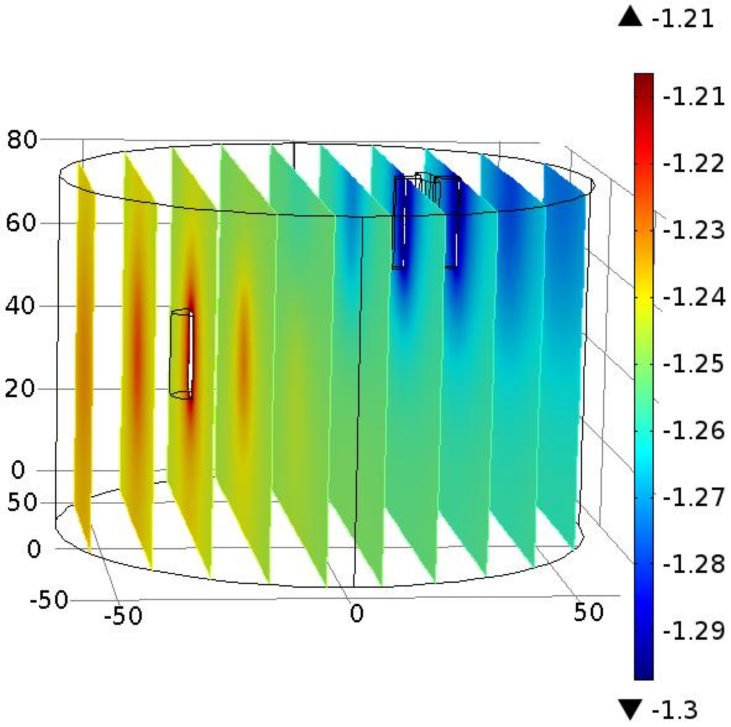

Fig. 5.5. Potential distribution along the cylindrical cathode as a slice surface

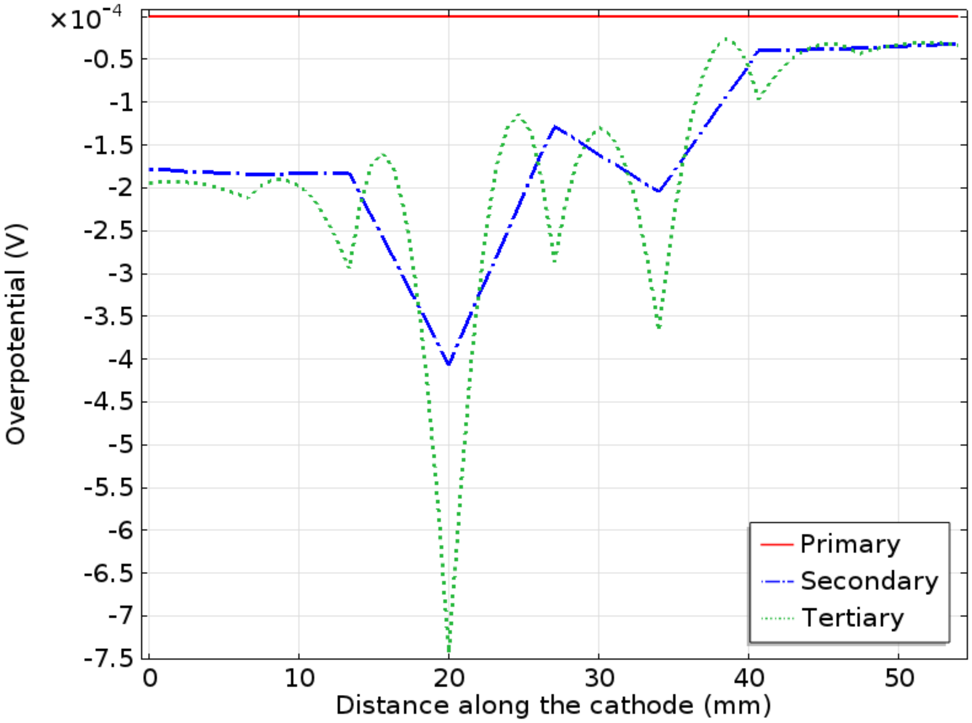

Fig. 5.6. Calculated overpotential vs distance along the cylindrical cathode

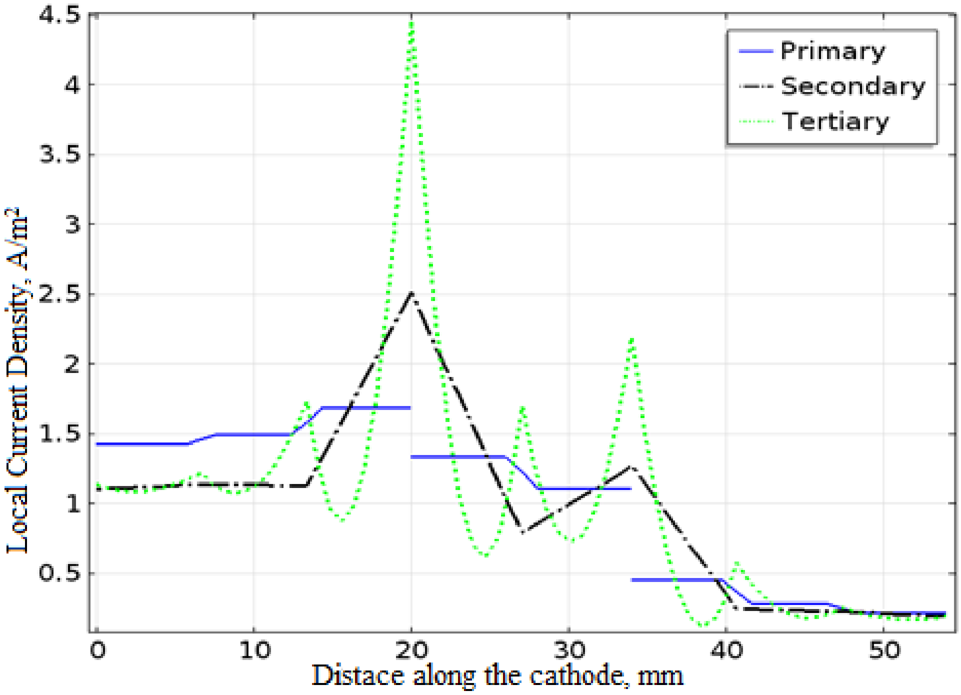

Fig. 5.7. Local current density distribution vs distance along the cylindrical cathode

5.4. Conclusions

A code was developed for electrorefining with a three cathodes of different shapes and with solid anode. The computations were carried out for the electrotransport of uranium from solid anode to solid cathode using the secondary, electrodeposition interface of electrochemistry module of COMSOL Multiphysics. The shape of the cathode plays an important role in electrodeposition in terms of uniform/non uniform potential and current density distributions, thickness of deposit, etc. There was very good agreement between the experimental values and simulation results for electrorefining with cathodes of equal surface area. Similar computations were also carried out for the cathodes of three different shapes and equal heights of immersion in the electrolyte.

Chapter 6

Summary, Conclusions and scope for future work

6.1. Summary and Conclusions

Molten salt electrorefining is the key step of the pyrochemical reprocessing process flow sheet for metallic fuels wherein the actinide fuel materials, U and Pu are separated from the fission products in the spent fuel to refabricate the fuel. Development of the metal fuel cycle is in progress in our Institute. Scaled up process studies are needed to develop the industrial process. In the design of an engineering scale high throughput electrorefiner, the following factors play a very important role

- the distance between the electrodes
- surface area
- Use of multiple electrodes and their mutual arrangement in the electrorefiner
- Shapes of the electrodes

All the above factors need to be optimized for designing an electrorefiner. In this thesis, modeling studies were carried out on the effect of the above parameters in the performance of a molten salt electrorefiner. The results of these studies are summarized as follows.

6.1.1. Modelling the electrotransport of U and Pu

The electrotransport of uranium from a liquid cadmium anode through molten LiCl-KCl eutectic salt to solid cathode was modeled using the three modules of COMSOL Multiphysics. They are

(1) The secondary current distribution (siec) interface of electrochemistry module is used for simulating electrochemical reactions at the electrode surfaces and the potential and current density distribution in the electrochemical cell.

(2) Transport of diluted species (tds) interface of chemical species transport module is used for simulating the mass transfer of each species through the diffusion layer.

(3) ODE and DAE interfaces (Global ODE and DAEs (ge)) of Mathematics module is used for solving the material balance equation for each species.

The above three modules were coupled to each other and solved simultaneously. A 2D axisymmetric model was used due to symmetry in the electrochemical cell. Mapped mesh (user-controlled mesh) was used in the diffusion layer region whereas triangular mesh was used in the other regions. The number of mesh elements was varied from 12213 to 139633 (12213, 18278, 105465 and 139633). It was observed that, the time required for solving was higher by 300% with physics controlled mesh elements of 105465 compared to that with the user controlled mesh elements of 12213.

The present numerical model for molten salt electrorefining process is based on the following important assumptions:

- ✓ The molten salt phase and liquid cadmium phase are thoroughly mixed and there is no concentration gradient of any metal ions/metal in each of the phases
- ✓ The thickness of each of the diffusion layer is constant and same for each of the metal ions. There is one layer at the solid rod cathode/ molten salt interface, one on the cadmium side and one on the salt side of the liquid cadmium anode/ salt interface.
- ✓ Most of the concentration gradients of metal ions/ metal lie in this diffusion layer.

- ✓ The mass transfer of metal ions/ metal in this diffusion layer is due to diffusion only and mass transfer due to convection and migration is neglected.

The model has the capability to predict the following

- ✓ The variation of concentration of U and Pu in the molten salt with time
- ✓ The variation in concentration of U and Pu in the liquid cadmium anode
- ✓ The amounts of U and Pu deposited on the solid cathode with the progress of electrorefining with time could be predicted
- ✓ The cell voltage

The model was validated with the experimental results of Tomczuk et al. from literature and the results are in good agreement, the variation being less than 10% for the U and Pu concentration changes in liquid Cd anode and molten salt, and U deposit on solid cathode. This model can be used effectively to predict the performance of electrorefining process of similar electrode configurations. These are discussed in Chapter 3.

6.1.2. Modelling the electrotransport from various anodes to cathodes

The electrotransport of uranium from a liquid cadmium anode through molten LiCl-KCl eutectic salt to solid cathode, that from a liquid cadmium anode to liquid Cd cathode and that from a solid anode to solid cathode were modeled for various electrode configurations using the primary current distribution (piec) interface of electrochemistry module of COMSOL Multiphysics. It was used to estimate the ohmic losses in simplified models of electrochemical cells, where the overpotential of the electrode reactions are small compared to the ohmic voltage drops in the electrolyte and electrodes. A 2D/2D axisymmetric geometry model was used to evaluate the potential and current distributions. The effects of the following parameters on the performance of the electrorefiner were evaluated:

- Configuration having two pairs of electrodes in parallel /staggered arrangement
- Center to center distance between the electrodes
- Having a solid cathode with and without insulation at the bottom
- Variations in the elevations of Cd cathode
- Cathode surface area.
- Sensitivity analysis of the cell parameters was also carried out.

6.1.2.1. Parallel and staggered arrangement of electrodes

In this study, a pair of perforated anode baskets and a pair of solid cathodes were configured to be in two different arrangements (parallel and staggered) to study the effect of these configurations on the potential and current profiles in the electrorefiner. A 2D geometry was created for the electrotransport of uranium from the perforated anode basket to the solid cathode and the primary current distribution was simulated. The potential and current density distributions were evaluated for both the electrode configurations. It was observed that in the parallel arrangement, only one side of the electrodes is effective, whereas in the staggered arrangement, both sides of the electrodes are effective. In the parallel arrangement of electrodes, the potential was distributed only in the space between the electrodes and electrodeposition occurred only on one face of the cathodes. The current distribution was also observed between one anode and one cathode facing each other in the parallel arrangement, whereas for the staggered arrangement, current distribution was observed from all the four faces of the anodes to all the sides of the two cathodes. The calculated cell resistance was 0.33 ohm for the parallel arrangement and it dropped to 0.18 ohm for the staggered arrangement which can be expected from the differences in the current distribution patterns for the two configurations. The cell resistances were calculated using the model and compared with the values from the experiments carried out in the present study. The calculated and experimental values are in good agreement ~ 10% for the staggered arrangement and ~20% for the parallel arrangement. Computations were also carried out using COMSOL Multiphysics for the electrorefiner configuration for which Kobayashi et al. have also done computations. The two sets of computed values were compared and there is good agreement between the two sets of computed values.

6.1.2.2. Effect of variation of the distance between the electrodes

A 2D geometry was created and the primary current distribution (piec) for electrotransport of uranium from perforated anode basket to solid cathode was computed with various distances (2-8 cm) of cathode. The potential and current density distributions were calculated for various center to center distances of cathode from fixed position of anode. The potential and current distributions were similar to that observed for the parallel arrangement of electrodes. The cell resistance increased with increase in center to center distance between the electrodes. The computed cell resistances using the model are in very good agreement with the experimentally determined values.

6.1.2.3. Effect of having an insulating disc at the bottom of the solid cathode

A 2D axisymmetric model was developed for the electro-deposition of uranium for with and without an insulating ceramic disc at the bottom of the solid cathode and liquid cadmium layer at the bottom of the electrochemical cell used as anode. There is no significant difference in the potential and current profiles for the two configurations. It was observed that the solid cathode with insulation had an advantage of avoiding uranium dendrites growth towards liquid cadmium anode without any significant loss in the performance, as the increase of cell resistance is only 11 % for the solid cathode with insulation compared to that without insulation. The present computed cell resistance values were also compared with those of Kobayashi et al. who have published their results based on computation for similar cell parameters. Both the sets of data are in good agreement with each other.

6.1.2.4. Effect of various elevations of the Cd cathode

Liquid cadmium taken in an alumina crucible was used as the cathode and the cadmium pool at the bottom of the electrorefiner was used as the anode, for these studies. A 2D axisymmetric code was developed. Electrotransport of uranium from liquid cadmium anode to liquid Cd cathode was computed by changing surface area (S) of Cd cathode, changing the height of the empty space (h_2) of the crucible and changing the immersed height (h_1) of the crucible. The potential and current density distributions were evaluated. The cell resistances computed using the present model is compared with the experimental results. It was observed that with increase in the height of the immersed region (h_1) of the crucible, the cell resistance decreased due to the decrease in the distance between the anode and cathode. Increasing the height of empty space of crucible (h_2) resulted in increase in the cell resistance and increasing the Cd cathode surface area lead to decrease in the cell resistance. The model results were validated with the experiments carried out in the present study as well as with literature data.

6.1.2.5. Effect of solid cathode surface area

A 2D axisymmetric model was developed by changing the solid cathode surface area and with fixed liquid cadmium anode. The potential and current density distributions were evaluated. The measured cell resistances are compared with experimental cell resistances. It was observed that, with increase in the cathode surface area, the cell resistance decreased and current increased, which results in high throughput of electrorefiner. But further increase in surface area would lead to polarization of liquid Cd anode and electrotransport would be interrupted.

6.1.2.6. Cell resistance sensitivity study

A sensitivity analysis was performed to determine which of the two parameters, electrolyte conductivity and cell voltage, more significantly influences the cell resistance. The two parameters that were varied were the electrolyte conductivity and the cell voltage. Each parameter was perturbed by ±10%, 20%, 30%, 40% and 50% of its original value and the cell resistance was recalculated for every case. It is observed that the cell resistance is more sensitive to the electrolyte conductivity and there is no change in cell resistance with cell voltage. All these are discussed in Chapter 4.

6.1.3. Effect of the shape of the cathode

In chapter 5, the studies on the effect of shapes of the cathode are discussed. The code was developed for electrotransport between a solid anode and three cathodes of different shapes using the secondary, electrodeposition interface of electrochemistry module of COMSOL Multiphysics. The shapes of the cathode plays an important role in electrodeposition in terms of uniform/non uniform potential and current density distributions resulting in the variation in the thickness of deposit during electrodeposition. The amount of deposit on each cathode was calculated from the current profiles for the three cathodes of different shapes but same surface area. A very good agreement among the experimental values and simulation results was found for equal surface area. Electrode thickness changes, Overpotential during electrodeposition were simulated for cathodes of different shapes but same immersion heights. Primary, secondary and tertiary current density distributions were compared and observed that effect of concentration overpotential is minimum.

6.2. Scope for the future work

- Developing the model for electrotransport behavior of multispecies under various possible conditions i.e. varying the compositions of electrolyte and liquid cadmium cathode
- Effect of rotation of cruciform and cylindrical anodes
- continuous electrorefiner for single and multispecies
- To improve the model to minimize the assumptions made by the present model.
- To develop the model to predict the morphology (e.g. dendrites) formation of the deposit on the solid cathode.

References

[1] S. David, Future scenarios for fission based reactors, Nucl. Phy. A. 751 (2005) 429c-441c.

[2] R. Chidambaram and C. Ganguly, Plutonium and Thorium in the Indian Nuclear programme, Curr. Sci. (India), 70 (1996) 21-35.

[3] Baldev Raj, H.S. Kamath, R. Natarajan, P.R. Vasudeva Rao, A Perspective on Fast Reactor Fuel Cycle in India, Prog. Nucl. Energ. 47 (2005) 369 – 379.

[4] R.B. Grover, Green growth and role of nuclear power: A perspective from India, Energy strategies reviews, 1(4) (2013) 255

[5] C.V. Sundaram, Nuclear fuels, Curr. Sci. (India), 70(1) (1996) 1

[6] http://rupe-india.org/48/atomic.html.

[7] J.L. Swanson, W.W. Schulz, L.L. Burger, J. D. Navratil, K. P. Bender, PUREX flow sheets, In: Science and Technology of tributyl phosphate, Vol. III, L.L.BCRC Press, Boca Raton, 1984.

[8] C. Bernard, J.P. Moulin, P. Lederman, P. Pradel, M. Viala, Advanced PUREX Process for the New French Reprocessing Plants. Future Nuclear Systems: Emerging Fuel Cycles and Waste Disposal Options, p.57, Seattle, 12-17 Sept, 1993.

[9] L. Costanzo, Thorp - the guided tour, Nuclear Fuel cycle and fuel materials, Atom, 25(13) (1994) 28-29, 31-32.

[10] M. Toyota, Outline of Rokkasho reprocessing plant project, Proceedings of the third international Conference on Nuclear Fuel Reprocessing and Waste Management, RECOD'91, p.38, Sendal (1991).

[11] L. Koch, J.F. Babelot, J.P. Glatz and *G*. Nicolaou, Proc. of the 3rd International

Exchange Meeting on Actinide and Fission Product Separation and Transmutation, Cadarache, OECD/NEA 1994.

[12] L. Koch, J.P. Glatz, R.J.M. Konings, J. Magill, Nuclear Waste Treatment: Partitioning Process. ITU Annual Report 1999, EUR 19054, p 34. 29 CAPITULO 2 VERSION 15.doc.

[13] Status of Developments in the Back End of the Fast Reactor Fuel Cycle, IAEA Nuclear Energy Series, No. NF-T-4.2, 2011.

[14] W.H. Hannum, The benefits of an Advanced Fast Reactor Fuel Cycle for Plutonium Management, Rep. ANL/ESH/CP-91629 (CONF-9610244-1), USDOE (1996).

[15] Hannum W, The technology of the integral fast reactor and its associated fuel cycle, Special Issue, Prog. Nucl. Energ. 311/2 (1997) 12–17.

[16] Non aqueous reprocessing of irradiated fuel, Bibliographical series No.26, International atomic energy agency, Vienna, 1967.

[17] T. Shimada, A study on the technique of spent fuel reprocessing with supercritical fluid direct extraction method (Super-DIREX Method), J. Nucl. Sci. Technol. Suppl. 3 (2002) 757–760.

[18] H. Kofuji, F. Sato, M. Myochin, S. Nakanishi, M.V. Kormilitsyn, V.S. Ishunin, A.V. Bychkov, MOX Co-deposition Tests at RIAR for SF Reprocessing Optimization, J. Nucl. Sci. Technol. 44(3) (2007) 349–353.

[19] R.H. Allardice, Fast Reactor Fuel Cycles (Proc. Int. Conf. London, 1981), BNES, London (1982).

[20] M.A. Demiyanovich, Russian Institute for Atomic Reactors, Fluorination of Spent Uranium-plutonium Oxide Fuel in the Flame Reactor, Rep. RIAR, Dimitrovgrad,

RIAR-50 (1982) 565 (in Russian).

[21] Status of National Programmes on Fast Reactors (Proceedings of the 26th Meeting of the International Working Group on Fast Reactors, Vienna, 4–7 May 1993), IAEA-TECDOC-741, IAEA, Vienna (1994) 85–103.

[22] K.M. Harmon and G. Jansen, The salt cycle process, Prog. Nucl. Eng. Pergamon Press, Series III, Process Chemistry 4 (1970) 429–460.

[23] D.C. Wade and Y.I. Chang, The integral fast reactor (IFR) concept: physics of operation and safety, Nucl. Sci. Eng. 100 (1988) 507–524.

[24] Y.I. Chang, The integral fast reactor, Nucl. Technol. 88 (1989) 129–138.

[25] C.E. Till and Y.I. Chang, Plentiful Energy: The Story of the Integral Fast Reactor, CreateSpace, Lexington, KY, 2012.

[26] Y.I. Chang, Actinide recycle potential in the integral fast reactor (IFR) fuel cycle, Trans. Am. Nucl. Soc. 62 (1990) 73.

[27] S. Ghosh, S. Vandarkuzhali, P. Venkatesh, G. Seenivasan, T. Subramanian, B. Prabhakara Reddy, K. Nagarajan, Electrochemical studies on the redox behaviour of zirconium in molten LiCl–KCl eutectic, J. Electroanal. Chem. 627 (2009) 15–27.

[28] S. Ghosh, S. Vandarkuzhali, N. Gogoi, P. Venkatesh, G. Seenivasan, B. Prabhakara Reddy, K. Nagarajan, Anodic dissolution of U, Zr and U–Zr alloy and convolution voltammetry of $Zr^{4+}|Zr^{2+}$ couple in molten LiCl–KCl eutectic, Electrochim. Acta. 56 (2011) 8204–8218.

[29] A. Venkatesh, S. Ghosh, S. Vandarkuzhali, B. Prabhakara Reddy, K. Nagarajan, P.R. Vasudeva Rao, Modeling the anodic behavior of U, Zr, and U-Zr alloy in molten LiCl-KCl eutectic, Nucl. Technol. 182 (2013) 98-110.

[30] K. Nagarajan, B. Prabhakara Reddy, S. Ghosh, G. Ravisankar, K.S. Mohandas, M.U. Kamachi, K.V.G Kutty, K.V.K. Viswanathan, C. Anand Babu, P. Kalyanasundaram, P.R. Vasudeva Rao, Baldev Raj, Development of pyrochemical reprocessing for spent metal fuel, Energ. Proce. 7 (2011) 431-436.

[31] B. Prabhakara Reddy, S. Vandarkuzhali, T. Subramanian, P. Venkatesh, Electrochemical studies on the redox mechanism of uranium chloride in molten LiCl–KCl eutectic, Electrochim. Acta. 49 (2004) 2471–2478.

[32] S. Vandarkuzhali, P. Venkatesh, Suddhasattwa Ghosh, G. Seenivasan, B. Prabhakara Reddy, T. Subramanian, N. Sivaraman, K. Nagarajan, Electrochemistry of rare earth oxy ions REO^+ (RE = Ce, La, Nd) in molten MgCl2–NaCl–KCl eutectic, J. Electroanal. Chem. 611 (2007) 181–191.

[33] S. Ghosh, B.P. Reddy, K. Nagarajan, P.R. Vasudeva Rao, PRAGAMAN: A computer code for simulation of electrotransport during molten salt electrorefining, Nucl. Technol. 170 (2010) 430-443.

[34] S. Ghosh, B. Prabhakara Reddy, K. Nagarajan, K.C. Hari Kumar, Experimental investigations and thermodynamic modelling of KCl–LiCl–UCl3system, CALPHAD: Computer Coupling of Phase Diagrams and Thermochemistry 45 (2014) 11–26.

[35] K. Nagarajan, T. Subramanian, B. Prabhakara Reddy, P.R. Vasudeva Rao, Baldev Raj, Current status of pyrochemical reprocessing research in India, Nucl. Technol. 162 (2008) 259-263.

[36] W.E. Miller, M.J. Steindler, L. Burris, Advanced electrorefiner design, W-31-109-ENG-38, 1997.

[37] J.H. Lee, Y.H. Kang, S.C. Hwang, E.H. Kim, J.H. Yoo, H.S. Park, Separation

characteristics of a spent fuel surrogate in the molten salt electrorefining process, J. Mater. Proc. Technol. 189 (2007) 268–272.

[38] P. Soucek, R. Malmbeck, C. Nourry, J. P. Glatz, Pyrochemical reprocessing of spent fuel by electrochemical techniques using solid aluminium cathodes, Energ. Proce. 7 (2011) 396–404.

[39] J.G. Kim, S.J. Lee, S.B. Park, S.C. Hwang, H. Lee, High-throughput electrorefining system with graphite cathodes and a bucket-type deposit retriever, Proce. Chem. 7 (2012) 754 – 757.

[40] J.J. Laidler, J.E. Battles, W.E. Miller, J.P. Ackerman, E.L. Carls, Development of pyroprocessing technology, Prog. Nucl. Energ. 31 (1997) 131–140.

[41] R.W. Benedict and S.P. Henslee, EBR-II spent fuel treatment demonstration project status, in: 5th international nuclear conference on recycling, conditioning and disposal 98, Nice, France, 25–28 October, 1998, pp. 149–155.

[42] J.L. Willit, W.E. Miller, J.E. Battles, Electrorefining of uranium and plutonium- a literature review. J. Nucl. Mater. 195 (1992) 229-249.

[43] F. Kobayashi, T. Ogawa, M. Akabori, Y. Kato, Anodic dissolution of uranium mononitride in lithium chloride-potassium chloride eutectic melt, J. Am. Ceram. Soc. 78 (1995) 2279-2281.

[44] S.X. Li and M.F. Simpson, Anodic process of electrorefining spent driver fuel in molten LiCl-KCl-UCl3 /Cd system, Miner. Metall. Process. 22 (2005) 192–198.

[45] I. Johnson, The thermodynamics of pyrochemical processes for liquid metal reactor fuel cycles, J. Nucl. Mater. 154 (1988) 169–180.

[46] J. P. Ackerman, Chemical Basis for Pyrochemical Reprocessing of Nuclear Fuel, Ind.

Eng. Chem. Res. 30 (1) (1991) 141–145.

[47] T. Kobayashi and M. Tokiwai, Development of TRAIL, a simulation code for the molten salt electrorefining of spent nuclear fuel, J. Alloy. Comp. 197 (1993) 7-16.

[48] Z. Tomczuk, J. P. Ackerman, R. D. Wolson, W. E. Miller, Uranium transport to solid electrodes in pyrochemical reprocessing of nuclear fuel, J. Electrochem. Soc. 139 (12) (1992) 3523–3528.

[49] T. Kobayashi, R. Fujita, H. Nakamura, T. Koyama, Evaluation of cadmium pool potential in a electrorefiner with ceramic partition for spent metallic fuel, J. Nucl. Sci. Technol. 34 (1) (1997) 50–57.

[50] H.P. Nawada and N.P. Bhat, Thermochemical modeling of electrotransport of uranium and plutonium in an electrorefiner, Nucl. Eng. Des. 179 (1998) 75–99.

[51] R. K. Ahluwalia, T. Q. Hua, H. K. Geyer, Behavior of uranium and zirconium in direct transport tests with irradiated EBR-II fuel, Nucl. Technol. 126 (1999) 289-302.

[52] R.K. Ahluwalia and T.Q. Hua, Electrotransport of uranium from a liquid cadmium anode to a solid cathode, Nucl. Technol. 140 (2002) 41–50.

[53] M. Iizuka, K. Kinoshita, T. Koyama, Modeling of anodic dissolution of U–Pu–Zr ternary alloy in the molten LiCl–KCl electrolyte, J. Phys. Chem. Solid. 66 (2005) 427-432.

[54] M. Iizuka, Studies on electrorefining and electroreduction processes for nuclear fuels in molten chloride systems, Dissertation, Kyoto University, Japan, 2010.

[55] J.H. Lee, Y.H. Kang, S.C. Hwang, H.S. Lee, E.H. Kim, S.W. Park, Assessment of a high-throughput electrorefining concept for a spent metallic nuclear fuel-I: computational fluid dynamics analysis, Nucl. Technol. 162 (2008) 107-116.

[56] J.H. Lee, K.H. Oh, Y.H. Kang, H.S. Lee, J.B. Shim, E.H. Kim, S.W. Park, Assessment of a high-throughput electrorefining concept for a spent metallic nuclear fuel-II: electro hydrodynamic analysis and validation, Nucl. Technol. 165 (2009) 370-379.

[57] K.R. Kim, J.D. Bae, B.G. Park, D.H. Ahn, S. Paek, S.W. Kwon, J.B. Shim, S.H. Kim, H.S. Lee, E.H. Kim, I.S. Hwang, Modeling and analysis of a molten-salt electrolytic process for nuclear waste treatment, J. Rad. Analytic. Nucl. Chem. 280 (2) (2009) 401–404.

[58] S.Y. Choi, J.Y. Park, K.R. Kim, H.S. Jung, I.S. Hwang, B.G. Park, K.W. Yi, H.S. Lee, D.H. Ahn, S.W. Paek, Three-dimensional multispecies current density simulation of molten salt electrorefining, J. Alloy. Compd. 503 (2010) 177-185.

[59] J.D. Bae, H.O. Nam, K.W. Yi, B.G. Park I.S. Hwang, Numerical assessment of pyrochemical process performance for PEACER system, Nucl. Eng. Des. 240 (2010) 1679-1687.

[60] I.S. Hwang, S.H. Jeong, B.G. Park, W.S. Yang, K.Y. Suh, C.H. Kim, The concept of proliferation-resistant, environment-friendly, accident-tolerant, continual and economical reactor (PEACER), Prog. Nucl. Energ. 37 (2000) 217-222.

[61] R.O. Hoover, S. Phongikaroon, M.F. Simpson, S.X. Li, T. Yoo, Development of computational models for the MARK-IV electrorefiner effect of uranium, plutonium, and zirconium dissolution at the fuel basket salt interface, Nucl. Technol. 171 (2010) 276-284.

[62] S. Choi, J. Park, R.O. Hoover, S. Phongikaroon, M.F. Simpson, K.R. Kim, I.S. Hwang, Uncertainty studies of real anode surface area in computational analysis for molten salt electrorefining, J. Nucl. Mater. 416 (2011) 318–326.

[63] S.H. Kim, S.B. Park, S.J. Lee, J.G. Kim, H.S. Lee, J.H. Lee, Computer assisted design and experimental validation of multielectrode electrorefiner for spent nuclear fuel treatment using a tertiary model, Nucl. Eng. Des. 257 (2013) 12–20.

[64] R.M. Cumberland and M.S. Yim, Estimation of uranium and plutonium exchange current densities on solid electrodes in lithium chloride-potassium chloride eutectic melts, International pyroprocessing research conference, Fontana (Geneva), (2012) 1800-1930.

[65] R.M. Cumberland and M.S. Yim, A computational meta analysis of UCl3 cyclic voltammograms in LiCl-KCl electrolyte, J. Electrochem. Soc. 161(4) (2014) D147-D149.

[66] J. Zhang, Kinetic model for electrorefining, part I: Model development and validation, Prog. Nucl. Energ. 70 (2014) 279-286.

[67] COMSOL Multiphysics 4.4, Users guide, COMSOL Inc., 2013.

[68] H.A. Laitinen, W.S. Ferguson, R.A. Osteryoung, Preparation of pure fused lithium chloride-potassium chloride eutectic solvent, J. Electrochem. Soc. 104(8) (1957) 516-520.

[69] A. Nakayoshi, S. Kitawaki, M. Fukushima, T. Murakami, M. Kurata, Investigation of a LiCl–KCl–UCl_3 system using a combination of X-ray diffraction and differential thermal analyses, J. Nucl. Mater. 441 (2013) 468-472.

[70] G. Baptista, M. Bosteels, S. Ilie, C. Schafer, Experimental study on oxygen and water removal from gaseous streams for future gas systems in LHC detectors, Report from European organization for nuclear research, June 2000.

[71] P. H. Riger, Electrochemistry, Second edition, Chapman & Hall, Inc. United States of

America, 1993.

[72] F. Scholz (Ed.), Electroanalytical methods-Guide to experiments and applications, Springer, New York, 2005.

[73] K. B. Oldham, J. C. Myland, Fundamentals of electrochemical science, Academic Press, Inc. USA, 1994.

[74] http://electrochem.cwru.edu/encycl/art-e01-electroplat.htm.

[75] http://www.comsol.com.

[76] E.J.F. Dickinson, J.G. Limon-Peterson, R.G. Compton, J. Solid State Electrochem. 15 (2011) 1335-1345.

[77] E.R.V. Artsdalen, I.S. Yaffe, Electrical conductance and density of molten salt systems: KCl-LiCl, KCl-NaCl, and KCl-KI, J. Phys. Chem. 59(2) (1955) 118-127.

[78] S.A. Kuznetsov, H. Hayashi, K. Minato, M.G. Escard, Electrochemical transient techniques for determination of rare earth metal separation coefficients in molten salts Elctrochem. Acta. 51 (2006) 2463-2470.

[79] D. Yamada, T. Murai, K. Moritani, T. Sasaki, I. Takagi, H. Moriyama, K. Kinoshita, Diffusion behavior of actinide and lanthanide elements in molten salt for reductive extraction, J. Alloy. Comp. 444-445 (2007) 557-560.

[80] I. Johnson, M.G. Chasanov, R.M. Yonco, Pu-Cd system: thermodynamics and partial phase diagram, Trans. Metall. Soc. AIME. 233 (1965) 1408-1414.

[81] I. Johnson and H.M. Feder, Thermodynamics of the uranium-cadmium system, Trans. Metall. Soc. AIME. 224 (1962) 468-473.

[82] T. Koyama, T.R. Johnson, D.F. Fischer, Distribution of actinides in molten chloride salt / cadmium metal system, J. Alloy. Comp. 189 (1992) 37-44.

[83] T. Kobayashi, M. Tokiwai, E.C. Gay, Investigation of cell resistance for molten salt electrorefining of spent nuclear fuel, J. Nucl. Sci. Technol. 32(1) (1995) 68-74.

[84] T. Nishimura, T. Koyama, M. Iizuka, H. Tanaka, Development of an environmentally benign reprocessing technology – pyrometallurgical reprocessing technology, Prog. Nucl. Energ. 32(3/4) (1998) 381-387.